Title
Mitochondrial Control of Cellular Lipid Metabolism in Adipose Tissue

Author
Veliova, Michaela

Publication Date
2021

Peer reviewed|Thesis/dissertation

UNIVERSITY OF CALIFORNIA

Los Angeles

Mitochondrial Control of Cellular Lipid Metabolism in Adipose Tissue

A dissertation submitted in partial satisfaction of the requirements for the degree

Doctor of Philosophy in Molecular and Medical Pharmacology

by

Michaela Veliova

2021

ABSTRACT OF THE DISSERTATION

Mitochondrial Control of Cellular Lipid Metabolism in Adipose Tissue

by

Michaela Veliova

Doctor of Philosophy in Molecular and Medical Pharmacology

University of California, Los Angeles, 2021

Professor Orian Shirihai, Co-Chair

Professor Marc Liesa-Roig, Co-Chair

Proper regulation of cellular lipid storage and oxidation is indispensable for the maintenance of cellular energy homeostasis and health. Mitochondrial function has been shown to be a main determinant of functional lipid storage and oxidation, which is of particular interest for the adipose tissue as it is the main site of triacylglyceride storage in lipid droplets (LDs). Obesity stems from an imbalance between energy intake and energy expenditure, leading to increased lipid storage. Therefore, a better understanding of the

mechanisms by which LD break-down and build-up are regulated can be crucial in the development of treatments against metabolic diseases.

Blocking mitochondrial pyruvate import in brown adipocytes induces energy wasting via lipid cycling

Combined fatty acid esterification and lipolysis, termed lipid cycling, is an ATP consuming process that contributes to energy expenditure. Therefore, interventions that stimulate energy expenditure through lipid cycling are of great interest. Here we find that pharmacological and genetic inhibition of the mitochondrial pyruvate carrier (MPC) in brown adipocytes activates lipid cycling and energy expenditure, even in the absence of adrenergic stimulation. We show that the resulting increase in ATP demand elevates mitochondrial respiration coupled to ATP synthesis and fueled by lipid oxidation. We identify that glutamine consumption and the **M**alate-**A**spartate **Sh**uttle are required for the increase in **E**nergy **E**xpenditure induced by MPC inhibition in **B**rown **A**dipocytes (MAShEEBA). We thus demonstrate that energy expenditure through enhanced lipid cycling can be activated in brown adipocytes by decreasing mitochondrial pyruvate availability. We here present a new mechanism to increase energy expenditure and fat oxidation in brown adipocytes, which does not require adrenergic stimulation of mitochondrial uncoupling.

The role of mitochondria attached to Lipid droplets in cellular energy and lipid metabolism

Recent studies have identified a subpopulation of mitochondria attached to LDs, peridroplet mitochondria (PDM) that can be separated from cytoplasmic mitochondria

(CM) by centrifugation. PDM have distinct bioenergetics, proteome, cristae organization and dynamics that support LD build-up. However, most of our knowledge on PDM function is based on PDM isolated from brown adipose tissue (BAT), mostly due to a lack of available protocols to isolate PDM from other tissues such as white adipose tissue (WAT). Here we show an optimized protocol to isolate PDM from BAT and WAT with high yield and purity by adding a proteolytic treatment. Using this protocol, we show that PDM attached to differently sized LDs have unique bioenergetics characteristics. Thus, our new isolation protocol has the potential to improve our understating of PDM function in WAT and BAT in different populations of LDs.

The dissertation of Michaela Veliova is approved.

Heather Christofk

Ajit S. Divakaruni

Caius G. Radu

Karen Reue

Marc Liesa-Roig, Committee Co-Chair

Orian S. Shirihai, Committee Co-Chair

University of California, Los Angeles

2021

DEDICATION

I would like to dedicate this work to my loving family. My parents Vladimir Veliov and Losana Veliova, my sisters Elena Sohani and Radina Veliova and my grandparents Elena Veliova, Nikola Peshev and Radka Pesheva, who have supported me throughout my life.

TABLE OF CONTENTS

ABSTRACT OF THE DISSERTATION....ii

DEDICATION....vi

TABLE OF CONTENTS....vii

LIST OF FIGURES AND TABLES....ix

ACKNOWLEDGMENTS....xi

CURRICULUM VITAE....xiii

INTRODUCTION....1

Obesity epidemic and treatment....1

Adipose Tissue Lipid Storage and Endocrine Function....1

Mitochondria in Adipose Tissue....3

Uncoupling vs. ATP-consuming Futile Cycles as Energy Wasting Mechanisms in Adipocytes....6

Chapter 1: Blocking mitochondrial pyruvate import in brown adipocytes induces energy wasting via lipid cycling....8

INTRODUCTION....8

RESULTS....10

DISCUSSION....24

MATERIALS AND METHODS....30

FIGURES....38

Chapter 2: The role of mitochondria attached to lipid droplets in adipose tissue function. 61

INTRODUCTION 61

Mechanisms for PDM interaction with lipid droplets 63

PDM visualization and isolation methodologies 67

RESULTS 70

DISCUSSION 77

MATERIALS AND METHODS 79

FIGURES 86

CONCLUSIONS AND FUTURE DIRECTIONS 98

Potential for PDM as therapeutic target 98

REFERENCES 104

LIST OF FIGURES AND TABLES

Figure 1: Inhibition of the mitochondrial pyruvate carrier increases energy expenditure fueled by fatty acid oxidation. 38

Figure 2: MPC1 inhibition stimulates mitochondrial respiration coupled to ATP synthesis in brown adipocytes..... 41

Figure 3: Glutamine metabolism is required for increased energy expenditure induced by MPC inhibition. 43

Figure 4: The malate-aspartate shuttle supports the increase of both glutamine and fatty acid metabolism induced by MPC inhibition. 45

Figure 5: MPC inhibition induces ATP utilization by lipid cycling. 48

Figure 6: Proposed mechanism by which MPC inhibition induces lipid cycling and and the activation of the malate-aspartate shuttle. 51

Figure EV1: Assessment of respiratory rates in permeabilized adipocytes. 52

Figure EV2: Pharmacological or genetic blockage of the MPC does not affect brown adipocyte differentiation. 54

Figure EV3: Effects of UK5099 treatment on cellular metabolites 55

Figure EV4: The malate-aspartate shuttle is required for increased Norepinephrine-stimulated energy expenditure induced by MPC inhibition. 56

Figure EV5: Effects of UK5099 on ATP demand and lipid cycling. 58

Table 1: Primers for qPCR 60

Figure 2-1: Peridroplet Mitochondria (PDM) and Cytoplasmic Mitochondria (CM). 86

Figure 2-2: PDM isolation by high-speed centrifugation does not strip all mitochondria from lipid droplets. 87

Figure 2-3: Proteolytic treatment of the fat layer increases the yield of PDM stripped from BAT and WAT lipid droplets. 89

Figure 2-4: Isolation of PDM with ProtK does not inhibit mitochondrial function..... 91

Figure 2-5: Proteinase K treatment enables the isolation of mitochondria attached to smaller LDs. 93

Figure 2-6: PDM from Fx2 have unique characteristics..... 95

Table 2: Mechanisms of Mitochondria-Lipid Droplet Interaction..... 96

Figure 3-1: Possible role of PDM and CM in protection from lipotoxicity. 102

Table 3: Benefits and Pathologies related to PDM 103

ACKNOWLEDGMENTS

I would like to thank my mentor Orian Shirihai, for his patience, guidance, support and unique mentoring style with lots of humor. I am especially grateful to him for putting emphasis on creative thinking and commination and teaching me the importance of communicating our science in a way that is understandable for a broad audience. I also want to thank him for creating a lab environment that feels like a family.

I would like to thank Marc Liesa for his invaluable advice on experimental planning, data interpretation and writing. He taught me the importance of critically analyzing data and considering alternative interpretations. His open door policy helped countless times during experiments, for which I am incredibly grateful.

I would also like to thank Marcus Oliveira for his mentorship and kind support. I am very grateful for all his advice on troubleshooting experiments and for keeping me on track while preparing my manuscripts. Even though he lives on the other side of the world, he always managed to support me in every step of the way.

Lastly, I would like to thank all the members of the Shirihai/Liesa lab, for all their support, great collaborations, friendships, and for making my time in the lab the happiest time I could imagine.

Published work included in this thesis

Chapter one is adapted from Veliova et al. Blocking mitochondrial pyruvate import in brown adipocytes induces energy wasting via lipid cycling. *EMBO Rep* 21. 2020, DOI: 10.15252/embr.201949634

Parts of introduction and conclusions are adapted from Veliova et al. The biology of lipid droplet-bound mitochondria. Seminars in Cell and Developmental Biology 108: 55–64. 2020, DOI: 10.1016/j.semcdb.2020.04.013

CURRICULUM VITAE

Education

INSTITUTION AND LOCATION	DEGREE	Completion Date MM/YYYY	FIELD OF STUDY
University of Natural Resources and Life Sciences, Vienna, Austria	B.S	09/2012	Food Science and Biotechnology
University of Natural Resources and Life Sciences, Vienna, Austria	M.S.	06/2015	Biotechnology

Positions and Employments:

2011-2012 Research Assistant in Prof. Florian Rüker's lab, Department of Biotechnology, University of Natural Resources and Life Sciences, Vienna, Austria

2012-2012 Research Assistant, Baxter Innovations, Orth an der Donau/Austria

2012-2013 Teaching Assistant, Department of Applied Genetics and Cell Biology, University of Natural Resources and Life Sciences, Vienna, Austria

2013-2013 Research Assistant in Dr. Irina Druzhinina, Institute of Chemical Engineering, University of Technology, Vienna, Austria

2014-2014 Visiting Researcher in Prof. Caius Radu's lab, Department of Molecular and Medical Pharmacology, University of California, Los Angeles

Since 2015 Graduate Student, Department of Molecular and Medical Pharmacology, University of California, Los Angeles

Since 2016 Graduate Student Researcher in Prof. Orian Shirihai's lab, Department of Medicine, University of California, Los Angeles

Other Experience and Professional Memberships:

2019 Member, The American Society for Cell Biology

2019 Organizer, UCLA Mitochondria Symposium

2019 Co-Director, SPARK101, Outreach program for middle school students

2020 Director, UCLA Mitochondria Symposium

Honors:

2013	Erasmus Mundus Mobility Program: Exchange Student at "Universitat Autònoma de Barcelona", Spain
2014	Scholarship for short-term scientific research work abroad (KUWI), Austria
2018	1st prize for best 3-Minute Thesis Talk at UCLA Molecular and Medical Pharmacology Retreat
2019	UCLA Dissertation Year Fellowship

Publications (in reverse chronological order)

Ngo J, Benador IY, Brownstein AJ, Vergnes L, **Veliova M**, Shum M, Acín-Pérez R, Reue K, Shirihai OS & Liesa M (2021) Isolation and functional analysis of peridroplet mitochondria from murine brown adipose tissue. *STAR Protoc* 2: 100243

Jones AE, Sheng L, Acevedo A, **Veliova M**, Shirihai OS, Stiles L & Divakaruni AS (2020) Forces, Fluxes, and Fuels: Tracking mitochondrial metabolism by integrating measurements of membrane potential, respiration, and metabolites. *Am J Physiol-Cell Physiol*

Veliova M, Ferreira CM, Benador IY, Jones AE, Mahdaviani K, Brownstein AJ, Desousa BR, Acín-Pérez R, Petcherski A, Assali EA, *et al* (2020a) Blocking mitochondrial pyruvate import in brown adipocytes induces energy wasting via lipid cycling. *EMBO Rep* 21

Veliova M, Petcherski A, Liesa M & Shirihai OS (2020b) The biology of lipid droplet-bound mitochondria. *Semin Cell Dev Biol* 108: 55–64

Acin-Perez R, Benador IY, Petcherski A, **Veliova M**, Benavides GA, Lagarrigue S, Caudal A, Vergnes L, Murphy AN, Karamanlidis G, *et al* (2020) A novel approach to measure mitochondrial respiration in frozen biological samples. *EMBO J* 39

Assali EA, Jones AE, **Veliova M**, Acín-Pérez R, Taha M, Miller N, Shum M, Oliveira MF, Las G, Liesa M, *et al* (2020) NCLX prevents cell death during adrenergic activation of the brown adipose tissue. *Nat Commun* 11

Benador IY, **Veliova M**, Liesa M & Shirihai OS (2019) Mitochondria Bound to Lipid Droplets: Where Mitochondrial Dynamics Regulate Lipid Storage and Utilization. *Cell Metab* 29: 827–835

Benador IY, **Veliova M**, Mahdaviani K, Petcherski A, Wikstrom JD, Assali EA, Acín-Pérez R, Shum M, Oliveira MF, Cinti S, *et al* (2018) Mitochondria Bound to Lipid Droplets Have Unique Bioenergetics, Composition, and Dynamics that Support Lipid Droplet Expansion. *Cell Metab* 27: 869–885.e6

INTRODUCTION

Obesity epidemic and treatment

The prevalence of obesity worldwide has substantially increased, concurrently with the vast array of obesity-associated diseases, including type 2 diabetes, dyslipidemia, hypertension heart disease, and different types of cancer. The fundamental cause of obesity is an energy imbalance between calories consumed and calories expended leading to their excessive accumulation in the form of triglycerides in adipose tissue. Sustained lipid/nutrient overload can negatively affect adipose tissue function and overall metabolic homeostasis. Efficacious treatment for obesity is currently severely limited. Diet, exercise, and lifestyle modifications are the primary methods of treatments but have limited long-term success. Drug therapies include compounds that directly inhibit nutrient absorption from the gut or curb appetite by acting on satiety receptors in the central nervous system. For qualified patients, bariatric surgery is used as a measure to limit nutrient intake and absorption when other approaches fail. Thus, there is a critical need to identify novel treatments for obesity.

Adipose Tissue Lipid Storage and Endocrine Function

There are two major types of adipose tissue in mammals, the white adipose tissue (WAT) and the brown adipose tissue (BAT). The majority of adipose tissue in adult humans is WAT, however under certain conditions there is an increase in BAT depots and the biogenesis of other thermogenic adipocytes called beige or brite adipocytes. Detailed

discussions of the different types of adipocytes, their cell lineage, and differentiation were published in recent reviews (Peirce *et al*, 2014; Harms & Seale, 2013).

Apart from its function as lipid storing tissue, WAT has an important role as an endocrine organ, secreting adipokines such as leptin and adiponectin, involved in whole body metabolic regulation (Kershaw & Flier, 2004). Similar to WAT, BAT also serves as lipid storing and endocrine tissue, however in addition to that, BAT plays a crucial role in adaptive thermogenesis. In this sense, stimuli such as cold exposure, stress or certain diets will increase circulating norepinephrine levels, which then activate the β3-adrenergic receptors on BAT, promoting an increase in nutrient oxidation and the generation of heat (Cannon, 2004).

Being the main tissue for lipid storage, the adipose tissue is specialized in storing and releasing fatty acids upon stimulation. Thus, the adipose tissue plays a central role in controlling whole body lipid levels, and protecting from toxicity induced by high levels of non-esterified fatty acids (NEFA), namely lipotoxicity (Carobbio *et al*, 2017). Under conditions such as starvation, adipose tissue lipolysis is activated and fatty acids are released to other tissues for the generation of ATP by fatty acid oxidation (FAO) (Duncan *et al*, 2007; Zechner *et al*, 2012). This process needs to be highly regulated, as uncontrolled release of NEFA can, not only be detrimental to surrounding tissues, but can also cause damage to the adipocyte itself. Therefore, in order to reduce circulating fatty acids and prevent damage such as ER stress, part of these liberated fatty acids are re-esterified, forming a futile energy consuming cycle. This process was shown to be dependent on DGAT1, as adipocyte specific knock-out of DGAT1 resulted in increased levels of circulating fatty acids, and ER stress in adipocytes (Chitraju *et al*, 2017, 1). White

adipocyte mitochondria provide the ATP required for fatty acid esterification and release, as shown by decreased fatty acid release induced by oligomycin and the absence of adipose tissue expansion in mice with deficiencies in mitochondrial oxidative function (Kusminski *et al*, 2012; Vernochet *et al*, 2014; Angel *et al*, 1971; Fain & Rosenthal, 1971). Therefore, in white adipocytes, mitochondria are expected to play an integral role in the futile cycle of lipolysis and fatty acid re-esterification (Hammond & Johnston, 1987), as the ability of mitochondria to oxidize fatty acids is blocked in mature white adipocytes (Wang *et al*, 2010; Harper & Saggerson, 1975). In contrast, brown and beige adipocyte mitochondria are specialized in oxidizing fatty acids to generate heat via UCP1-mediated and other mechanisms (Wu *et al*, 2012; Heaton *et al*, 1978; Bertholet *et al*, 2017), thereby reducing susceptibility to lipotoxicity Here, NEFA play a role activating uncoupled respiration and fatty acid oxidation (Fedorenko *et al*, 2012).

Mitochondria in Adipose Tissue

Mature white adipocytes typically consist of one large LD, with a diameter in the 100 µm range (unilocular adipocytes), which covers most of the cytoplasm. Numerous studies have observed various levels of heterogeneity among white adipocytes, both in terms of their LD size and composition and function. Detailed reviews on this topic were published recently (Luong *et al*, 2019; Kwok *et al*, 2016). Compared to brown adipocytes, white adipose tissue and adipocyte cell lines have significantly fewer mitochondria. However, during WAT differentiation mitochondrial biogenesis plays an important role, as mitochondria are critical to meet the ATP demand of the differentiation process and provide substrates for lipogenesis. Interestingly, terminal differentiation to mature white adipocytes is associated with removal of mitochondria by autophagy (Goldman *et al*,

2011; Wilson-Fritch *et al*, 2003; Zhang *et al*, 2009). Accordingly, adipose-specific knock-out of autophagy gene Atg7 leads to a concurrent impairment of the adipocyte differentiation program and accumulation of mitochondria, as well as showing small LDs similar to immature white adipocytes (Zhang *et al*, 2009). The fact that mature WAT removes mitochondria generated during differentiation seems to suggest that mitochondrial function needs to be limited in mature WAT. However, several studies have demonstrated the importance of mitochondrial function in WAT physiology (Kusminski & Scherer, 2012; Kusminski *et al*, 2012; Wang *et al*, 2010; Wilson-Fritch *et al*, 2003, 2004; Vernochet *et al*, 2014; Yin *et al*, 2014). Indeed mitochondrial function was found to be crucial for adiponectin production (Koh *et al*, 2007). Furthermore, adipocyte specific knock-out of TFAM, a key regulator of mitochondrial transcription, resulted in severe lipodystrophy, insulin resistance and hepatosteatosis (Vernochet *et al*, 2014). Supporting the contribution of decreased mitochondrial function in WAT to metabolic diseases, there seems to be a negative correlation between mitochondrial mass in the WAT and obesity. In this context, white adipocytes from *ob*/*ob* mice had significantly lower mitochondrial mass and oxygen consumption rates compared to lean control mice, which could partially be improved by PPARgamma agonist rosiglitazone (Wilson-Fritch *et al*, 2004).

With a remarkable resemblance to immature white adipocytes (Zechner *et al*, 2012), mature brown adipocytes are characterized by numerous small and medium sized LDs, with diameters ranging from nm range to around 15 µm (multilocular adipocytes), which are surrounded by numerous mitochondria. (Napolitano & Fawcett, 1958; Benador *et al*, 2018). Studies observed that BAT undergoes “whitening”, a process that is accompanied by reduced mitochondrial mass and a decrease in the number of lipid droplet, becoming

unilocular (Kotzbeck *et al*, 2018). Conversely, the process of “browning” is typically associated with an increase in mitochondrial mass and activity, the expression of thermogenic markers such as UCP1 and Prdm16, and the number of lipid droplets per adipocyte in white adipose tissue, which leads to improvements in whole body metabolism (Seale *et al*, 2011). Remarkably, rosiglitazone was shown to increase both fatty acid oxidation and lipolysis/re-esterification in white adipose tissue, before browning is found (Wilson-Fritch *et al*, 2004). Therefore, one could propose that, in white adipose tissue, the fatty acid oxidation stimulation induced by rosiglitazone is confined to browning of white adipocytes, while mature white adipocytes only showed enhanced re-esterification (not browned).

Both WAT and BAT are innervated by the sympathetic nervous system (SNS), and their activation is dependent on hormonal stimulation by the SNS (Blaszkiewicz *et al*, 2019). In this context, mitochondria play an indispensable role in adipose tissue thermogenesis, a process enabled by the uncoupling protein 1 (UCP1), a mitochondrial protein expressed exclusively in thermogenic adipocytes. UCP1 uncouples mitochondrial nutrient oxidation from ATP synthesis to generate heat (Wu *et al*, 2012; Heaton *et al*, 1978). UCP1-mediated thermogenesis is activated after stimulation of β3-adrenergic receptors by Norepinephrine released from sympathetic neurons, which induce fatty acid release from LDs and mitochondrial fragmentation in a PKA-dependent manner (Cannon, 2004; Divakaruni & Brand, 2011). Mitochondrial fragmentation and the fatty acids released activate UCP1 to mediate uncoupling. Activated BAT elevates its metabolic activity, causing an increase in glucose uptake as well. Thus, active BAT is detectable in mice and humans using positron emission tomography–computed tomography (PET-CT) to

monitor ^{18}flurodeoxyglucose (^{18}FDG) uptake, this glucose uptake being reduced with aging or obesity (Cypess *et al*, 2009a; van Marken Lichtenbelt *et al*, 2009a; Virtanen *et al*, 2009; Pfannenberg *et al*, 2010; Yoneshiro *et al*, 2011). In this context, a recent study showed that mitochondrial lipoylation is reduced in aged BAT and serves likely as a key driver in age-related decline in BAT thermogenic activity (Tajima *et al*, 2019). In addition to an increase in mitochondrial oxygen consumption upon BAT stimulation, mitochondrial dynamics play a central role in BAT thermogenic capacity. Wikstrom et al. showed that upon adrenergic stimulation BAT mitochondria undergo PKA mediated fragmentation by activating the mitochondrial fission protein Drp1 (Wikstrom *et al*, 2014). Moreover, the study showed that Drp1 activation and mitochondrial fragmentation are necessary for BAT thermogenesis using a dominant-negative form of Drp1 (Wikstrom *et al*, 2014). Furthermore, our recent study has shown a tight interaction between mitochondria and LDs, and that BAT mitochondria detach from LDs upon cold exposure (Benador *et al*, 2018).

Uncoupling vs. ATP-consuming Futile Cycles as Energy Wasting Mechanisms in Adipocytes

Recent evidence demonstrated that BAT and beige adipocytes can increase energy expenditure by activating ATP-consuming futile cycles. This need for ATP means that mitochondria can remain coupled to sustain ATP demand and fuel these futile cycles, which prevents the potential risks associated with large depolarization characteristic of mitochondrial uncoupling. Remarkably, these ATP-consuming futile cycles recently identified in BAT and beige adipocytes were already shown to promote energy expenditure in skeletal muscle.

A futile cycle consists of a set of biochemical reactions that concurrently run in opposite directions, consuming ATP in one of the directions. As the product of the first reaction is the substrate of the second reaction, and the product of the second reaction is the substrate of the first reaction, such a cycle will lead to a net decrease in (Newsholme *et al*, 1983). Thus, mitochondria or any other ATP generating processes will need to consume energy to provide this ATP, resulting in a net increase in energy dissipation.

Chapter 1: Blocking mitochondrial pyruvate import in brown adipocytes induces energy wasting via lipid cycling

INTRODUCTION

Brown adipose tissue (BAT) is the main site of non-shivering thermogenesis (Cannon, 2004; van Marken Lichtenbelt *et al*, 2009b; Virtanen *et al*, 2009; Cypess *et al*, 2009b). Fat oxidation is activated in BAT when the sympathetic nervous system releases norepinephrine after sensing cold temperatures, which activates adrenergic receptors on BAT to increase thermogenesis. This activation causes a stimulation of lipolysis, mediated by Protein Kinase A actions on lipolytic proteins, ultimately activating mitochondrial uncoupling protein 1 (UCP1) by free fatty acids (Cannon, 2004; Divakaruni & Brand, 2011). UCP1 is exclusively expressed in thermogenic adipocytes and dissipates the energy of mitochondrial proton gradient to generate heat, instead of conserving it as ATP (Cannon, 2004). Numerous studies demonstrated the beneficial effects of BAT activation in the treatment of metabolic disorders (Poekes *et al*, 2015). Although recent publications have proposed mechanisms to increase energy expenditure in BAT independent of hormonal stimulation (Kazak *et al*, 2015; Ikeda *et al*, 2017; Deng *et al*, 2018; Mahdaviani *et al*, 2017), currently there is only one known pharmacological approach to increase BAT energy expenditure in humans, which is the use of β3-adrenergic receptor agonists, such as mirabegron (O'Mara *et al*, 2020). While promising, potential undesirable side effects may arise from systemic β3-adrenergic stimulation.

Increased glucose uptake is a hallmark of BAT activation, as shown by ^{18}fluorodeoxyglucose positron emission tomography–computed tomography (^{18}F-PET-

CT) images in humans and mice (Cypess *et al*, 2009b; van Marken Lichtenbelt *et al*, 2009b; Virtanen *et al*, 2009; Hankir *et al*, 2017). Pyruvate, the end-product of glycolysis, has multiple metabolic fates in the cytosol and in the mitochondria. The first step of mitochondrial pyruvate oxidation requires pyruvate import across the inner membrane, which is mediated by the mitochondrial pyruvate carrier (MPC) (Herzig *et al*, 2012; Bricker *et al*, 2012). MPC is a protein complex that transports pyruvate in a proton motive force-dependent manner (Papa *et al*, 1971; Herzig *et al*, 2012). Several studies have shown that MPC activity determines the fuel oxidized by mitochondria, with direct consequences to cell function and fate (Vacanti *et al*, 2014; Yang *et al*, 2014a; Vanderperre *et al*, 2016; Divakaruni *et al*, 2017; Vanderperre *et al*, 2015). Once in the matrix, mitochondrial pyruvate undergoes simultaneous decarboxylation to acetyl-CoA and condensation with oxaloacetate to produce citrate. Citrate can then be used as a precursor of malonyl-CoA, the first intermediate of *de novo* fatty acid synthesis. At the same time, malonyl-CoA also inhibits the rate-controlling step of mitochondrial fatty acid oxidation by blocking carnitine palmitoyl transferase 1 (CPT1). The role of mitochondrial pyruvate oxidation driven by MPC activity in brown adipocytes remains elusive, as the assumptions are that; i) pyruvate might not be required as a fuel in BAT mitochondria, as brown adipocytes mostly oxidize fatty acids when mitochondrial uncoupling is adrenergically activated to generate heat and ii) the preferred fate of pyruvate from increased glycolysis in BAT would be lactate, to allow glycolysis to compensate for uncoupling and provide the ATP not produced by uncoupled mitochondria. To gain insight into the role of mitochondrial pyruvate transport and metabolism in BAT energy metabolism, we determined the effects of blocking the MPC on energy expenditure. Here, we show that pharmacological and

genetic inhibition of the MPC activates coupled fat oxidation in the absence of adrenergic stimulation, thus demonstrating that MPC inhibition increases ATP demand and fat expenditure. The increased flux in coupled fatty acid oxidation induced by MPC blockage is supported by glutamine consumption and the malate-aspartate shuttle (MASh), a previously unstudied metabolic pathway in BAT. Interestingly, we show that acute MPC blockage has an additive effect promoting energy expenditure in adrenergically stimulated brown adipocytes, suggesting that MPC inhibition enhances fatty acid oxidation for ATP synthesis in mitochondria in which UCP1 is not activated. Finally, we demonstrate that the ATP-consuming glycerolipid/free fatty acid (GL/FFA) cycling (Prentki & Madiraju, 2008; Reshef *et al*, 2003) is responsible for increased ATP demand in response to MPC inhibition. Thus, we show that MPC activity limits energy expenditure in resting and activated brown adipocytes, rather than facilitating it. We conclude that MPC activity regulates BAT energy metabolism and its inhibition may represent a novel target to increase fat oxidation and energy expenditure independent of adrenergic stimuli, with potential benefits for treatment of metabolic diseases.

RESULTS

Inhibition of the mitochondrial pyruvate carrier increases energy expenditure fueled by fatty acid oxidation.

To determine the role of the mitochondrial pyruvate import in BAT fuel preference, we sought to assess the effects of MPC inhibition on fatty acid utilization in non-stimulated brown adipocytes. Mitochondrial pyruvate import was blocked using UK5099, a pharmacological inhibitor that covalently binds the MPC (Halestrap, 1975). To confirm

that UK5099 at the concentrations used inhibited pyruvate oxidation by blocking pyruvate import and not by causing mitochondrial dysfunction, we compared the acute effect of UK5099 on mitochondrial respiration fueled by pyruvate vs. succinate. To directly test mitochondrial pyruvate and succinate oxidation, cells were permeabilized to allow direct provision of pyruvate and succinate to mitochondria. Permeabilization prevented any metabolic rewiring induced by MPC blockage in intact cells to preserve mitochondrial ATP synthesis by using other available fuels. UK5099 decreased oxygen consumption rates (OCR) in a dose-dependent manner in permeabilized brown adipocytes under pyruvate and malate (**Fig. EV1A**), but not under succinate and rotenone (**Fig EV1B**). These data are in agreement with previous studies showing a specific effect of UK5099 on pyruvate oxidation at low micromolar concentrations (Divakaruni *et al*, 2013, 2017).

Previous studies demonstrated that upon MPC inhibition, fat mobilization and oxidation increased (Vacanti *et al*, 2014; Yang *et al*, 2014a; Vanderperre *et al*, 2016; Divakaruni *et al*, 2017; Vanderperre *et al*, 2015). To test the role of the MPC in the fate of fatty acids in brown adipocytes, we used the fluorescent fatty acid analog Bodipy C12 558/568 (Bodipy C12), which can be oxidized and/or incorporated into lipid droplets (LDs) as triacylglycerides (TAGs). Primary brown adipocytes were incubated overnight with Bodipy C12 to stain lipid droplets and chase lipid droplet size and fluorescence after 120 min of UK5099 treatment. Lipid droplets were imaged using high resolution airyscan confocal microscopy in living cells (**Fig 1A**). We found that treatment with UK5099 significantly reduced lipid droplet content (**Fig 1A-B**). Reduced lipid droplet content by MPC inhibition was similar to the reduction induced by norepinephrine (NE) in brown adipocytes (**Fig 1B**), strongly suggesting that UK5099 increased lipolysis. Next, we tested

whether MPC inhibition increased utilization of extracellular fatty acids by measuring the fate of exogenous fluorescently-labeled fatty acid using thin layer chromatography (TLC). We pulsed brown adipocytes with Bodipy C12 for 24 h in the presence of either 100 nM UK5099, 1 µM NE or vehicle. Lipids were extracted from both media and cells and resolved by TLC (**Fig 1C**) (Rambold *et al*, 2015; Benador *et al*, 2018). Treatment with UK5099 increased Bodipy C12 uptake from the media similarly to NE, indicating that fatty acid uptake and utilization were increased upon MPC inhibition (**Figs 1C-D**). To measure C12 incorporation into TAGs, we quantified the amount of TAGs containing exogenously added C12 per amount of C12 uptake. We found that both UK5099 and NE induced a reduction in C12 incorporation into TAGs (**Fig 1D**). Altogether, these data provide evidence that MPC inhibition promotes fatty acid uptake by brown adipocytes, with the majority of these fatty acids going towards oxidation rather than storage as TAGs.

Based on the results in figures 1 A-D, we reasoned that MPC inhibition might affect mitochondrial respiration fueled by fatty acids. Thus, we measured the effects of MPC inhibition by UK5099 on mitochondrial OCR in non-stimulated brown adipocytes. We observed that inhibition of the MPC resulted in a dose-dependent increase in mitochondrial OCR of intact brown adipocytes (**Fig 1E**). The maximal increase in OCR by UK5099 was observed at 10 µM. This observation raised two questions: i) what are the fuels driving the increase in OCR: ii) what are the ATP-requiring processes that are activated upon MPC inhibition. We first wanted to examine what substrates were being oxidized to fuel the enhanced respiratory rates. Given that both lipolysis and fatty acid uptake were increased under UK5099 treatment (**Figure 1A-D**), we tested the requirement for fatty acids in UK5099-induced increase in OCR. We hypothesized that, if

increased mitochondrial respiration induced by UK5099 is dependent on a rise in intracellular levels of fatty acids, then their sequestration would prevent the boost in respiratory rates upon MPC inhibition. To assess the role of increased free fatty acids availability in UK5099-induced OCR we supplemented the respirometry media with 0.1 % fatty acid free albumin (BSA-FAF), which sequesters the excess intracellular free fatty acids (Alsabeeh *et al*, 2018). BSA-FAF prevented the stimulatory effects of UK5099 on mitochondrial respiration, suggesting that increased fatty acids availability supports respiration when MPC is inhibited (**Fig EV1C**).

To further test whether the increase in mitochondrial respiration induced by UK5099 is fueled by fatty acids, we used etomoxir to block a rate-controlling step of mitochondrial fatty acid oxidation catalyzed by carnitine palmitoyl transferase 1 (CPT1) (Kiorpes *et al*, 1984). The contribution of fatty acid oxidation to UK5099-induced respiration was assessed by determining the portion of OCR that is sensitive to etomoxir. Etomoxir was used at 40 μM, a concentration that specifically blocks CPT1 and has only minimal effects on other mitochondrial processes (**Fig EV1D**). Remarkably, the component of OCR that was sensitive to etomoxir was significantly higher in UK5099-treated brown adipocytes, strengthening our assertion that MPC inhibition promotes fatty acid oxidation (**Figs. 1F-G**). On the other hand, the etomoxir-insensitive component of OCR was not affected by MPC inhibition (**Fig 1G**). These data suggest that MPC inhibition is primarily inducing oxidation of fat as compared to other fuels in brown adipocytes.

The above observations indicate that increased respiratory rates meditated by MPC inhibition were prevented if fatty acid import to mitochondria was blocked. However, blocking fatty acid utilization with etomoxir could be upregulating the utilization of other

fuels to preserve mitochondrial ATP synthesis, thus underestimating the rates of fatty acid oxidation under MPC inhibition. Therefore, to unequivocally determine the real preference towards fatty acid oxidation when the MPC is inhibited, we measured the incorporation of palmitate-derived carbons into tricarboxylic acid (TCA) cycle intermediates using gas-chromatography/mass spectrometry (GC/MS) (**Fig 1H**). [U-$^{13}C_{16}$] Palmitate and 5 μM UK5099 or vehicle were concurrently provided to non-stimulated brown adipocytes for 24 h. Enrichment of ^{13}C in TCA cycle metabolites was quantified in polar metabolite extracts from total lysates (Cordes & Metallo, 2019). Figure 1I shows that UK5099 increased incorporation of ^{13}C from labelled palmitate into citrate and malate, indicating that MPC inhibition increases fatty acid oxidation to acetyl-CoA that enters the TCA cycle (**Fig 1I**). Collectively, our data indicate that in the absence of NE stimulation, inhibition of the MPC increases energy expenditure fueled by fatty acid oxidation in mitochondria.

MPC1 inhibition stimulates mitochondrial respiration coupled to ATP synthesis in brown adipocytes.

Sympathetic stimulation of brown adipocytes increases mitochondrial fatty acid oxidation by stimulating lipolysis uncoupling mitochondria. Consequently, acute treatment of brown adipocytes with norepinephrine (NE) increases mitochondrial fat oxidation to produce heat by activating UCP1. Thus, we next aimed to determine whether MPC inhibition would further increase fatty acid oxidation in activated brown adipocytes or whether it would be inert, as expected with MPC1 inhibition in uncoupled and depolarized mitochondria. We find that MPC inhibition by UK5099 further increased OCR in NE-stimulated brown adipocytes (**Figs 2A-B**). Next, we determined whether UK5099-

mediated increase in mitochondrial respiration was caused by an increase in uncoupled fat oxidation. To this end, we injected ATP-synthase inhibitor oligomycin, to block coupled respiration, and etomoxir, to block fatty acid oxidation, sequentially in NE stimulated brown adipocytes. MPC inhibition via UK5099 treatment increased both uncoupled and coupled (ATP-synthesizing) respiration, where the effect on coupled respiration was twice as large as the effect on uncoupled respiration (**Figs 2A-B**). Furthermore, the component of NE-stimulated respiration sensitive to etomoxir was significantly higher in cells treated with UK5099 compared to vehicle-treated cells. Altogether, these data indicate that MPC inhibition promotes an increase in both coupled and uncoupled fatty acid oxidation during adrenergic stimulation (**Figs 2A-B**). To address the possibility that UK5099 increased coupled respiration by decreasing UCP1 content, we measured UCP1 expression in cells treated with UK5099. Western blot and qPCR analyses showed that UK5099 treatment did not affect UCP1 expression and protein content (**Fig EV2A**).

MPC is a protein heterodimer composed of MPC1 and MPC2 subunits, which are required for mitochondrial pyruvate import and consequently pyruvate oxidation (Herzig *et al*, 2012; Bricker *et al*, 2012; Vigueira *et al*, 2014). To validate that the effects on respiration observed were not off-target effects of UK5099, we silenced the expression of *Mpc1* and then assessed energy expenditure and fatty acid oxidation. Brown adipocytes were transfected with an siRNA for *Mpc1* (MPC1-KD), or a control scramble RNA (Scramble). Successful knock-down was confirmed by Western blot (**Figs 2C-D**) and by qPCR (**Fig 2E**). Both MPC1 and MPC2 protein levels were reduced when cells were transfected with MPC1 siRNA (**Fig 2D**). However, only the transcript levels of *Mpc1*, but not *Mpc2*, were reduced in cells transfected with *Mpc1* siRNA (**Fig 2E**). As MPC1

stabilizes MPC2 by being in the same complex, similar effects of downregulation of MPC2 protein levels by the silencing of MPC1 were reported in previous studies (Bricker *et al*, 2012; Divakaruni *et al*, 2013; Gray *et al*, 2015). Next, we tested the effects of MPC1-KD on energy expenditure and fatty acid oxidation. Assessment of OCR in non-stimulated brown adipocytes showed that MPC1-KD increased energy expenditure compared to control, thereby confirming the observed effect of pharmacological MPC inhibition (**Figs 2F-G**). Furthermore MPC1-KD increased the etomoxir-sensitive proportion of NE-stimulated respiration in brown adipocytes, indicating that genetic downregulation of *Mpc1* recapitulated the effects of UK5099 (**Fig 2G**). Interestingly, MPC1-KD did not further increase NE-stimulated OCR when compared to scramble (**Fig 2G**). The apparent difference between the effects of pharmacological and genetic interference on NE-induced energy expenditure suggests that a long-term reduction of MPC activity recruits compensatory mechanisms to control the thermogenic response to NE. To further confirm that the effects of UK5099 on increased fat oxidation are a consequence of MPC1 blockage, we measured the effects of 100 nM UK5099 on mitochondrial respiration in scramble RNA and MPC1-KD brown adipocytes. UK5099 treatment increased mitochondrial respiration in unstimulated brown adipocytes expressing scramble RNA, similar to the effect observed in non-transfected cells (**Figs 2A, 2B and 2H**). However, this stimulatory effect of UK5099 on OCR was lost in MPC1-KD cells (**Fig 2H**), indicating that increased energy expenditure caused by UK5099 treatment is dependent on MPC. As in UK5099 treated brown adipocytes, qPCR analysis confirmed that MPC1 KD did not reduce UCP1 expression or affect brown adipocyte differentiation markers compared to control cells (**Fig EV2B**). Overall, our data suggest that MPC inhibition further increases

NE-stimulated energy expenditure and mitochondrial respiration coupled to ATP synthesis.

Glutamine metabolism is required for increased energy expenditure induced by MPC inhibition.

Fatty acid oxidation generates acetyl-CoA (2 carbons) which then condenses with oxaloacetate (4 carbons) to generate citrate (6 carbons) through the citrate synthase reaction. Since this metabolic step requires both substrates, the two carbons input provided by acetyl-CoA must be matched with oxaloacetate, which is provided by anaplerotic reactions from pyruvate or amino acid metabolism (Cannon & Nedergaard, 1979). As we observed that MPC inhibition increased fatty acid oxidation (**Figs 1F, 1G, 2A, 2B, 2F, and 2G**), we hypothesized that brown adipocytes switch to an alternative source for oxaloacetate when mitochondrial pyruvate transport is limited. Previous work in hepatocytes, neurons and myoblasts showed that cells shift towards glutamate metabolism when the MPC is inhibited, which can provide carbons for oxaloacetate production (Divakaruni *et al*, 2017; Vacanti *et al*, 2014; Yang *et al*, 2014a). We therefore assessed the dependency of UK5099-stimulated increase in mitochondrial respiration on glutamine in brown adipocytes. Glutamine was required for UK5099-mediated increase in OCR in both non-stimulated and NE-stimulated brown adipocytes (**Figs 3A-B**). In media lacking glutamine, pharmacological inhibition of the MPC had no effect on non-stimulated OCR and reduced NE-stimulated respiration (**Figs 3A-B**). Furthermore, use of glutamine depleted media prevented the stimulatory effects of UK5099 on both coupled and uncoupled respiration, as well as etomoxir-sensitive respiration (**Figs 3A-B**). These

data indicate that glutamine is a necessary nutrient to sustain the increase in mitochondrial fat oxidation induced by MPC inhibition (**Figs 3A-B**). Glutamine catabolism is a source for oxaloacetate, which is necessary for acetyl-CoA generated by fatty acid oxidation to enter the TCA cycle. Thus, to test whether glutamine catabolism was necessary for UK5099-mediated increase in mitochondrial fat oxidation, we tested the effects of glutaminase inhibitor CB839 on UK5099-induced mitochondrial fat oxidation. Figure 3C shows that CB839 prevented the increases in mitochondrial coupled and uncoupled respiration and etomoxir-sensitive OCR caused by MPC inhibition, supporting our hypothesis that glutaminolysis is required to support enhanced mitochondrial fatty acid oxidation after MPC inhibition (**Fig 3C**). One pathway to fuel the TCA cycle with glutamine is the aspartate aminotransferase reaction, a reaction with converts glutamate (from glutamine) and oxaloacetate into alpha-ketoglutarate (used by the TCA cycle) and aspartate. Therefore, we reasoned that the aspartate:glutamate ratio would serve as an indicator of glutamine oxidation by the TCA cycle (Vacanti *et al*, 2014; Divakaruni *et al*, 2017). Indeed, we find that UK5099 treatment increased aspartate:glutamate ratio indicating increased aspartate aminotransferase activity (**Fig 3D**).To specifically determine the metabolic fate of glutamine into the TCA cycle intermediates, we traced the incorporation of glutamine carbons to polar metabolites, using uniformly labeled glutamine [U-$^{13}C_5$] and quantifying labeled metabolite enrichment by GC-MS (**Fig EV3B**). UK5099 significantly increased the incorporation of glutamine-derived carbons into aspartate, glutamate, α-ketoglutarate and malate, thereby supporting the hypothesis that glutamine is required for TCA anaplerosis, when mitochondrial pyruvate import is limited (**Fig EV3C**). Intriguingly, the isotopomer distribution shows, that most of the increase in

glutamine derived carbons were in the M+3 mass isotopomer (**Fig EV3D**), which may be indicative of reductive carboxylation of glutamine linked to ATP citrate lyase activity (Zhang *et al*, 2014).

The malate-aspartate shuttle supports the increase of both glutamine and fatty acid metabolism induced by MPC inhibition.

Glutamine derived carbons can enter the TCA cycle by glutamic oxaloacetic transaminase- (GOT) dependent conversion of aspartate to oxaloacetate. GOT is a critical component of the malate aspartate shuttle (MASh), a cyclic pathway that allows the transfer of reduced equivalents from the cytosol to the mitochondrial matrix (**Fig 4A**). Since our metabolomics data indicated increased aminotransferase activity upon UK5099 treatment (**Fig 3D**), we sought to test the role of the MASh in UK5099-induced energy expenditure in brown adipocytes. To determine whether MASh could be contributing to the increase in respiration induced by MPC inhibition, we inhibited GOT using aminooxyacetic acid (AOA) (Kauppinen *et al*, 1987). The increase in mitochondrial respiration induced by UK5099 was dose-dependently reduced by AOA, reaching complete inhibition at 1 mM AOA (**Figs 4B and EV4A**). In the absence of UK5099, AOA caused no apparent effects on brown adipocyte respiration (**Figs 4B and EV4A**). To further confirm the involvement of the MASh in the metabolic effects caused by UK5099, and address potential off-target effects of AOA (Cornell *et al*, 1984; Yang *et al*, 2008), we then silenced the expression of oxoglutarate carrier 1 (*SLC25A11* or *OGC1*), a key component of MASh. OGC1 mediates the electroneutral exchange of malate and α-ketoglutarate between mitochondrial intermembrane space and the matrix, transporting

malate to mitochondrial matrix to generate oxaloacetate (**Fig 4A**) (Indiveri *et al*, 1987). Adenovirus-mediated knock-down of *OGC1* was confirmed by qPCR in primary brown adipocytes (**Fig EV4B**). OGC1 KD prevented the UK5099-induced increase in OCR in non-stimulated and NE-stimulated brown adipocytes (**Figs 4C-D and EV4C**). Furthermore, OGC1 KD abrogated the increase in etomoxir-sensitive OCR caused by UK5099 (**Fig 4E**). The involvement of the MASh in UK5099-induced energy expenditure was further assessed by silencing another MASh component, the mitochondrial aspartate/glutamate carrier (*SLC25A12* or *Aralar1*). Aralar1 catalyzes the calcium-dependent exchange of aspartate efflux and glutamate uptake across the mitochondrial inner membrane (Palmieri *et al*, 2001). Aralar is found as two isoforms 1 and 2 (*Aralar1* or *SLC25A12*, and *Aralar2* or citrin or *SLC25A13),* with Aralar1 being the most abundant isoform in BAT (Forner *et al*, 2009; Geiger *et al*, 2013). siRNA-mediated knock-down of *Aralar1* was confirmed by qPCR in primary brown adipocytes (**Fig EV4D**). Similar to OGC1 KD cells, Aralar1 KD reversed the stimulatory effects of MPC inhibition on respiratory rates in non-stimulated and NE-stimulated brown adipocytes (**Figs 4F-G, EV4E)**. Furthermore, knock-down of *Aralar1* reversed the effects of MPC inhibition on NE-stimulated mitochondrial fat oxidation as revealed by the lack of an increase in etomoxir-sensitive respiration following UK5099 treatment (**Fig 4H**).

Next, we sought to determine whether the MASh is required for the increase in glutamine metabolism. To test this hypothesis, we analyzed the effect of UK5099 treatment on glutamate and aspartate abundance in Aralar1 KD as compared to scrambled siRNA treated brown adipocytes. Here we applied the same principle as in Figure 3D where the ratio of aspartate to glutamate is used as a measure of aspartate

aminotransferase activity and associated glutamine catabolism. Knock-down of *Aralar1* resulted in partial reversal of the increase in aspartate:glutamate ratio induced by MPC inhibition (**Fig 4I**). Partial reversal was expected, given that glutamine can provide glutamate and alpha-ketoglutarate independently of the MASh, through glutaminase and glutamate dehydrogenase. Thus, our data indicate that the **M**alate-**A**spartate **Sh**uttle is required to allow an increase in **E**nergy **E**xpenditure in **B**rown **A**dipocytes (MAShEEBA) via glutamate and fatty acid oxidation under MPC inhibition. Having mapped the metabolic reprogramming associated with the increased energy expenditure, we then asked which ATP-requiring processes were increased upon MPC inhibition.

MPC inhibition Induces ATP utilization by lipid cycling.

Intracellular handling of nutrients, particularly of fatty acids, is an ATP demanding process. Our data and other's demonstrated that when mitochondria do not have access to pyruvate, a cellular response elicits a switch to use fatty acids as an oxidative fuel in the mitochondria to synthesize ATP (Vacanti *et al*, 2014; Gray *et al*, 2015). Accordingly, in addition to the increase in mitochondrial fat oxidation induced by MPC inhibition, we find that UK5099 treatment increased ATP-synthesizing respiration both in NE-stimulated **(Fig. 2A, 3B)** and non-stimulated brown adipocytes in a dose-dependent manner (**Fig 5A-B**, **EV5D**). This was accompanied by an increase in mitochondrial proton leak in response to UK5099 treatment (**Fig 5A-B**), which may be the result of increased membrane potential associated with a shift to fatty acid oxidation and the engagement of complex II (Nicholls & Ferguson, 2013). Analysis of TMRE fluorescence intensity confirmed an increase in mitochondrial membrane potential in response to treatment with

UK5099 (**Fig EV5A-B**). To confirm that increase TMRE fluorescence is not due to increased cytosolic concentration of TMRE we show that TMRE fluorescence intensity in the nuclear area, which represents a non-mitochondrial TMRE level in the cell, is unchanged **(Fig EV5C)**.

We reasoned that if ATP demand is elevated by MPC inhibition, then UK5099 treatment should have no effect on mitochondrial respiration when cellular ATP demand is clamped, by controlling cytoplasmic ADP concentrations. To test this hypothesis, we clamped the ADP concentration by permeabilizing brown adipocytes and supplementing the assay buffer with 5 mM ADP. OCR was measured after concurrently providing all fuels (pyruvate, malate, palmitoyl-CoA and carnitine). UK5099 treatment did not change mitochondrial respiration in permeabilized cells when given all substrates and 5 mM ADP (**Fig 5C**). This observation strengthens the finding that increased mitochondrial respiration in intact brown adipocytes induced by MPC inhibition is mainly driven by increased ATP demand.

Brown and white adipocytes re-esterify free fatty acids that are produced by lipolysis, in a process termed glycerolipid and free fatty acid (GL/FFA) cycling or lipid cycling (**Fig 5D**) (Prentki & Madiraju, 2008; Hammond & Johnston, 1987; Gorin *et al*, 1969; Mottillo *et al*, 2014). This ATP-consuming process is inevitable in cells storing and mobilizing fatty acids. Indeed, lipid cycling contributes to the basal ATP demand and is a key mechanism for preventing toxicity caused by excessive levels of free fatty acids and glucose (Prentki & Madiraju, 2008; Mottillo *et al*, 2014). A metabolic signature of lipid cycling is the diversion of glycolytic intermediates towards glycerol-3-phosphate (G3P) production to support FFA re-esterification into triglycerides (Reshef *et al*, 2003). Since

MPC inhibition activated lipolysis and fatty acid oxidation (**Fig 1**), we hypothesized that increased lipid cycling could explain the increased ATP-demand observed upon UK5099 treatment in brown adipocytes. If this were the case, G3P/DHAP would be increased by MPC inhibition. Indeed, the G3P/DHAP ratio was increased in brown adipocytes treated with UK5099 (**Figs 5D-E),** via an increase in G3P, rather than a decrease in DHAP content (**Fig EV5E)**. We then reasoned that inhibition of lipolysis or lipid re-esterification should prevent UK5099-induced increase in ATP demand. Figure 5F shows that specific inhibition of adipose triglyceride lipase (ATGL) by Atglistatin, which impairs the first step of lipolysis, completely prevented the increase in basal and ATP-synthesizing respiration induced by MPC inhibition in non-stimulated brown adipocytes (**Fig 5F,G**). Remarkably, Atglistatin treatment had no significant effects on maximal (uncoupled) respiratory rates in intact brown adipocytes (**Fig EV5F**), underscoring the concept that increased ATP demand associated with lipolysis drives the increase in respiration induced by MPC inhibition.

Lipid cycling can involve the entire cycle from TAG synthesis to free fatty acid and glycerol, or be limited to shorter sub-cycles that involve break-down and regeneration of mono- and di-glycerides. Importantly, full or partial cycling are both ATP-demanding processes (Prentki & Madiraju, 2008). To assess the potential role of TAG synthesis in UK5099-mediated activation of lipid cycling, we blocked the last step of TAG synthesis catalyzed by diglyceride acyltransferase 1 and 2 (DGAT1/2) using pharmacological inhibitors (JNJ-DGAT1-A inhibitor (Qi *et al*, 2010) and PF-06424439). The UK5099-induced increases in respiration were insensitive to DGAT inhibition (**Figs 5H-I**). These results suggest that ATP-demand induced by MPC inhibition does not involve the last

step of TAG synthesis. We then blocked acyl-CoA synthetase (ACS) by using Triacsin C, thereby blocking a sub-cycle of lipid cycling (**Figure 5D**). The UK5099-induced increase in ATP-synthesizing respiration was highly sensitive to Triacsin C, reaching values close to vehicle treated cells (**Figs 5J-K**). In the absence of UK5099, Triacsin C reduced basal and ATP-synthesizing respiration in non-stimulated brown adipocytes, in agreement with previous studies showing that lipid esterification contributes to basal ATP demand in adipose tissue (Mottillo *et al*, 2014). We confirmed that Triacsin C and UK5099 treatment did not affect maximal (uncoupled) respiratory rates, strengthening that inhibition of ACS only decreases mitochondrial ATP-demand and does not affect mitochondrial fuel availability and respiratory function (**Fig EV5G**). Collectively, our data suggest that MPC inhibition increases ATP-demand and OCR in non-stimulated brown adipocytes by activating a sub-cycle of lipid cycling pathway.

DISCUSSION

Our study identified that inhibition of mitochondrial pyruvate transport is a novel mechanism to increase the energy demand and expenditure in non-stimulated brown adipocytes through the activation of lipid cycling (**Figure 6**). Non-stimulated brown adipocytes store most of their intracellular lipids as TAGs in lipid droplets, which are consumed upon adrenergic stimulation (Cannon & Nedergaard, 2004). Therefore, increasing fat oxidation in non-stimulated BAT, and potentially other types of adipose tissues, could be a promising way to reduce circulating fatty acids and shrink fat depots. Our data suggest that MPC inhibition increases lipolysis and fatty acid oxidation in both non-stimulated and NE-stimulated brown adipocytes. Fatty acid oxidation was assessed

by measuring [U-$^{13}C_{16}$] palmitate incorporation into TCA cycle metabolites and using the CPT1 inhibitor etomoxir in respirometry assays. As etomoxir has been reported to have off-target effects particularly at higher doses (Divakaruni *et al*, 2018), we confirmed that the dose of etomoxir used in this study does not affect the oxidation of substrates that are independent of CPT1 activity (**Fig EV1C**). Interestingly, a recent study showed that whole body MPC1 KO mice was embryonically lethal, unless the pregnant mice were fed a ketogenic diet (Vanderperre *et al*, 2016). Further evidence reinforced the shift towards fat oxidation in heterozygous MPC1 KO mice, which exhibit reduced body weight and increased expression of genes associated with lipolysis and fatty acid oxidation (Zou *et al*, 2018a). Additionally data in C2C12 cells and muscle specific MPC1 KO mice show increased fatty acid oxidation (Vacanti *et al*, 2014; Sharma *et al*, 2019). These observations agree with our results showing increased lipid droplet consumption and fatty acid oxidation in brown adipocytes upon MPC inhibition. Our data also indicate that MPC inhibition acutely increases fatty acid oxidation and therefore could be envisioned as a potential target for obesity and associated metabolic disorders by promoting fat oxidation in vivo. Recent studies demonstrated that genetic deletion of mice MPC in UCP1+ adipocytes improved insulin sensitivity and increased circulating ketones, consistent with our data showing increased fat oxidation in isolated brown adipocytes (Panic *et al*, 2019). It remains to be determined whether MPC inhibition can promote fat oxidation and lipid cycling in white adipocytes, which would be especially interesting considering that most depots of human adipose tissue are white or beige.

Multiple groups have demonstrated that modulation of MPC activity acts as a mitochondrial fuel preference switch in various tissues and conditions (Divakaruni *et al*,

2017; Gray *et al*, 2015; Vacanti *et al*, 2014; Zou *et al*, 2018a, 2018b; Schell *et al*, 2017; Yang *et al*, 2014b). However, in these studies, pharmacological inhibition, or genetic deletion of the MPC led to reduced or unchanged mitochondrial respiration. By contrast, in brown adipocytes MPC inhibition increased non-stimulated and adrenergically stimulated mitochondrial oxygen consumption. One possible reason that could explain this discrepancy is that the brown adipocyte is a cell type specialized to store and oxidize fat. Therefore, it is conceivable that brown adipocytes are more efficient for switching their fuel to fatty acids when mitochondrial pyruvate import is limited. Enhanced fatty acid oxidation is often associated with an increase in mitochondrial proton leak through UCP1 activation (Fedorenko *et al*, 2012). Surprisingly, we show that MPC inhibition indeed activated mitochondrial fatty acid oxidation coupled to ATP synthesis by oxidative phosphorylation. We find that UK5099 increases ATP-linked OCR even in brown adipocytes stimulated with NE, suggesting that MPC inhibition can increase fat oxidation to produce ATP in mitochondria in which UCP1 was not successfully activated. In this regard, UCP1 expression varies between different brown adipocytes, and even between different mitochondria inside the same cell (Wikstrom *et al*, 2014). Interestingly the effect of knock-down of MPC1, while being similar to effects of UK5099-treatment in the absence of NE, did not reproduce the same effect in NE-stimulated brown adipocytes. The difference between the effects of pharmacological and genetic interference on NE-induced energy expenditure may be attributed to differences in level of MPC inhibition between UK5099 and genetic knock-down of MPC1 or recruitment of compensatory mechanisms in MPC1 knock-down cells that are not induced upon 2 hours of UK5099 treatment.

We show that MPC in brown adipocytes increases energy expenditure through the activation of ATP-demanding lipid cycling. Using pharmacological inhibitors of various steps in TAG break-down or esterification we show that ATGL-dependent lipolysis and ACS-dependent fatty acid esterification are required for the increased energy demand induced by MPC inhibition (**Figs 5F-K**). Remarkably we find that inhibition of DGAT enzymes had no effect on energy demand under UK5099 treatment (**Figs 5H-I**). These data suggest that MPC inhibition activates a sub-cycle in the lipid cycling pathway which involves ACS-dependent esterification of lipids. Furthermore, our data suggest that the majority of the lipids used in the sub-cycle are from endogenous TAG stores that are released from LDs in an ATGL-dependent manner. However, it is conceivable that DGAT inhibition using pharmacological inhibitors was incomplete and therefore had no apparent effect on energy demand following MPC inhibition. It remains to be determined by which mechanism inhibition of the MPC stimulates lipolysis and lipid cycling. In this regard, ROS activate lipolysis in white adipocytes (Krawczyk *et al*, 2012) and blocking MPC decreases the synthesis of the ROS-scavenger glutathione, by diverting glutamine away from glutathione biosynthesis (Tompkins *et al*, 2019). Thus, it is a possibility that lipolysis and the concomitant lipid cycling are initiated by redox-signaling induced by MPC blockage.

Our data support that glycolytic intermediates are diverted towards lipid cycling, instead of downstream glycolysis to pyruvate and lactate, as G3P/DHAP ratio increased upon MPC inhibition (**Figs 5E and EV5B**). As opposed to increasing energy wasting by mitochondrial uncoupling, activation of lipid cycling would be a safer and more controlled way to increase energy wasting. Recent publications proposed UCP1-independent futile cycles as possible mechanisms to increase energy expenditure in adipose tissue (Deng

et al, 2018; Kazak *et al*, 2015; Ikeda *et al*, 2017; Mahdaviani *et al*, 2017). Future studies will determine whether lipid cycling can be activated by MPC inhibition in white and beige adipose tissue as well.

In addition to increased oxidation of fatty acids, our data indicate that glutamine supports energy expenditure induced by MPC inhibition, as previously shown in other tissues (Divakaruni *et al*, 2017; Vacanti *et al*, 2014; Yang *et al*, 2014b). Besides the increase in fatty acid oxidation and glutamine catabolism to provide oxaloacetate and TCA intermediates, we find that MPC inhibition in brown adipocytes requires the MASh carriers to increase mitochondrial respiration by transferring more NADH from the cytosol to the mitochondria. Furthermore our glutamine-tracing experiments suggest reductive carboxylation of glutamine, which could be a mechanism for brown adipocytes to sustain *de novo* lipogenesis despite reduced mitochondrial pyruvate import (Zhang *et al*, 2014; Yoo *et al*, 2008). Therefore, the identification that **MASh** supports **E**nergy **E**xpenditure in **B**rown **A**dipocytes (or MAShEEBA) represents a novel mechanism for regulation of energy expenditure in BAT. Wang et al. showed that acetyl-CoA derived from fatty acids can acetylate and thereby activate components of the MASh, which could be the mechanism by which MPC inhibition increases MASh flux (Wang *et al*, 2018). Intriguingly the only described posttranslational modification of the MPC is acetylation of MPC2, which was shown to have an inhibitory effect on MPC activity (Vadvalkar *et al*, 2017). The observation that acetylation has activating effects on the MASh, and inhibitory effects on the MPC might suggest a functional link between MASh activity and MPC activity. However, the functional role of MASh under physiological stimulation of non-shivering thermogenesis in BAT remains to be determined.

In conclusion, we identified a novel mechanism to activate futile lipid cycling and increase energy expenditure in brown adipocytes through inhibition of the MPC. Importantly, FDA-approved drugs such as thiazolidinediones (TZDs) were shown to target the MPC at clinically relevant concentrations (Divakaruni *et al*, 2013). Remarkably, TZDs were shown to promote glyceroneogenesis and lipid cycling through increased expression of glycerol kinase (GK) in human adipose tissue (Tan *et al*, 2003). However, this effect was a result of PPARgamma mediated activation of GK transcription, and therefore can likely not be attributed to TZDs effect on the MPC. Further work is required to assess the contribution of lipid cycling and the MASh in the beneficial effects of TZDs. Nevertheless, our data suggests that the MPC could be a safe target to increase energy expenditure in brown adipocytes and potentially improve whole body metabolic health in patients with obesity and cardiometabolic disorders linked to nutrient excess.

MATERIALS AND METHODS

Animals

Primary brown adipocytes were isolated from 4-5 weeks old wild-type male C57BL/6J mice (Jackson Laboratory, Bar Harbor, ME). Animals were fed standard chow (mouse diet 9F, PMI Nutrition International, Brentwood, MO) and maintained under controlled conditions (19–22^{o}C and a 14:10 hour light-dark cycle) until euthanasia by isofluorane, followed by cervical dislocation. All animal procedures were performed in accordance with the Guide for Care and Use of Laboratory Animals of the NIH and were approved by the ARC/IACUC of the University of California, Los Angeles.

Primary brown adipocyte culture

Primary brown adipocytes were isolated and cultured as described in detail [1]. In brief, BAT was dissected from interscapular, subscapular, and cervical regions of four male mice. Tissue was digested using Collagenase Type II (Worthington, Lakewood, NJ). Digested tissue was filtered through a 100 µm and 40 µm mesh and centrifuged. Cell pellet was re-suspended in brown adipocyte culture media (DMEM supplemented with 10 % newborn calf serum (Sigma-Aldrich, St. Louis, MO), 4 mM glutamine, 10 mM HEPES, 0.1 mg/mL sodium ascorbate, 100 U/mL penicillin, 100 µ/mL streptomycin) and plated in a 6-well plate. Cells were incubated in a 37°C, 8 % CO_2 incubator. 72 hours after isolation the cells were lifted using STEMPro Accutase (Thermo Fisher Scientific, Roskilde, Denmark), counted, and re-plated in final experimental vessel. 24 hours later media was changed to differentiation media (growth media supplemented with 1 µM rosiglitazone maleate (Sigma-Aldrich, St. Louis, MO) and 4 nM human insulin (Humulin R, Eli Lilly,

Indianapolis, IN). Cells were differentiated for 7 days and media was changed every other day.

Gene silencing

Adenoviral Transduction

On day 3 of differentiation, adipocytes were incubated with 1.5 µL/mL of adenoviral preparation (10^9 particles/ml) for 24 h in complete culture media containing 1 µg/mL polybrene (hexadimethrine bromide, Sigma-Aldrich, St. Louis, MO). Respirometry, metabolomics and gene expression were measured on day 7 of differentiation. Ad-mSLC25A11 and Ad-mKate2 shControl were generated and purchased from Welgen (Worcester, MA).

siRNA transfection

Undifferentiated pre-adipocytes were transfected with scramble RNA, MPC1 siRNA or Aralar1 (Slc25a12) siRNA using Lipofectamine 3000 reagent (Thermo Fisher Scientific, Roskilde, Denmark) according to manufacturer's protocol. In brief, culture media was removed from cells and cells were incubated with Opti-MEM media (Thermo Fisher Scientific, Roskilde, Denmark), Lipofectamine 3000 reagent and 100 nM scramble RNA or siRNA for 4 hours. Then DMEM with 1 % fetal bovine serum (Thermo Fisher Scientific, Roskilde, Denmark) was added to the cells and incubated overnight. The next day media was replaced with differentiation media. Respirometry, gene expression and protein expression were measured on day 7 of differentiation. The following siRNAs were used: ON-TARGETplus Non-targeting Pool (D-001810-10-05), ON-TARGETplus Mouse Mpc1

(55951) siRNA (L-040908-01-0005), and ON-TARGETplus Mouse Slc25a12 siRNA (L-064268-01-0005) from Dharmacon (Lafayette, CO)

Respirometry measurements

Respirometry in intact cells: Pre-treatments were performed in brown adipocyte culture media. The following compounds were used for pre-treatments: 50 nM - 20 µM UK5099 (Sigma-Aldrich, St. Louis, MO), 40 µM Atglistatin (Selleck Chemicals, Houston, TX), 200 µM – 1 mM aminooxyacetic acid (Sigma-Aldrich, St. Louis, MO), 5 µM Triacsin C (Sigma-Aldrich, St. Louis, MO), PF-06424439 (Sigma-Aldrich, St. Louis, MO). The JNJ-DGAT1-A inhibitor (Qi et al., 2010) was a generous gift from Janssen Research and Development LLC (Spring House, PA) and is available from MedKoo Biosciences Inc. Prior to respirometry measurements, culture media was replaced with respirometry media (Seahorse XF Base medium (Agilent Technologies, Santa Clara, CA) supplemented with 5 mM glucose and 3 mM glutamine and incubated for 30-45 minutes at 37°C (without CO_2). Where indicated, respirometry media was supplemented with 0.1 % fatty acid free bovine serum albumin (Sigma-Aldrich, St. Louis, MO). During this incubation period, the ports of the Seahorse cartridge were loaded with the compounds to be injected during the assay (50 µL/port) and the cartridge was calibrated. Oxygen consumption rates were measured using the Seahorse XF24-3 extracellular flux analyzer (Agilent Technologies, Santa Clara, CA). The following compounds were used for injections during the assay: 1 µM norepinephrine (Levophed), 4 µM oligomycin A (Calbiochem, San Diego, CA), 40 µM etomoxir (Sigma-Aldrich, St. Louis, MO), 4 µM antimycin A (Sigma-Aldrich, St. Louis, MO), 2 µM Carbonyl cyanide 4-(trifluoromethoxy)phenylhydrazone (FCCP;Sigma-Aldrich,

St. Louis, MO). After the assay, cells were fixed using 4 % paraformaldehyde (Thermo Fisher Scientific, Roskilde, Denmark). To normalize the data for possible differences in cell number, nuclei were stained with 1 µg/mL Hoechst 33342 (Thermo Fisher Scientific, Roskilde, Denmark) and nuclei were counted using the Operetta High-Content Imaging System (PerkinElmer, Waltham, MA).

Respirometry in permeabilized cells: Experiments were performed as previously described in detail (Mahdaviani *et al*, 2015). In brief, differentiated primary brown adipocytes were permeabilized using 5 nM XF PMP reagent (Agilent Technologies, Santa Clara, CA). Respirometry assay was performed in MAS buffer (660 mM mannitol, 210 mM sucrose, 30 mM KH2PO4, MgCl2, HEPES, EGTA, 1 mM GDP, 1% (w/v) fatty-acid free BSA). The following substrates were used: 5 mM pyruvate, 0.5 mM or 3 mM malate, 5 mM succinate, 2 µM rotenone, 0.1 mM palmitoyl-CoA, 0.5 mM carnitine, 0.1 mM palmitoyl-carnitine, 5 mM ADP. The following compounds were injected: 5 µM oligomycin, 8 µM antimycin a, 0.5 mM N,N,N',N'-Tetramethyl-p-phenylenediamine (TMPD), 1 mM ascorbic acid, 50 mM sodium azide. Oxygen consumption rates were measured using the Seahorse XF24-3 extracellular flux analyzer (Agilent Technologies, Santa Clara, CA).

Quantitative real time PCR

Samples from cells transduced with adenovirus or transfected with siRNA were collected on day 7 of differentiation. RNA was extracted using the Direct-zol RNA Miniprep Plus Kit ® (Zymo Research, Irvine, CA) following the manufacturer's instructions. A sample corresponding to 1 µg RNA from each sample was used to perform cDNA synthesis by the High-Capacity cDNA Reverse Transcription Kit ® (Applied Biosystems, Foster City,

CA). QPCR were performed using 0.4 ng/µL cDNA and 240 nM of each primer, whose sequences are listed in Table 1.

Western blot

Protein was isolated using RIPA lysis buffer (Santa Cruz Biotechnology, Dallas, TX) containing protease and phosphatase inhibitor cocktail (Thermo Fisher Scientific, Roskilde, Denmark), and protein concentration was determined using a BCA protein assay (Thermo Fisher Scientific, Roskilde, Denmark). Samples of 10-15 µg isolated protein were diluted in NuPAGE LDS Sample Buffer (Thermo Fisher Scientific, Roskilde, Denmark) containing β-mercaptoethanol (Thermo Fisher Scientific, Roskilde, Denmark), and incubated at 95°C for 5 min. Samples were then loaded into 4 %–12 % Bis-Tris precast gels (Thermo Fisher Scientific, Roskilde, Denmark) and electrophoresed, using NuPAGE MES SDS Running Buffer (Thermo Fisher Scientific, Roskilde, Denmark). Proteins were transferred to methanol-activated Immuno-Blot PVDF Membrane (Bio-Rad, Hercules, CA). Blots were incubated over-night with primary antibody diluted in PBST (phosphate buffered saline with 1 mL/L Tween-20/PBS) + 5 % BSA (Thermo Fisher Scientific, Roskilde, Denmark) at 4°C. The next day, blots were washed in PBST and incubated with fluorescent secondary antibodies, diluted in PBST+ 5 % BSA for 1 hour at room temperature. Proteins were detected using the following antibodies: anti-MPC1 (BRP44L Polyclonal Antibody, Thermo Fisher Scientific, Roskilde, Denmark), anti-MPC2 (MPC2 (D4I7G) Rabbit mAb, Cell Signaling, Danvers, MA), anti-β-Actin (Abcam, Cambridge, United Kingdom), anti-UCP1 (ab10983, Abcam, Cambridge, United Kingdom), anti-Vinculin (V9131, Sigma-Aldrich, St. Louis, MO), Goat anti-Rabbit IgG

secondary antibody DyLight 800 (Thermo Fisher Scientific, Roskilde, Denmark). Blots were imaged on the ChemiDoc MP imaging systmen (Bio-Rad Laboratories, Hercules, CA). Band densitometry was quantified using FIJI (ImageJ, NIH).

Fluorescence confocal microscopy

Super resolution live cell imaging was performed on a Zeiss LSM880 using a 63x Plan-Apochromat oil-immersion lens and AiryScan super-resolution detector with humidified 5 % CO_2 chamber on a temperature controlled stage (37°C). Cells were differentiated in glass-bottom confocal plates (Greiner Bio-One, Kremsmünster, Austria). For Lipid droplet imaging cells were incubated with 1 µM Bodipy 558/568 C12 (Thermo Fisher Scientific, Roskilde, Denmark) overnight. The day of imaging cells were stained with 200 nM mitotracker green (MTG) (Thermo Fisher Scientific, Roskilde, Denmark) for 1 h. MTG and Bodipy 558/568 C12 were removed before imaging and cells were imaged in regular culture media. MTG was excited with 488 nm laser and Bodipy 558/568 C12 was excited with 561 nm laser. For membrane potential measurements cells were incubated with 200 nM MTG and 15 nM Tetramethylrhodamine Ethyl Ester Perchlorate (TMRE) (Thermo Fisher Scientific, Roskilde, Denmark) for 1 h. MTG was washed out prior to imaging and cells were imaged in presence of TMRE in regular culture media. Image Analysis was performed in FIJI (ImageJ, NIH). Image contrast and brightness were not altered in any quantitative image analysis protocols. Brightness and contrast were equivalently modified in the different groups compared, to allow proper representative visualization of the effects revealed by unbiased quantitation.

Thin layer chromatography

Cells were seeded and differentiated in 6-well plate. On day 7 of differentiation, cells were incubated with 1 µM Bodipy 558/568 C12 and DMSO, 100 nM UK5099 or 1 µM norepinephrine for 4 h and 24 h. Thin layer chromatography of intra-cellular lipids and extra-cellular lipids was performed as previously described (Rambold *et al*, 2015) with minor modifications. Intra-cellular lipids and lipids from media were extracted in 500 µL chloroform. Chloroform was evaporated using the Genevac EZ-2 Plus Evaporating System (Genevac, Ipswich, United Kingdom). Lipids were then dissolved in 15 µL Chloroform and 1 µL was spotted on a TLC plate (Silica gel on TLC Al foils, Sigma-Aldrich, St. Louis, MO). Lipids were resolved based on polarity in a developer solution containing ethylacetate and cyclohexane in a 2.5:1 ratio. TLC plates were imaged on the ChemiDoc MP imaging system (Bio-Rad Laboratories, Hercules, CA). Band densitometry was quantified using FIJI (ImageJ, NIH).

Metabolite tracing

For metabolomics and stable isotope tracing, cells were cultured and differentiated in 6-well plates using BAT differentiation media. On day 7 of differentiation cells were washed once and treated with 10 µM UK5099 or DMSO for 24 h in DMEM supplemented with phenol red, 10 mM glucose, 2 mM glutamine, and 10% NCS. For palmitate tracing experiments NCS was delipidated using fumed silica (Sigma-Aldrich, St. Louis, MO), and 200 µM [U-$^{13}C_{16}$] palmitate (Cambridge Isotope Laboratories, Tewksbury, MA) was added to the media, with unlabeled palmitate added to matched controls. Palmitate was added at a 4:1 palmitate:BSA complex. For glutamine tracing experiments, unlabeled glutamine

in the media was replaced with 2 mM [U-$^{13}C_5$] glutamine (Cambridge Isotope Laboratories, Tewksbury, MA). Metabolite extraction and GC/MS was performed as previously described in detail (Vacanti *et al*, 2014).

G3P and DHAP measurements

G3P and DHAP were measured using fluorimetric and colorimetric kits available from Sigma-Aldrich (MAK207 and MAK275, respectively). After differentiation in 6-well plates, cells were treated with DMSO (vehicle), 100 nM UK5099 or 1 µM Norepinephrine for 24 hours. Then, cells were washed with PBS and 60 µL of the respective assay buffer were added to each well. The suspension was centrifuged for 2,000 x g for 1 min and 10 µL of supernatant were used to measure G3P and DHAP according to the manufacturer instructions. For normalization purposes, 2 µL were used to measure protein concentration by a BCA protein assay kit (Thermo Fisher Scientific, Roskilde, Denmark).

Statistical analyses

Data were presented as mean ± SEM for all conditions. Comparisons between groups were done by one-way ANOVA with Tukey's or Holm Sidak's test for pair-wise multiple comparisons. When appropriate two-way ANOVA with Tukey's multiple comparisons test was employed. Pairwise comparisons were done by two-tailed Student's t-test. Differences of $p<0.05$ were considered to be significant. All graphs and statistical analyses were performed using GraphPad Prism 8 for Windows (GraphPad Software, San Diego, CA).

FIGURES

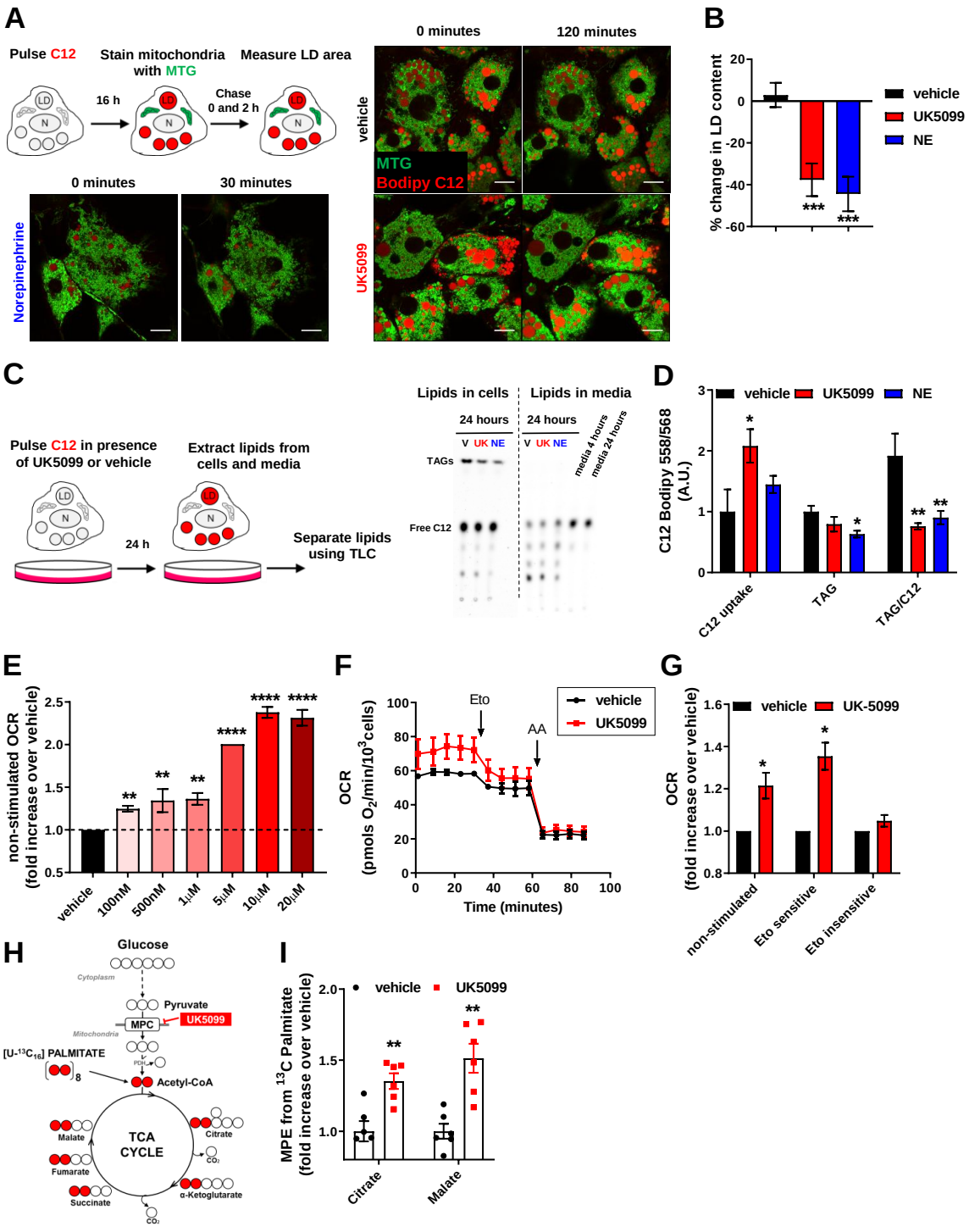

Inhibition of the mitochondrial pyruvate carrier increases energy expenditure fueled by fatty acid oxidation. (A,B) Effect of MPC inhibition on cellular lipid droplet

content. **(A)** Live-cell super-resolution confocal imaging of primary brown adipocytes pre-stained overnight with the fatty acid tracer BODIPY C12 558/568 (Bodipy C12, red). Cells were stained with mitotracker green (MTG, green) prior to imaging. Cells were imaged before and 120 minutes after treatment with either vehicle (DMSO) or 100 nM UK5099. As a positive control, cells were imaged 30 min after treatment with 1 µM norepinephrine. LD, lipid droplet; N, nucleus. Scale bar=10 µm. **(B)** Quantification of changes in lipid droplet cross-sectional area with indicated treatments from images shown in (A). Data are represented as percentage change in LD area at time=120 min compared to time=0 min. Data represent n=23-34 cells from 3 individual experiments. *** $p < 0.0001$ by ANOVA, relative to vehicle.

(C,D) Effect of MPC inhibition on fatty acid uptake and incorporation into triacylglycerides (TAGs) **(C)** Representative thin-layer chromatography (TLC) plate of lipids extracted from primary brown adipocytes and cell culture media. Cells were incubated with Bodipy C12 in presence of vehicle (V), 100 nM UK5099 (UK) or 1 µM norepinephrine (NE) for 24 h and triacylglyceride (TAG) synthesis (Lipids in cells) and fatty acid uptake (Lipids in media) were detected. The relative polarity of the lipid species determines the motility, with nonpolar TAG migrating the furthest. **(D)** Quantification of C12 uptake from media, TAG in cells and TAG per amount of free fatty acid uptake shown in (C), n=5 individual experiments. Note that UK5099 treatment decreases the amount of synthesized TAG per free fatty acid uptake, similarly to NE. * $p < 0.05$, ** $p < 0.01$ by ANOVA, relative to vehicle.

(E-G) Effect of UK5099 treatment on cellular energy expenditure. Fully differentiated primary brown adipocytes were pre-treated with vehicle (DMSO) or UK5099 at indicated concentrations for 2 h. Oxygen consumption rates (OCR) were measured in respirometry

media supplemented with 5 mM glucose and 3 mM glutamine in the presence of vehicle or UK-5099. **(E)** Quantification of non-stimulated OCR from n=3-7 individual experiments. Data were normalized to vehicle for each individual experiment. Note that UK5099 increases OCR in non-stimulated brown adipocytes. ** $p < 0.01$, **** $p < 0.0001$ by ANOVA, relative to vehicle. **(F)** Brown adipocytes were treated with 100 nM UK5099 or vehicle. Etomoxir (Eto; 40 µM) and antimycin A (AA; 4 µM) were injected where indicated. Representative OCR traces averaging 6 technical replicates. **(G)** Quantification of non-stimulated OCR, etomoxir sensitive, and etomoxir insensitive OCR from n=4 individual experiments. Data were normalized to vehicle for each individual experiment. * $p < 0.05$ compared to vehicle by Student t test.

(H,I) Effect of MPC inhibition on adipocyte fuel preference towards fatty acid. **(H)** Schematic representation of metabolite tracing using [U-$^{13}C_{16}$] palmitate. **(I)** [U-$^{13}C_{16}$] palmitate tracing in fully differentiated primary brown adipocytes treated with 5 µM UK5099 or vehicle for 24 h. Data shows mole percent enrichment (MPE) of isotope labeled substrate into respective metabolite. Data were normalized to vehicle for each individual replicate. n=6 technical replicates from 2 individual experiments. ** $p < 0.01$ compared to vehicle by Student t test.

Data information: All data are presented as mean ± SEM.

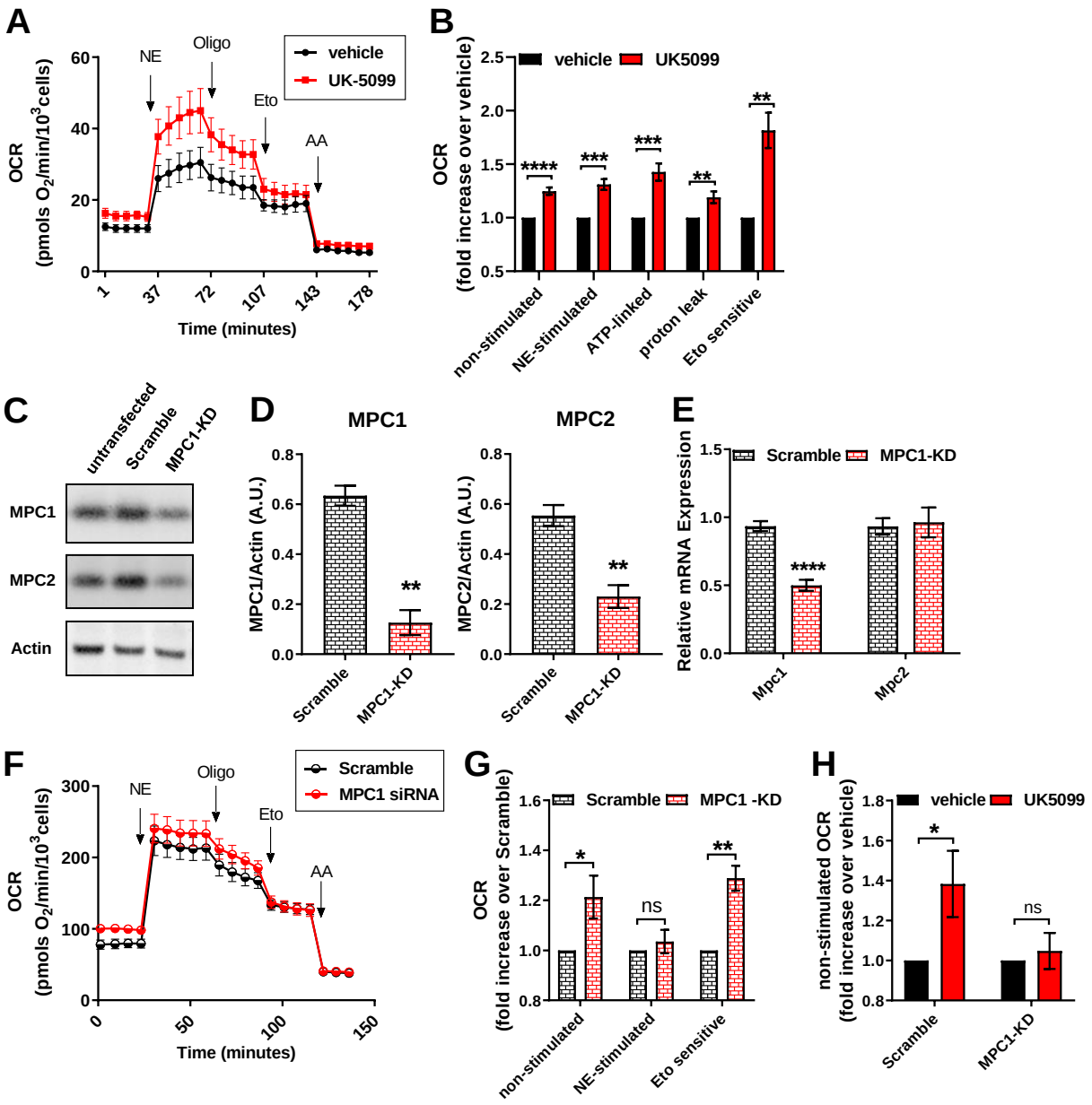

Figure 2: MPC1 inhibition stimulates mitochondrial respiration coupled to ATP synthesis in brown adipocytes.

(A,B) Effect of UK5099 treatment on norepinephrine-stimulated energy expenditure. Fully differentiated primary brown adipocytes were pre-treated with vehicle (DMSO) or 100 nM UK5099 for 2 h. OCR were measured in respirometry media supplemented with 5 mM glucose and 3 mM glutamine in the presence of vehicle or UK5099. Norepinephrine (NE;

1 µM), oligomycin A (Oligo; 4 µM), etomoxir (Eto; 40 µM) and antimycin A (AA; 4 µM) were injected where indicated. **(A)** Representative OCR traces averaging 4 technical replicates. **(B)** Quantification of non-stimulated OCR, NE-stimulated OCR, ATP-linked OCR, mitochondrial proton leak and Eto-sensitive OCR as shown in (A) from n=9 individual experiments. The effects of UK5099 treatment were normalized to vehicle for each experiment. ** $p < 0.01$, *** $p < 0.001$, **** $p < 0.0001$ compared to vehicle by Student´s t test.

(C-H) Primary brown adipocytes were transfected with MPC1 siRNA (MPC1 KD) or Scramble RNA (Scramble). **(C)** Representative Western Blot analysis of MPC1, MPC2 and actin. **(D)** Quantification of MPC1 and MPC2 expression normalized to actin from Western Blots in (C) from n=3 individual experiments. ** $p < 0.01$ compared to Scramble by Students t test. **(E)** mRNA levels of MPC1 and MPC2 from n=3 individual experiments. **** $p < 0.0001$ compared to Scramble by Student´s t-test. **(F)** Representative OCR traces of differentiated primary brown adipocytes averaging 6 technical replicates. OCR were measured in respirometry media supplemented with 5 mM glucose and 3 mM glutamine. Norepinephrine (NE; 1 µM), oligomycin A (Oligo; 4 µM), etomoxir (Eto; 40 µM) and antimycin A (AA; 4 µM) were injected where indicated. **(G)** Quantification of basal, NE-stimulated and Eto-sensitive OCR as shown in (F) from n=7 individual experiments. Data were normalized to Scramble RNA for each individual experiment. ns $p>0.05$, * $p < 0.05$, ** $p < 0.01$ compared to Scramble by Student´s t test. **(H)** Quantification of basal OCR in response to 100 nM UK5099 treatment in Scramble RNA of MPC1 siRNA transfected cells from n=5 individual experiments. Data were normalized to vehicle for each experiment. Note that UK5099 capacity to increase OCR in non-stimulated brown

adipocytes is absent in cells where MPC1 is downregulated. ns p>0.05, * p < 0.05 compared to vehicle by Student´s t test.

Data information: All data are presented as mean ± SEM.

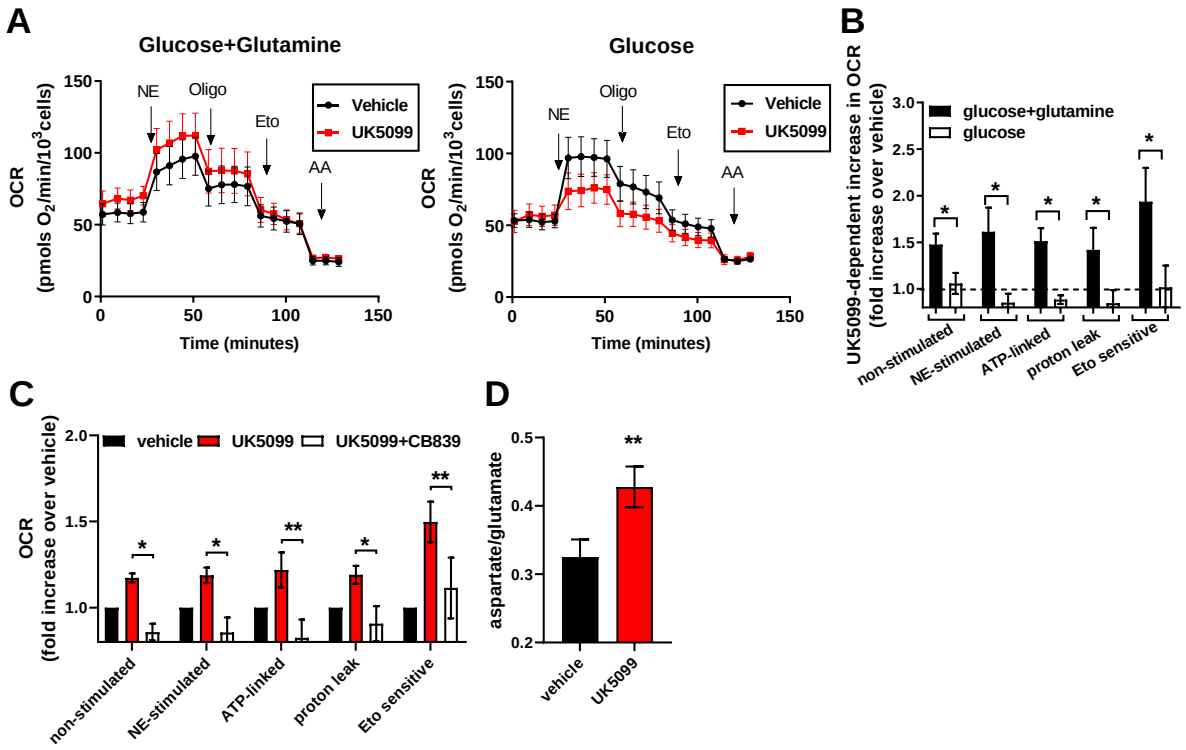

Figure 3: Glutamine metabolism is required for increased energy expenditure induced by MPC inhibition.

(A,B) Requirement for glutamine in UK5099-induced energy expenditure. Primary brown adipocytes were pre-treated with vehicle (DMSO) or 100 nM UK5099 for 2 h. OCR were measured in presence of either 5 mM glucose and 3 mM glutamine or 5 mM glucose alone. Norepinephrine (NE; 1 µM), oligomycin A (Oligo; 4 µM), etomoxir (Eto; 40 µM) and antimycin A (AA; 4 µM) were injected where indicated. **(A)** Representative OCR traces averaging 6 technical replicates. **(B)** Quantification of non-stimulated OCR, NE-stimulated OCR, ATP-linked OCR, mitochondrial proton leak and etomoxir-sensitive OCR

after vehicle or UK5099 treatment as shown in (A) from n=4 individual experiments. Data were normalized to vehicle for each experiment. Note that UK5099 treatment increased OCR only when cells were assayed in the presence of both glucose and glutamine. * $p < 0.05$, compared to vehicle by Student´s t test.

(C) Effect of glutaminase inhibitor on UK5099-induced energy expenditure. Primary brown adipocytes were pre-treated with either vehicle (DMSO), 100 nM UK5099, or 100 nM UK5099 + 2.5 µM CB839 for 2 h. OCR were measured in respirometry media supplemented with 5 mM glucose and 3 mM glutamine in the presence of vehicle, UK5099 or UK5099 + CB839 from n=5 individual experiments. Data were normalized to vehicle for each experiment. * $p < 0.05$, ** $p < 0.01$ by ANOVA.

(D) Effect of MPC inhibition on glutamate/aspartate ratio measurement. Glutamate/aspartate ratio was quantified using GC-MS as a measure of glutamine catabolism. Primary brown adipocytes were treated for 24 h with vehicle (DMSO) or 10 µM UK5099 from n=6 individual experiments. ** $p < 0.01$, compared to vehicle by Student´s t test.

Data information: All data are presented as mean ± SEM.

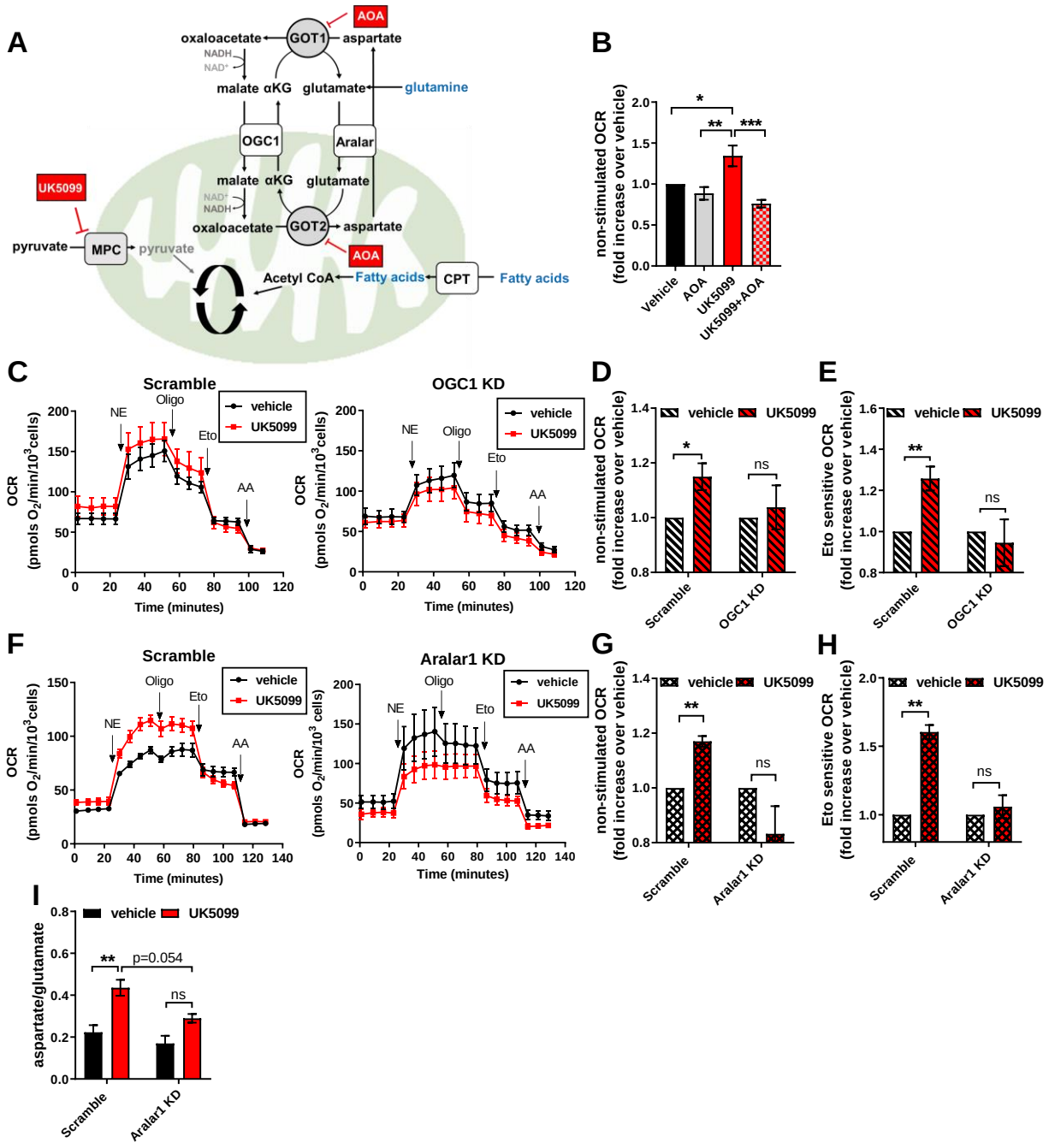

Figure 4: The malate-aspartate shuttle supports the increase of both glutamine and fatty acid metabolism induced by MPC inhibition.

(A) Schematic representation of proposed mechanism by which MPC inhibition engages the malate-aspartate shuttle (MASh). GOT1/2, glutamic-oxaloacetic transaminase; OGC1, oxoglutarate carrier 1; Aralar, mitochondrial aspartate-glutamate carrier; CPT,

Carnitine Palmitoyltransferase. The coordinated work of OGC1 and Aralar provide a mechanism to allow fatty acid oxidation in the absence of pyruvate. Fatty acid oxidation generates acetyl-CoA which condenses with oxaloacetate to generate citrate. In the absence of pyruvate, oxaloacetate can be generated by glutamine metabolism.

(B) Effect of transaminase inhibition on UK5099-induced energy expenditure. Brown adipocytes were pre-treated with vehicle (DMSO), 50-100 nM UK5099, 1 mM aminooxyacetic acid (AOA), or a combination of UK5099 and AOA for 2 h. OCR were measured in respirometry media supplemented with 5 mM glucose and 3 mM glutamine in the presence of the tested compounds. Data show quantification of non-stimulated OCR from n=5 individual experiments. Data were normalized to vehicle for each experiment. * $p < 0.05$, ** $p < 0.01$, *** $p < 0.001$ by ANOVA.

(C-E) Effect OGC1 downregulation on UK5099-induced energy expenditure. Primary brown adipocytes were transduced with Scramble RNA (Scramble) or shOGC1 (OGC1 KD) adenovirus. Cells were pre-treated for 2 h with vehicle (DMSO) or 100 nM UK5099 before OCR measurements. OCR were measured in respirometry media supplemented with 5 mM glucose and 3 mM glutamine in the presence of vehicle or UK5099. Norepinephrine (NE; 1 µM,) oligomycin A (Oligo; 4 µM), etomoxir (Eto; 40 µM) and antimycin A (AA; 4 µM) were injected where indicated. **(C)** Representative OCR traces averaging 4 technical replicates. **(D)** Quantification of non-stimulated OCR as measured in (C) from n=6 individual experiments. Data were normalized to vehicle for each experiment. ns $p>0.05$, * $p < 0.05$ compared to vehicle by Student´s t test. **(E)** Quantification of Eto-sensitive OCR as measured in (C) from n=6 individual experiments.

Data were normalized to vehicle for each experiment. ns p>0.05, ** p < 0.01 compared to vehicle by Student´s t test.

(**F-H**) Effect of Aralar1 downregulation on UK5099-induced energy expenditure. Primary brown adipocytes were transfected with Scramble RNA (Scramble) or siRNA for Aralar1 (Aralar1 KD). Cells were pre-treated for 2 h with vehicle (DMSO) or 100 nM UK5099 before OCR measurements. OCR were measured in respirometry media supplemented with 5 mM glucose and 3 mM glutamine in the presence of vehicle or UK5099. Norepinephrine (NE; 1 µM), oligomycin a (Oligo; 4 µM), etomoxir (Eto; 40 µM) and antimycin a (AA; 4 µM) were injected where indicated. **(F)** Representative OCR traces averaging 4 technical replicates. **(G)** Quantification of non-stimulated OCR as measured in (G) from n=4 individual experiments. Data were normalized to vehicle for each experiment. ns p>0.05, ** p < 0.01 compared to vehicle by Student´s t test. **(H)** Quantification of Eto-sensitive OCR as measured in (F) from n=4 individual experiments. Data were normalized to vehicle for each experiment. ns p>0.05, ** p < 0.01 compared to vehicle by Student´s t test.

(**I**) Brown adipocytes transfected with Scramble RNA or Aralar1 siRNA were treated for 24 hours with vehicle (DMSO) or 10 µM UK5099. Data shows quantification of the ratio of aspartate to glutamate abundance as measured by GC-MS from n=3 individual experiments. ns p>0.05, ** p < 0.01 by ANOVA. Note that both carriers of malate-aspartate shuttle, OGC1 and Aralar1, are required for UK5099-induced energy expenditure.

Data information: All data are presented as mean ± SEM.

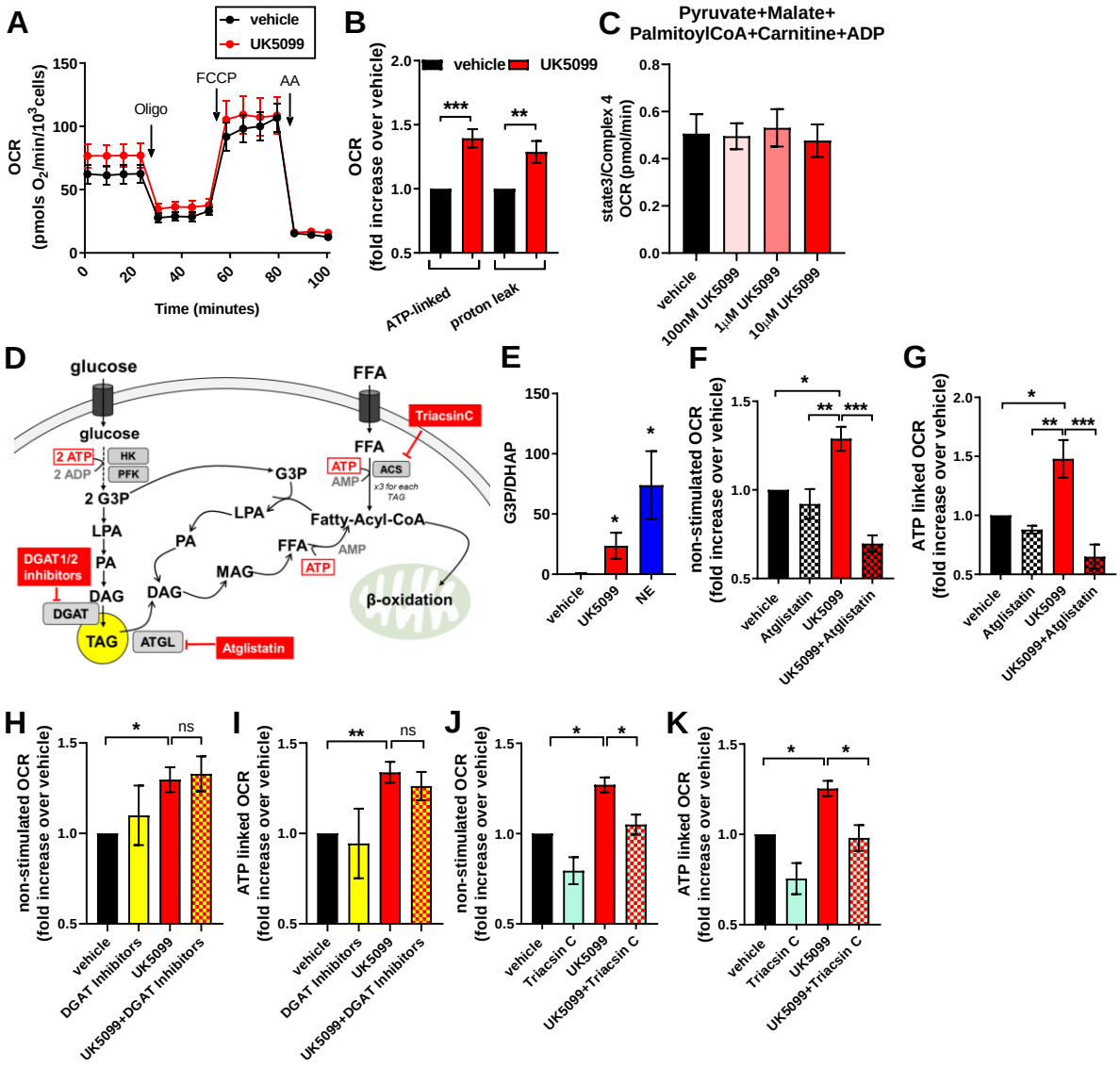

Figure 5: MPC inhibition induces ATP utilization by lipid cycling.

(A,B) Effect of UK5099 on energy expenditure contributed by ATP demand and by mitochondrial proton leak in non-stimulated brown adipocytes. Primary brown adipocytes were pre-treated with vehicle (DMSO) or 100 nM UK5099 for 2 hours. OCR were measured in respirometry media supplemented with 5 mM glucose and 3 mM glutamine in the presence of vehicle or UK5099. Oligomycin A (Oligo; 4 μM), mitochondrial uncoupler FCCP (2 μM) and antimycin A (AA; 4 μM) were injected where indicated. **(A)**

Representative OCR traces averaging 6 technical replicates. **(B)** Quantification of mitochondrial proton leak and ATP-linked OCR (oligomycin sensitive) as measured in (A) from n=9 individual experiments. Data were normalized to vehicle for each individual experiment. ** $p < 0.01$ ***, $p < 0.001$ compared to vehicle by Student´s t test.

(C) To determine the contribution of ATP demand to increased energy expenditure under UK5099 cells were permeabilized and cytosolic ADP concentrations were clamped. OCR were measured in the presence of 5 mM pyruvate, 3 mM malate, 0.1 mM palmitoyl-CoA, 0.5 mM carnitine and 5 mM ADP. Cells were treated with either 100 nM, 1 µM or 10 µM UK5099. Data shows maximal state 3 OCR normalized to maximal complex 4 activity from n=3 individual experiments. Note that when ATP demand is clamped, UK5099 had no effect on energy expenditure.

(D) Schematic representation of lipid cycling. HK, hexokinase; PFK, phosphofructokinase; ATGL, adipose triglyceride lipase; ACS, Acyl-CoA synthetase; TAG, triacylglyceride; DAG, diacylglyceride; MAG, monoacylglyceride; LPA, lysophosphatidic acid; FFA, free fatty acid; G3P, glycerol-3-phosphate

(E) Effect of MPC inhibition on glycerol 3-phosphate (G3P) and dihydroxyacetone phosphate (DHAP) generation. G3P/DHAP is used as a measure of acylglycerol synthesis. Brown adipocytes were treated with either vehicle, 100 nM UK5099 or 1 µM norepinephrine (NE) for 24 h from n=4 individual experiments. * $p < 0.05$ by ANOVA, relative to vehicle.

(F,G) Contribution of lipolysis to UK5099 induced energy demand. Primary brown adipocytes were pre-treated with either vehicle (DMSO), 100 nM UK5099, 40 µM Atglistatin or a combination of Atglistatin with UK5099 for 2 h. OCR were measured in

respirometry media supplemented with 5 mM glucose and 3 mM glutamine in the presence of vehicle, UK5099, or Atglistatin. **(F)** Quantification of non-stimulated OCR from n=4 individual experiments. * $p < 0.05$, ** $p < 0.01$, *** $p < 0.001$ by ANOVA. **(G)** Quantification of ATP-linked respiration from n=4 individual experiments. Data were normalized to vehicle for each individual experiment. * $p < 0.05$, ** $p < 0.01$, *** $p < 0.001$ by ANOVA.

(H,I) Contribution of TAG synthesis to UK5099 induced energy demand. Primary brown adipocytes were pre-treated with either vehicle (DMSO), 100 nM UK5099, 1 µM DGAT1 and 1 µM DGAT2 or a combination of DGAT1/2 inhibitors with UK5099 for 2 h. OCR were measured in respirometry media supplemented with 5 mM glucose and 3 mM glutamine in the presence of vehicle, UK5099, DGAT1/2 inhibitors, or UK5099 + DGAT1/2 inhibitors. **(H)** Quantification of non-stimulated OCR from n=6 individual experiments. Data were normalized to vehicle for each individual experiment. ns $p>0.05$, * $p < 0.05$ by ANOVA. **(I)** Quantification of ATP-linked OCR from n=6 individual experiments. Data were normalized to vehicle for each individual experiment. ns $p>0.05$, ** $p < 0.01$ by ANOVA.

(J,K) Contribution of ACS to UK5099 induced energy demand. Primary brown adipocytes were pre-treated with either vehicle (DMSO), 100 nM UK5099, 5 µM Triacsin C or a combination of 5 µM Triacsin C with UK5099 for 2 h. OCR were measured in respirometry media supplemented with 5 mM glucose and 3 mM glutamine in the presence of vehicle, UK5099, Triacsin C, or UK5099 + Triacsin C.

(J) Quantification of non-stimulated OCR from n=4 individual experiments. Data were normalized to vehicle for each individual experiment. * $p < 0.05$ by ANOVA.

(K) Quantification of ATP-linked OCR from n=4 individual experiments. Data were normalized to vehicle for each individual experiment. * $p < 0.05$ by ANOVA. Note that MPC-inhibition induced energy demand requires lipolysis and ACS dependent fatty acid activation, but not DGAT-dependent TAG synthesis, suggesting the activation of a sub-cycle in lipid cycling pathway.

Data information: All data are presented as mean ± SEM.

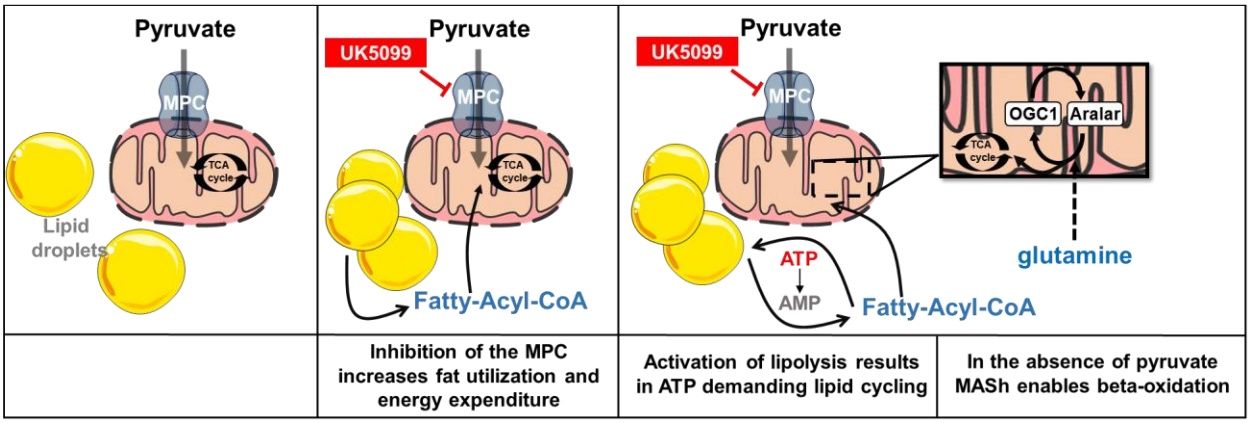

Figure 6: Proposed mechanism by which MPC inhibition induces lipid cycling and and the activation of the malate-aspartate shuttle.

Inhibition of mitochondrial pyruvate import in brown adipocytes results in the induction of lipolysis, a shift towards fatty acid utilization and an increase in energy expenditure. The increase in energy expenditure mediated by the addition of energy demand contributed by the activation of lipid cycling, involving a recurrent cycle of fatty acid release and re-esterification. To support fatty acid oxidation in the absence of pyruvate import the TCA cycle relies on carbons from glutamine and the activation of the malate-aspartate shuttle. Thus blocking mitochondrial pyruvate import can promote an increase in energy wasting even in the absence of adrenergic stimulation. LD, lipid droplet; MPC, mitochondrial pyruvate carrier; CPT1, Carnitine Palmitoyltransferase1; ATP, adenosine triphosphate;

AMP, adenosine monophosphate; OGC1, oxoglutarate carrier 1; Aralar, mitochondrial aspartate-glutamate carrier.

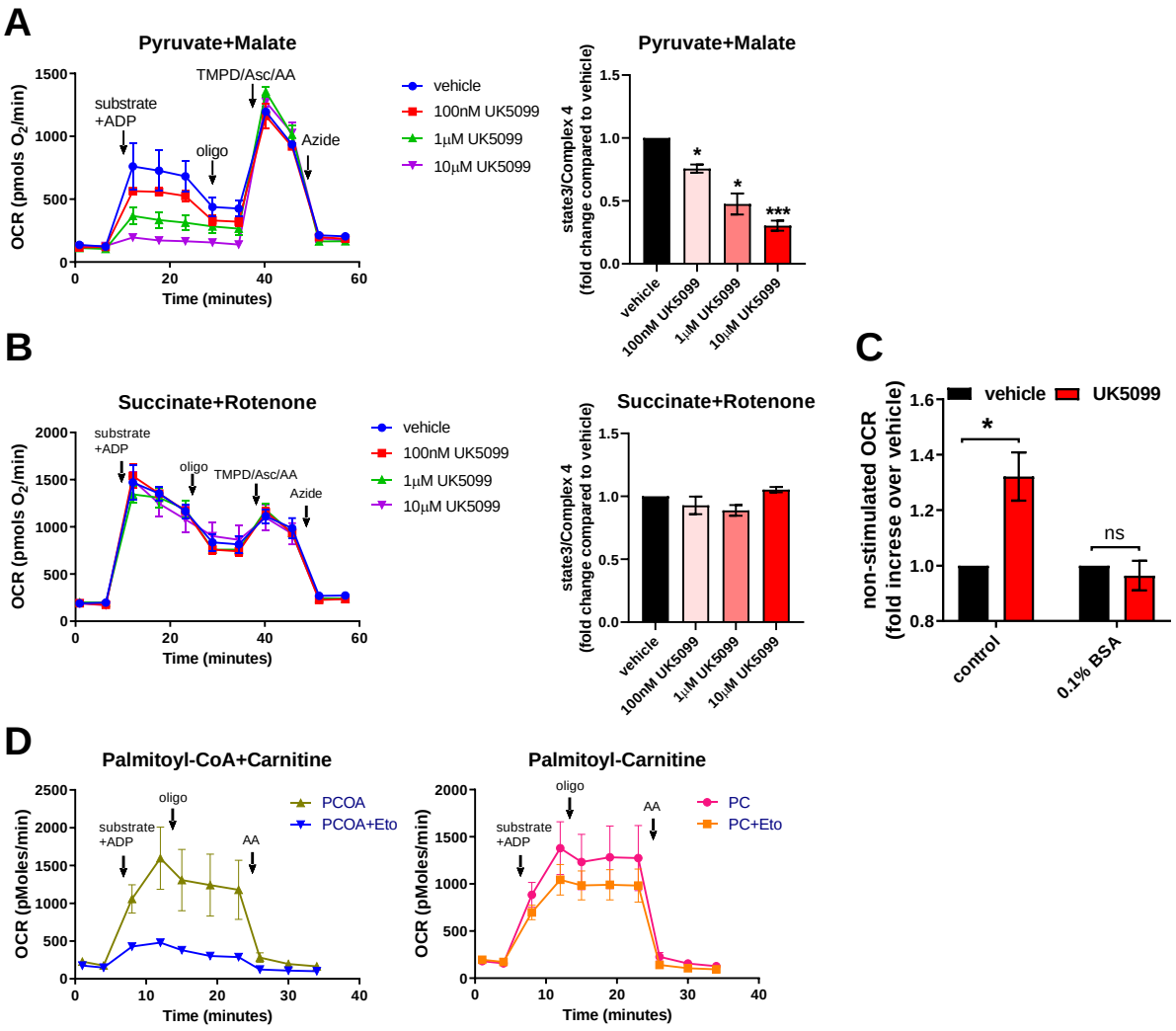

Figure EV1: Assessment of respiratory rates in permeabilized adipocytes. (A,B) Effect of MPC inhibitor UK5099 on respirometry in permeabilized brown adipocytes **(A)** OCR of permeabilized cells were measured in presence of 5 mM pyruvate, 0.5 mM malate and 5 mM ADP as substrates and treated with vehicle (DMSO) or indicted concentrations of UK5099. Chart on the left shows representative OCR traces averaging 3 technical replicates. Pyruvate and malate (substrate) + ADP, oligomycin a (Oligo; 4 μM), TMPD

(0.5 mM) + ascorbic acid (1 mM) + antimycin A (4 µM) (TMPD/Asc/AA) and sodium azide (50 mM, Azide) were injected where indicated. Bar-graph shows quantification of state 3 OCR normalized to complex 4 activity (measured as maximal TMPD+Ascorbate driven OCR). Data were normalized to vehicle for each individual experiment (n=4 individual experiments). Note that UK5099 dose-dependently reduced state3/complex 4 OCR. * $p < 0.05$, *** $p < 0.001$ by ANOVA **(B)** OCR of permeabilized primary brown adipocytes were measured in presence of 5 mM succinate, 2 µM rotenone and 5 mM ADP as substrates and treated with vehicle (DMSO) or indicted concentrations of UK5099. Chart on the left shows representative OCR traces averaging 3 technical replicates. Succinate and rotenone (substrate) + ADP, oligomycin a (Oligo; 4 µM), TMPD (0.5 mM) + ascorbic acid (1 mM) + antimycin A (4 µM) (TMPD/Asc/AA) and sodium azide (50 mM, Azide) were injected where indicated. Bar-graph shows quantification of state 3 OCR normalized to complex 4 activity (measured as maximal TMPD+Ascorbate driven OCR). Data were normalized to vehicle for each individual experiment (n=3 individual experiments).

(C) Brown adipocytes were pre-treated with vehicle (DMSO) or 100 nM UK5099 for 2 h prior to OCR measurements. OCR were measured in Seahorse base media with glucose and glutamine (control) or supplemented with 0.1% fatty acid free bovine serum albumin (BSA) where indicated. Quantification of non-stimulated OCR of brown adipocytes from n=3-7 individual experiments. Data were normalized to vehicle for each individual experiment. ns $p>0.05$, * $p < 0.05$ compared to vehicle by Student´s t test.

(D) Effect of CPT1 inhibitor Etomoxir on respirometry in permeabilized brown adipocytes OCR of permeabilized cells were measured in the presence of 0.1 mM palmitoyl-CoA+ 0.5 mM carnitine (PCOA) , a substrate that is dependent on CPT1, or in the presence of

0.1 mM palmitoyl-carnitine (PC) a substrate that does not require CPT1 activity. Substrate+ADP, oligomycin a (Oligo; 4 µM) and antimycin A (4 µM) were injected where indicated. Representative OCR traces averaging 3 technical replicates. Note that etomoxir (Eto) only inhibits OCR fueled by palmitoyl-CoA, a substrate that is dependent on CPT1 activity.

Data information: All data are presented as mean ± SEM.

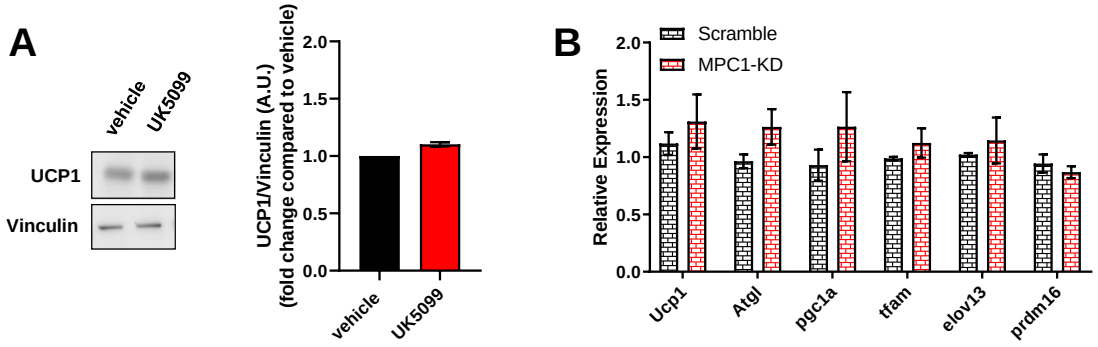

Figure EV2: Pharmacological or genetic blockage of the MPC does not affect brown adipocyte differentiation.

(A) Primary brown adipocytes were treated with 100 nM UK5099 or vehicle (DMSO) for 4 hours. Data shows representative Western Blot for UCP1 and Vinculin, and quantification of UCP1 normalized to Vinculin from n=3 individual experiments.

(B) mRNA levels of UCP1, Atgl, Pgc1alpha, Tfam, Elov13 and Prdm16 brown adipocytes transfected with scramble RNA (Scramble) or MPC1 siRNA (MPC1-KD) from n=3 individual experiments. mRNA levels were normalized to 36B4.

Data information: All data are presented as mean ± SEM.

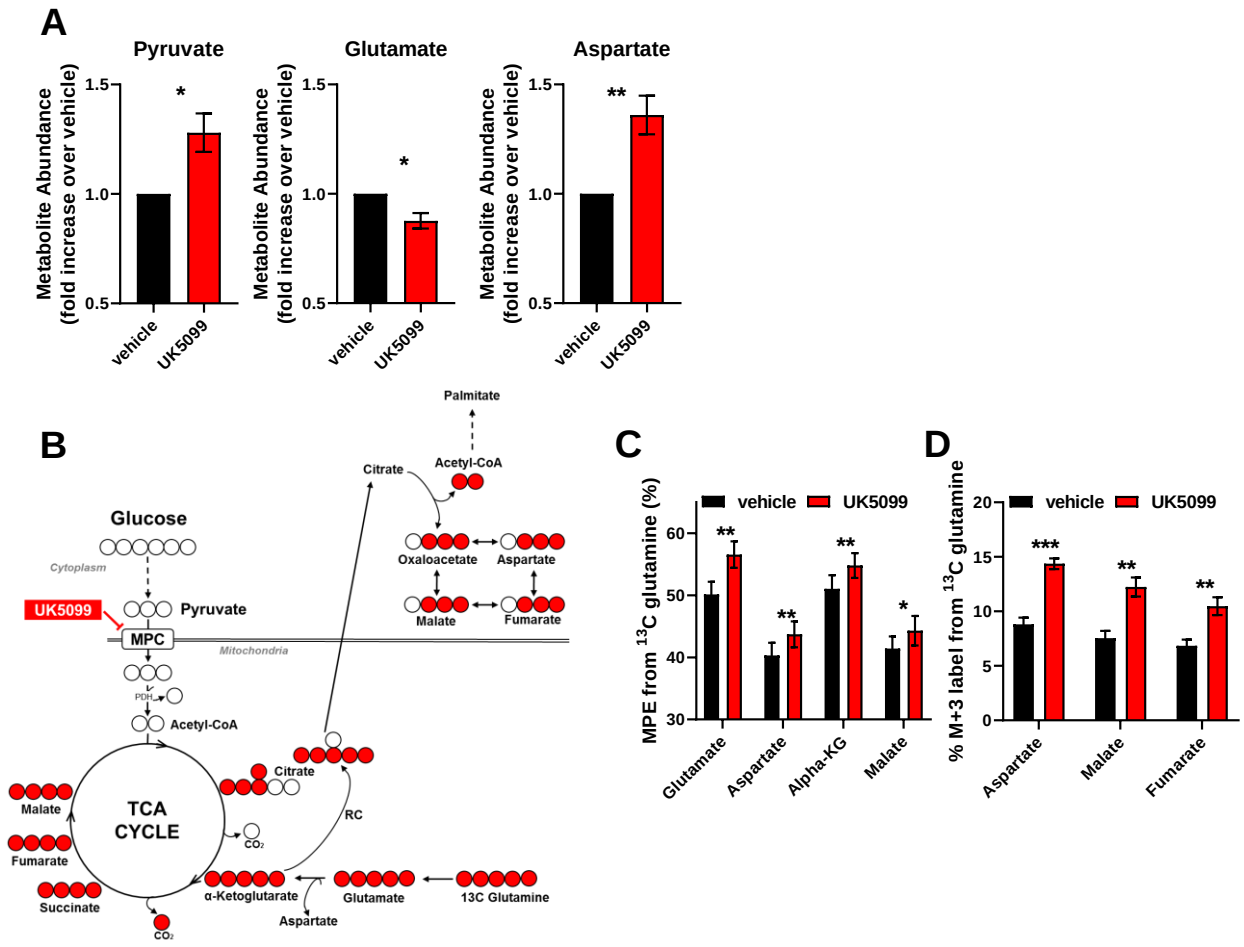

Figure EV3: Effects of UK5099 treatment on cellular metabolites

(A) Effect of MPC inhibition on polar metabolite abundance. Primary brown adipocytes were treated for 24 h with vehicle (DMSO) or 10 µM UK5099. Data shows total metabolite abundance measured by GC-MS from n=6 individual experiments. Data were normalized to vehicle for each individual experiment. * $p < 0.05$, ** $p < 0.01$ compared to vehicle by Student´s t test.

(B,C) Effect of MPC inhibition on glutamine catabolism and contribution to TCA cycle metabolites. **(B)** Schematic representation of metabolite tracing using [U-$^{13}C_5$] glutamine. **(C)** [U-$^{13}C_5$] glutamine tracing in primary brown adipocytes treated with vehicle (DMSO), or 10 µM UK5099. Data shows mole percent enrichment (MPE) of isotope labeled

substrate into respective metabolite from n=4 individual experiments. * $p < 0.05$, ** $p < 0.01$ compared to vehicle by Student´s t test.

(D) Quantification of percent M+3 label from [U-$^{13}C_5$] glutamine into respective metabolite from from experiment described in (C) (n=4 individual experiments). * $p < 0.05$, ** $p < 0.01$, *** $p < 0.001$ compared to vehicle by Student´s t test.

Data information: All data are presented as mean ± SEM.

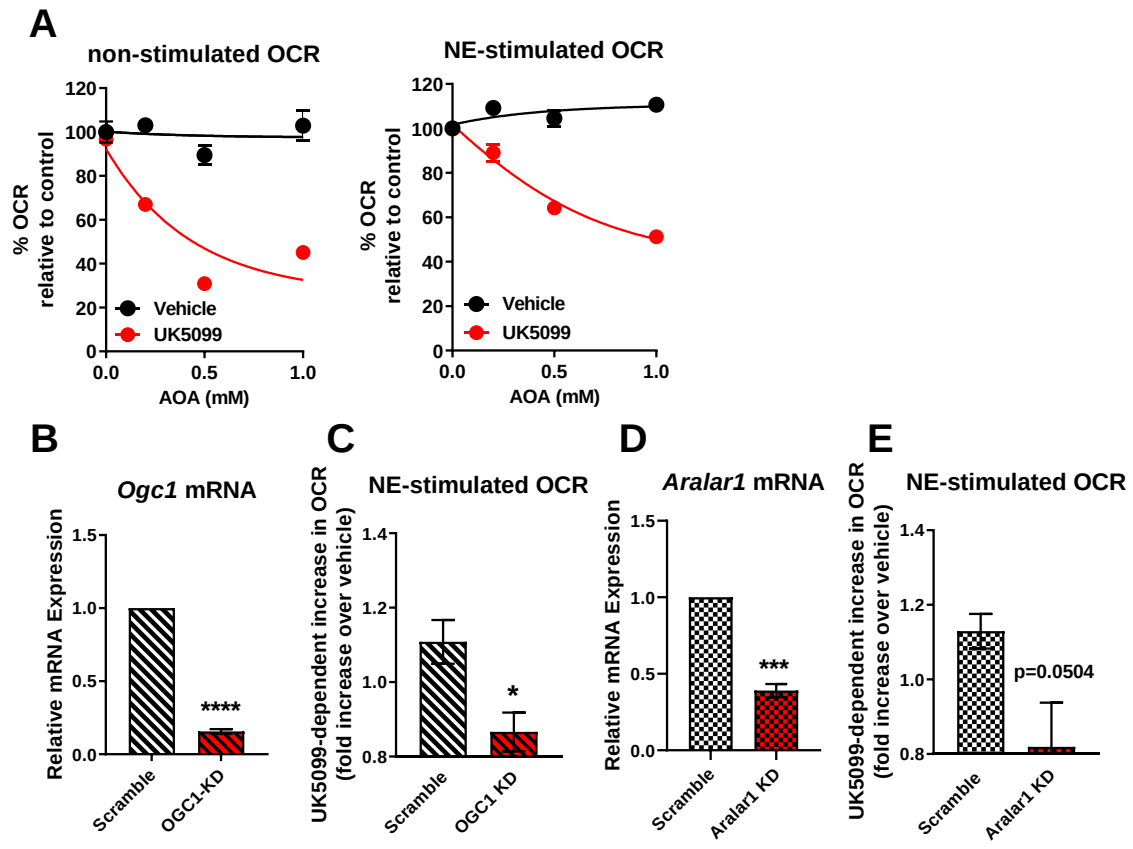

Figure EV4: The malate-aspartate shuttle is required for increased Norepinephrine-stimulated energy expenditure induced by MPC inhibition. (A) Brown adipocytes were pre-treated with vehicle (DMSO), 50 nM UK5099, aminooxyacetic acid (AOA) at various concentrations, or a combination. Oxygen consumption rates (OCR) were measured in respirometry media supplemented with 3 mM glucose and 3 mM glutamine

in the presence of the compounds. Data shows non-stimulated and norepinephrine stimulated OCR (n=3 individual experiments). Note that AOA has no effect in vehicle treated cells, but reduced OCR when cells are treated with UK5099.

(B) mRNA levels of OGC1 in brown adipocytes transduced with adenovirus carrying either scramble RNA (Scramble) or OGC1 shRNA (OGC1 KD). Data were normalized to vehicle for each individual experiment (n=3 individual experiments). **** $p < 0.0001$ compared to Scramble by Student´s t-test.

(C) Quantification of norepinephrine stimulated OCR after vehicle or UK5099 treatment in scramble RNA or OGC1 shRNA transduced cells. Data were normalized to vehicle for each individual experiment (n=5 individual experiments). * $p < 0.05$ compared to vehicle by Student´s t-test.

(D) mRNA levels of Aralar1 in brown adipocytes transfected scramble RNA (Scramble) or Aralar1 siRNA (Aralar1 KD). Data were normalized to vehicle for each individual experiment (n=4 individual experiments). *** $p < 0.001$ compared to Scramble by Student´s t-test.

(E) Quantification of NE-stimulated OCR after vehicle or UK5099 treatment in scramble RNA or Aralar1 siRNA transfected cells. Data were normalized to vehicle for each individual experiment (n=4 individual experiments). $p=0.0504$ compared to vehicle by Student´s t-test.

Data information: All data are presented as mean ± SEM.

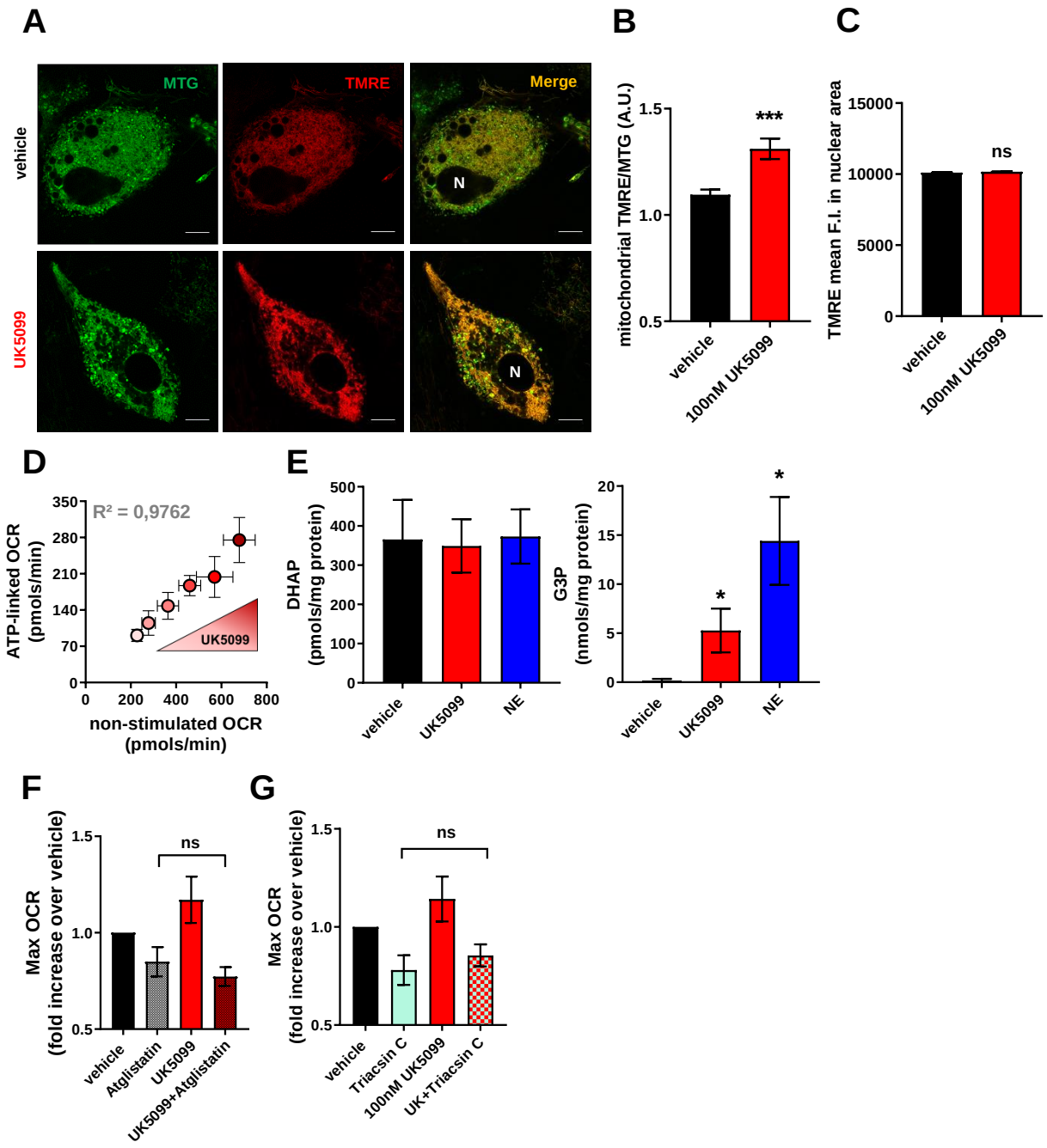

Figure EV5: Effects of UK5099 on ATP demand and lipid cycling.

(A) Live-cell super-resolution confocal imaging of primary brown adipocytes. Cells were stained with mitotracker green (MTG, green) and membrane potential sensitive dye

TMRE (red). Cells were treated with vehicle (DMSO) or 100 nM UK5099 for 2 h. N, nucleus. Scale bar=10 µm.

(B) Quantification of mitochondrial TMRE fluorescence intensity (F.I.) normalized to mitochondrial MTG F.I. from images shown in (A). Data represent 22-27 cells from 3 individual experiments. *** $p < 0.0001$ by Student´s t-test.

(C) Quantification of TMRE mean F.I. in nuclear area (N) from images shown in (A). Data represent 15 cells from 3 individual experiments. ns $p>0.05$ by Student´s t-test.

(D) Effect of increasing UK5099 concentrations (50 nM, 100 nM, 1 µM, 5 µM, 10 µM) on brown adipocytes respiratory rates. Note that the dose dependent increase in basal OCR following UK5099 treatment correlates with an increase in ATP linked OCR (n=3 individual experiments).

(E) Quantification of G3P and DHAP in brown adipocytes treated with vehicle, 100 nM UK5099 or 1 µM norepinephrine (NE) for 24 h (n=3 individual experiments). * $p < 0.05$ compared to vehicle by ANOVA.

(F) Brown adipocytes were treated with either vehicle (DMSO), 100 nM UK5099, 40 µM Atglistatin or Atglistatin in combination with UK5099. Maximal respiratory rates (Max OCR) were calculated after uncoupling by using the proton ionophore FCCP. Data were normalized to vehicle for each individual experiment (n=3 individual experiments). ns $p>0.05$ by ANOVA.

(G) Brown adipocytes were treated with either vehicle (DMSO), 100 nM UK5099, 5 µM Triacsin C , or Triacsin C in combination with UK5099. Maximal respiratory rates (Max OCR) were calculated after uncoupling by using the proton ionophore FCCP. Data were

normalized to vehicle for each individual experiment (n=4 individual experiments). ns p>0.05 by ANOVA.

Data information: All data are presented as mean ± SEM.

Table 1: Primers for qPCR

Gene	**Forward primer 5'-3'**	**Reverse Primer 5'-3'**
Mpc1	GAC TTT CGC CCT CTG TTG CTA	GAG GTT GTA CCT TGT AGG CAA AT
Mpc2	CCG CCG CGA TGG CAG CTG	GCT AGT CCA GCA CAC ACC AAT CC
SCL25A11	AGT CTC CTC TTG GGT GTT AGA	CTT CTG CTT TCT CCT GTC TCC
SCL25A12	TGGTTACCTACGAGCTTCTGC	ACCGATGTGATCGGGGTTG
Ucp1	GGC CTC TAC GAC TCA GTC CA	TAA GCC GGC TGA GAT CTT GT
Atgl	TCC GAG AGA TGT GCA AAC AG	CTC CAG CGG CAG AGT ATA GG
pgc1a	AAG ATC AAG GTC CCC AGG CAG TAG	TGT CCG CGT TGT GTC AGG TC
tfam	CAC CCA GAT GCA AAA CTT TCA	CTG CTC TTT ATA CTT GCT CAC AG
elov13	TCC GCG TTC TCA TGT AGG TCT	GGA CCT GAT GCA ACC CTA TGA
prdm16	GCC ATG TGT CAG ATC AAC GA	CCT TCT TTC ACA TGC ACC AA
36b4	GTC ACT GTG CCA GCT CAG AA	TCA ATG GTG CCT CTG GAG AT

Chapter 2: The role of mitochondria attached to lipid droplets in adipose tissue function.

INTRODUCTION

Various studies have observed a tight or transient (also known as “kiss-and-run”) interaction between LDs and mitochondria (Benador *et al*, 2018; Freyre *et al*, 2019; Herms *et al*, 2015; Tarnopolsky *et al*, 2007; Nguyen *et al*, 2017; Rambold *et al*, 2015; Cui *et al*, 2019; Yu *et al*, 2015). Interestingly multiple groups observed an increase in mitochondria-LD interaction upon conditions of starvation and were thus hypothesized to be a mechanism for increasing mitochondrial fatty acid oxidation (Herms *et al*, 2015; Rambold *et al*, 2015; Nguyen *et al*, 2017). However, only recently it was shown that mitochondria attached to LD have distinct bioenergetics, proteome, cristae organization and dynamics compared to cytoplasmic mitochondria (CM) (**Figure 2-1**). These mitochondria, termed peridroplet mitochondria (PDM) were successfully isolated from mature BAT by utilizing high-speed centrifugation to separate mitochondria from their associated lipid droplets (Benador *et al*, 2018). Benador et al. show that PDM have higher capacity to oxidize pyruvate and malate, but lower capacity for fat oxidation, compared to CM. Interestingly, PDM were shown to have a higher ATP synthesis capacity and higher expression levels of ATP synthase (Benador *et al*, 2018). ATP synthesis in PDM enabled esterification of lipids and expansion of LDs (**Figure 2-1**). Furthermore, it was found that PDM differ from CM in their dynamics, as they do not fuse and thus do not share content with their cytoplasmic neighbors, despite higher expression of mitochondrial fusion protein Mfn2 (Benador *et al*, 2018). However, due to their attachment to LDs, their motility is significantly lower, which is likely the reason for their reduced fusion activity (Benador

et al, 2018). Data in primary brown adipocytes using overexpression models of a PDM tethering protein suggest that forcing mitochondria to attach to the LD may be sufficient to give them the unique bioenergetics characteristics associated with PDM (Benador *et al*, 2018). However, it remains to the determined how LD attachment "transforms" mitochondria into PDM.

Despite the role of PDM in providing ATP for lipid synthesis in brown adipocytes, little is known about their function in other tissues, including white adipocytes. However, the finding that at least two types of mitochondria co-exist within a cell provides a mechanism of how seemingly antagonistic metabolic programs, such as lipogenesis and fatty acid oxidation can occur at the same. Thus, PDM may be particularly important for BAT and beige adipocytes, as this tissue needs to manage storage and oxidation of fatty acids, often at the same time.

Other metabolically highly active tissues could also benefit from having a population of mitochondria capable of assisting FFAs esterification. In cardiac tissue, conditions that induce a rapid increase in lipid droplet mass such as fasting or β-agonist treatment invariably led to induction of Plin5 expression and increase in mitochondria-lipid droplet contact sites (Varghese *et al*, 2019). PDM function may also protect cells from oxidative stress, through a yet unknown mechanism. In the HepG2 liver cell line, Tan et al., demonstrated that PLIN5 protein expression and the incidence of PDM was increased upon the induction of oxidative stress. Moreover, PLIN5 overexpression conferred protection from H_2O_2 induced apoptosis leading to the speculation that PDM can confer protection from oxidative stress (Tan *et al*, 2019). Interestingly, the transfer of anti- and pro-apoptotic factors from the outer mitochondrial membrane to the lipid droplet

membrane has been previously shown to be part of the stress response in yeast and mammalian cells (Bischof *et al*, 2017).

The possible role of PDM in other tissues such as muscle and liver and cancer were recently reviewed (Benador *et al*, 2019).

Mechanisms for PDM interaction with lipid droplets

Although mitochondria and LD contact has been described in multiple tissues and conditions, the exact mechanism by which this interaction is mediated remains inconclusive. In fact, several mechanisms for mitochondria-LD tethering were proposed in the literature, opening the possibility that PDM interaction with LDs is regulated on multiple levels, or in a tissue specific manner (**Table 2**).

One of the proposed PDM tethering proteins is Perilipin 5 (Plin5), a member of the Perilipin family of LD-coating proteins. Plin5 was shown to co-localize with mitochondria and LDs. Overexpression of Plin5 is sufficient to promote mitochondria-LD association in multiple cell types (Wang *et al*, 2011; Sztalryd & Kimmel, 2014; Benador *et al*, 2018). Importantly Plin5 is also a negative regulator of lipolysis via its interaction with ATGL, which makes studies analyzing the involvement of PDM recruitment to LD expansion challenging (Sztalryd & Kimmel, 2014). Interestingly, Wang et al. found that a conserved sequence at the C-terminus of the protein is required for Plin5 to tether mitochondria (Wang *et al*, 2011). However, expression of Plin5-mitochondria tethering sequence alone did not co-localize with mitochondria, indicating that Plin5 might form a complex with another protein that directly binds to mitochondria, or may indicate that specific protein folding is required for the tethering effect (unpublished data). A recent study showed that

Plin5 phosphorylation at S155, a PKA target, induces lipolysis without detaching mitochondria from the LD in cardiomyocytes (Kolleritsch *et al*, 2019). Adrenergic stimulation in brown adipocytes leads to detachment of PDM (Benador *et al*, 2018), however it remains to be determined if it is through PKA-mediated signaling on Plin5, or an alternative mechanism. Interestingly, Gallardo-Montejano et al. published that Plin5 translocates to the nucleus in a PKA dependent manner (Gallardo-Montejano *et al*, 2016), suggesting that Plin5 translocation to the nucleus could induce transcriptional changes to maintain PDM detached from the LD.

Another proposed mitochondria-LD tether is Diglyceride-Acyltransferase 2 (DGAT2). DGAT2, together with DGAT1, is responsible for the last step in TAG synthesis. DGAT2 was shown to co-localize with LDs, mitochondria and the ER, thereby bringing these three organelles in direct contact (Stone *et al*, 2009). Stone et al. showed that the N-terminus of DGAT2 contains a mitochondrial targeting sequence, which is necessary and sufficient for its mitochondrial localization. Accordingly, introducing the targeting sequence alone into Cos7 cells was sufficient to target a fluorescent probe to mitochondria. Interestingly Irshad et al. showed that, in contrast to DGAT1, which is required for TAG synthesis from circulating free fatty acids, DGAT2 was necessary for esterification of TAGs derived from de novo lipogenesis (Irshad *et al*, 2017). It remains to be determined, if loss of DGAT2 leads to a decrease in PDM, and if that further affects TAG synthesis from de novo lipogenesis.

Furthermore, the outer mitochondrial membrane protein Mitofusin 2 (Mfn2) has been suggested as a possible tethering protein between LD and mitochondria (Boutant *et al*, 2017), and between mitochondria and the ER (de Brito & Scorrano, 2008). Knock-out of

Mfn2 in BAT leads to a 50% reduction in mitochondria-LD interaction, and Mfn2 pull-down experiments showed co-immunoprecipitation of Mfn2 with LD- coating protein Plin1 in MEFs (Boutant *et al*, 2017). Moreover, the outer membrane mitochondrial protein Mfn2 was recently demonstrated to participate in the transfer of phospholipid precursors from the ER to mitochondria to enable phospholipid synthesis (PE) (Hernández-Alvarez *et al*, 2019). LDs have a monolayer of phospholipids to encapsulate the neutral lipids stored. Consequently, one could hypothesize that the interaction between mitochondria and LDs might allow an efficient transfer of de novo synthesized phospholipids to facilitate LD expansion. Various reviews have discussed the function of Plin5 (Sztalryd & Kimmel, 2014; Wang & Sztalryd, 2011), DGAT2 (Yen *et al*, 2008; Bhatt-Wessel *et al*, 2018) and Mfn2 (Liesa *et al*, 2009; Schrepfer & Scorrano, 2016) aside from their proposed role as mitochondria-LD tethering proteins.

A recent study identified Mitoguardin 2 (MIGA2) as a tethering protein between mitochondria and LDs in white adipose tissue (Freyre *et al*, 2019). Detailed analysis of various truncations of MIGA2 revealed that an amphipatic sequence at the C-terminus of the protein was necessary and sufficient to mediate mitochondria-LD interaction (Freyre *et al*, 2019). Indeed, expression of this mitochondria-recruiting sequence was able to target a fluorescent probe to mitochondria (Freyre *et al*, 2019). In addition, fusion of this sequence to Calnexin, an ER protein that does not co-localize with mitochondria, was sufficient to mediate Calnexin-mitochondria interaction (Freyre *et al*, 2019). Interestingly, the study supports that MIGA2 acts as a connection between mitochondria, the ER and LDs, similarly to DGAT2 (Freyre *et al*, 2019; Stone *et al*, 2009, 2). MIGA2 interaction with the ER was mediated by a FFAT-motif binding to VAP-A/B in the ER. While MIGA2-

mediated tethering promotes de novo lipogenesis, the role of MIGA2-mediated PDM recruitment in the esterification of pre-existing fatty acids into triglycerides remains to be determined (Freyre *et al*, 2019). On the other hand, Plin5-mediated PDM recruitment increased TAG esterification from pre-existing fatty acids, but whether Plin5 increases de novo lipogenesis remains to be determined (Benador *et al*, 2018). The observation that DGAT2, a PDM tethering protein, was shown to be required for TAG synthesis coming from de novo lipogenesis (Stone *et al*, 2009; Irshad *et al*, 2017), similar to MIGA2 (Freyre *et al*, 2019), as opposed to PDM recruitment by Plin5, which promoted esterification of external fatty acids (Benador *et al*, 2018), suggests that different tethers might assign different functions to PDM. Since two of the proposed tethers for PDM are also tethering the ER to the LD, and the ER is known to be the site of LD-budding (Walther & Farese, 2009; Murphy & Vance, 1999), it is interesting to speculate that PDM are involved in the generation of new LDs, or the expansion of existing LDs, or both.

The observation that MIGA2 acts as a tethering protein for PDM in WAT, a tissue that expresses little to no Plin5 (Wolins *et al*, 2006; Freyre *et al*, 2019), supports that PDM attachment and function might be regulated in a tissue-specific manner. Furthermore, it is conceivable that depending on the tether used, PDM could have beneficial vs. detrimental effects on systemic lipid metabolism. Additionally, it is possible that certain tethers like MIGA2 are expressed during cell differentiation to aid in this process, whereas others, like Plin5 or DGAT2 are needed for metabolic regulations in the fully differentiated state.

PDM visualization and isolation methodologies

While previous studies have observed mitochondria associated with LD, the type of visualization and quantitation varied greatly between these studies. Therefore, this section of the review focuses on the various methodologies to visualize and quantify PDM association, and furthermore discuss published isolation protocols and their limitations. Noteworthy is that the different analyses and isolation methods may detect different types of interactions of PDM to LDs. Different levels of strength of association (permanent vs transient) are detected with varying isolation and detection methods, which are outlined below, and might explain why different groups propose opposing roles for PDM. However, it remains to be determined whether the type of strength of PDM interaction with LD corresponds to a different biological function.

Electron Microscopy

The first observations of mitochondria-LD interactions were made using electron microscopy (EM) by Palade in 1959 (Palade, G.E., 1959). Indeed EM images provide the highest resolution, and multiple groups have observed seemingly tight interaction of mitochondria and LD using this method (Freyre *et al*, 2019; Benador *et al*, 2018; Herms *et al*, 2015; Tarnopolsky *et al*, 2007; Bleck *et al*, 2018; Arruda *et al*, 2014). This tight interaction can be seen as an electron dense region that connects the PDM and LD (Benador *et al*, 2018; Bleck *et al*, 2018; Herms *et al*, 2015; Tarnopolsky *et al*, 2007). A clear advantage of this method is the high resolution of EMs, which allows the detection of PDM even in cells that do not have many or big LDs (Nielsen *et al*, 2010; Tarnopolsky *et al*, 2007). Furthermore, EM images can give interesting information on cristae arrangement in PDM. In that regard, several groups observed a perpendicular

arrangement of mitochondrial cristae towards the LD (Benador *et al*, 2018; Herms *et al*, 2015). However, the biological significance of this observation remains to be determined.

Live-cell confocal imaging

A variety of studies have observed mitochondria LD interaction using live-cell fluorescence imaging (Benador *et al*, 2018; Freyre *et al*, 2019; Rambold *et al*, 2015; Stone *et al*, 2009; Wang *et al*, 2011). A clear advantage of live-cell imaging to monitor mitochondria-LD interactions is the real-time component. Along with other organelles in the cells, both mitochondria and LDs are in constant movement and their juxtapositions may be dynamic. A life-cell imaging approach thus can provide important information on the nature of PDM interaction; whether these are permanent or transient interactions. Furthermore, responses to pharmacological interventions can be studied more easily using a life-cell imaging approach. Recent studies have described approaches for spatial life cells imaging with novel analysis approaches that provide high-resolution information and a more accurate assessment of organelle interactions. (Valm *et al*, 2017; Pribasnig *et al*, 2018). Improved imaging technology paired with accurate analysis platforms will likely improve our understating of the nature of PDM and their interactions with LDs.

Analyses of cell-free LD fraction

Multiple studies have isolated LD fractions by centrifugation and measured mitochondrial content in this lipid fraction by fluorescence microscopy (Benador *et al*, 2018; Cui *et al*, 2019), western blot analyses (Freyre *et al*, 2019; Yu *et al*, 2015; Cui *et al*, 2019), quantitative proteomics (Zhang *et al*, 2011; Yu *et al*, 2015) or with fluorescent plate reader assay (unpublished data). Using these approaches only strong interactions between

mitochondrial and LD will be detected, but relatively weakly attached PDM might be missed. Furthermore, depending on the speed of centrifugation different groups may have assessed a different pool of PDM, depending on the strength of the interaction.

PDM isolation heterogeneity

Several studies have attempted to isolate PDM and separate them from the LDs using centrifugation with or without salts or detergents (Benador *et al*, 2018; Yu *et al*, 2015; Cui *et al*, 2019). While Benador et al. showed successful isolation of PDM using a centrifugation of 10.000xg (Benador *et al*, 2018), other studies showed that centrifugation is not sufficient to strip all mitochondria from the lipid droplet, requiring proteinase treatments to isolate them (Yu *et al*, 2015; Cui *et al*, 2019). These discrepancies could be attributed to; 1. differences in the ionic strength of the buffers used for tissue homogenization 2. the type of homogenization technique (e.g. dounce homogenizer, filtration through mesh) 3. the strength of homogenization (number and force of strokes used). Further work needs to be done on optimizing isolation protocols, tissue differences and properly defining the nature of the interaction between mitochondria and LDs. In addition, these differences might be suggestive of heterogeneity of peridroplet mitochondria, by itself an exciting aspect. It is conceivable that depending on the strength of interaction there is a subgroup of PDM specialized to provide ATP, while another subgroup could potentially be involved in lipogenesis or other processes regulating lipid metabolism.

Based on the questions posed in this introduction we carried out a series of experiments to optimize the PDM isolation protocol for BAT and WAT, and assess the possible heterogeneity between PDM attached to differently sized LDs.

RESULTS

PDM isolation by high-speed centrifugation does not strip all mitochondria from lipid droplets.

While our published method enabled us to isolate PDM from BAT using high-speed centrifugation of the fat layer (Benador *et al*, 2018; Ngo *et al*, 2021), some mitochondria remained tightly associated with LDs (**Figure 2-2A and B**). Moreover, we noticed that mitochondria attached to small LDs were the mitochondria that remained attached to LD after high-speed centrifugation with higher frequency (**Figure 2-2A**). We further observed that smaller LDs have more mitochondria attached to them when compared to larger LDs, both in brown adipocytes (**Figure 2-2C**) and in a cultured white adipocyte cell line (3T3-L1) (**Figure 2-2D**). Together these data support that PDM are heterogeneous in terms of LD binding, with this heterogeneity being determined by LD size. Such heterogeneity supports that mitochondria attached to smaller LDs might have a higher activity promoting LD expansion or other unique roles that remain to be characterized.

Proteolytic treatment of the fat layer increases the yield of PDM stripped from BAT and WAT lipid droplets.

Mitochondria-LD interactions are mediated by a variety of protein tethers and complexes (Wang *et al*, 2011; Boutant et al, 2017; Stone *et al*, 2009; Freyre *et al*, 2019). We, therefore, hypothesized strong protein-protein interactions explained why some mitochondria that remained attached to LDs after high-speed centrifugation. We reasoned that incubation with a protease could cleave the strong protein tethers between mitochondria and LD, allowing to strip more mitochondria. To test our hypothesis we treated the fat layer containing PDM with proteinase K, followed by high speed centrifugation and proteinase K inactivation (**Figure 2-3A**). Briefly, we split the homogenate from WAT and BAT into two fractions, one fraction used to isolate PDM using proteinase K and the second fraction using our old protocol. To control for a potential over-digestion of mitochondria leading to their respiratory dysfunction, we added ProtK to the supernatant from which CM are isolated. ProtK was incubated for 15 minutes following high-speed centrifugation. We found that ProtK treatment significantly increased protein content in PDM fractions, without changing protein content in CM fractions (**Figure 2-3B**).

We next sought to verify that the increase in protein content in PDM fraction was explained by an increase in mitochondria content, not by other contaminant organelles tethered to LDs. To assess this possibility we analyzed PDM and CM fractions isolated from BAT by Western blot, to quantify the amount of mitochondrial proteins per microgram or protein. We analyzed both outer membrane proteins (VDAC), which could be degraded by ProtK, and components of the electron transport chain in the inner membrane (total OXPHOS), which would not be accessed by ProtK in intact mitochondria. As expected, after freezing PDM and CM fractions from the fat layer treated

with Prot K, both the content of outer mitochondrial membrane protein VDAC and the electron transport chain complexes, particularly complex 3 were decreased (**Figure 2-3B,C**). To preserve the integrity of mitochondrial proteins of PDM isolated from Prot K treated fat layers, we treated treated the fat layer with phenylmethylsulfonyl fluoride (PMSF) right after the ProtK treatment and before freezing. Indeed, PMSF prevented both VDAC and Oxphos degradation in BAT mitochondria in PDM fractions from Prot K treated fat layers, while still preserving the increase in yield in PDM isolation (**Figure 2-3C**). Interestingly PMSF treatment in the absence of ProtK resulted in decreased VDAC and Oxphos subunit content when compared to the old PDM stripping protocol, possibly suggesting that PMSF can have side effects on protein stability and mitochondrial isolation if proteinase K is absent. Similar results were also observed in CM isolated from WAT (**Figure 2-3D**).

Together these data suggest that ProtK treatment can increase the yield of PDM isolated from BAT and WAT, resulting in a fraction more enriched in mitochondrial content. In addition, PMSF addition even prevented the degradation of some outer mitochondrial membrane proteins, such as VDAC. Thus, our data supports that our proteolytic protocol degrades the protein tethers between mitochondria and LD.

Isolation of PDM with ProtK does not inhibit mitochondrial function

ProtK is a serine protease, which will cleave any protein with a serine residue and can thus degrade components of the mitochondria that are essential for mitochondrial function. Despite our Western Blot data supported that our Prot K treatment combined with PMSF prevented VDAC degradation, we wanted to determine whether our new

protocol could be changing mitochondrial respiratory function. We measured both maximal and state 3 respiratory capacity of PDM isolated from BAT using ProtK , with state 3 reflecting respiration at maximal ATP synthesis rates. Our data show that state 3 and maximal respiratory capacity were not affected in CM and PDM from BAT isolated with ProtK (**Figure 2-4A, B**). Moreover, our data confirms our previously published findings, that BAT PDM have higher state 3 and maximal respiration than CM under pyruvate and malate as substrates (Benador *et al*, 2018). To further confirm that mitochondrial ATP synthesis and release are not affected by ProtK, we measured ATP synthesis rates using firefly luciferase luminescence. Figure 3C shows that ProtK did not affect BAT CM or PDM capacity to synthesize ATP. We furthermore were able to reproduce the previous observation that BAT PDM have higher ATP synthesis rates than BAT CM (Benador *et al*, 2018).

We then performed the same respirometry measurements in WAT mitochondria and found that ProtK treatment did not affect state 3 or maximal respiratory capacity in CM and PDM from WAT (**Figure 2-4D**). Surprisingly, PMSF treatment led to reduced state 3 OCR in CM and reduced state 3 and maximal OCR in WAT PDM (**Figure 2-4E**). Furthermore, our data revealed that WAT PDM have lower respiratory capacity than CM, which can be suggesting that the demand for CM pyruvate oxidation in WAT can be higher than in BAT, as CM in BAT oxidize fatty acids (**Figure 2-4D and E**). Interestingly, we find that ProtK treatment increased ATP synthesis rate in WAT CM and PDM (**Figure 2-4F**), further supporting the idea that the addition of ProtK results in a fraction with higher yield of mitochondria.

Overall, these data suggest, that ProtK does not inhibit mitochondrial function and that PMSF is only needed if mitochondria are frozen, as disruption of mitochondrial membranes by freeze-thawing gives Prot K access to inner membrane proteins.

Proteinase K treatment enables the isolation of mitochondria attached to smaller LDs

Previous studies have shown that there is a distribution of various sizes of LDs within an individual cell and that these differently sized LDs can have distinct metabolic functions (Zhang *et al*, 2016). Furthermore, our preliminary data suggest that small LDs, despite having less perimeter of contact area, recruit more mitochondria (**Figure 2-2C**). We thus hypothesized that mitochondria bind to small LD with higher affinity, being the population that is selectively enriched by proteinase K treatment. To test this hypothesis, we developed an approach to separate lipid droplets of different sizes by performing two consecutive centrifugations at different speeds. The first centrifugation is at 500 x g which creates a fat layer consisting of large LDs (Fx1), followed by the second centrifugation at 2000 x g which results in a fat layer consisting of smaller LDs (Fx2) (**Figure 2-5A**). To confirm that these centrifugation steps indeed separated two fractions with differently sized LDs, we imaged the lipid droplets of Fx1 and Fx2 obtained from WAT using confocal microscopy after staining them with Bodipy493. Fx1 isolated from WAT is enriched with LDs that have a significantly larger size than Fx2 **(Figure 2-5B)**. To measure whether Fx2 is associated with more mitochondria than Fx1, we measured PDM amount using a plate reader assay, based on Bodipy493 and mitotracker deep red staining of the fractions. The

fluorescent ratio of MTDR/Bodipy493 was used to estimate mitochondria recruitment per lipid content. Our data show that WAT Fx2 contains more mitochondria per lipid content than Fx1, thus supporting our hypothesis that small LDs are more associated with mitochondrial than large LDs (**Figure 2-5C**). To validate the increased recruitment of mitochondria in smaller lipid droplets (Fx1), we quantified mitochondrial OXPHOS protein content determined by Western blot of WAT and BAT total homogenates, Fx1 and Fx2 (**Figure 2-5D**). To normalize for LD content, we probed the western blot membrane for Perilipin 1 (Plin1), an LD protein ubiquitously expressed on all LDs whose content tracks with LD size. Our data shows that Fx2 contains higher levels of OXPHOS, including ATP synthase; both in WAT and BAT (**Figure 2-5D**). These data further support that small LDs are more associated with PDM than large LDs.

PDM from Fx2 have unique characteristics

Previous studies have shown that small lipid droplets are more metabolically active than larger lipid droplets (Zhang *et al*, 2016). In addition, we observed heterogeneity in PDM function and composition when measured in intact cells, with some PDM having higher ATP synthase content than others (Benador et al., 2018). We therefore hypothesized that PDM attached to small LDs are more active than PDM attached to large lipid droplets. To test this hypothesis, we stripped PDM from Fx1 and Fx2 using our new protocol including ProtK to isolate them and measure their respiratory rates. In BAT we find that PDM from Fx1 have increased maximal and ATP-synthesizing respiration capacity than PDM from Fx2. Remarkably, complex 4 driven respiration measured using TMPD/Ascorbate, a substrate that donates electrons directly to complex 4, was the same in Fx1 and Fx2 (**Figure 2-6A**). Interestingly Fx1 PDM from WAT respire lower than CM for all

mitochondrial states measured (**Figure 2-6C**), while Fx2 PDM have significantly higher respiratory rates than PDM from Fx1 reaching similar levels to CM (**Figure 2-6C**). These data suggest that, as opposed to BAT, WAT PDM do not have higher respiratory capacity than CM under pyruvate and malate as fuel. This might speak to LD in BAT being more dynamic and active than in WAT, as a major function of WAT is to store lipids.

A major hallmark of PDM in BAT is their lower capacity to oxidize fatty acids compared to CM. We, therefore, wanted to test whether this holds true for WAT PDM and how BAT and WAT PDM from Fx2 respire on fatty acids. To test this we measured respiratory rates when given palmitoyl-carnitine and malate as substrate (**Figure 2-6B and D**). We find that both WAT PDM and CM have similar capacities to oxidize palmitoyl-carnitine and malate, which is again in contrast to BAT PDM that had lower fatty acid oxidation capacity than CM. As the total mitochondrial oxidative capacity in WAT is much lower than in BAT, and the differences fractions had different oxidative capacities as well, we needed to perform some normalizations to determine the oxidative capacity for each nutrient (i.e. pyruvate versus fatty acids). We then quantified mitochondrial fuel preference as the ratio of maximal OCR fueled by pyruvate+malate divided by maximal OCR fueled by palmitoyl-carnitine+malate. Our data show that BAT PDM from Fx1 have a higher preference for pyruvate and malate than CM (**Figure 2-6E**), with this ratio recapitulating what we previously published in total PDM from BAT (Benador *et al*, 2018). Interestingly Fx2 PDM have a lower capacity to oxidize pyruvate and malate than Fx1 PDM (**Figure 2-6E**). In WAT differences in fuel preference between CM and PDM from Fx1 and Fx2 are not significant (**Figure 2-6F**). Together these data suggest that in both BAT and WAT there are at least two populations of mitochondria with unique bioenergetic function.

Furthermore, our data suggest that WAT PDM have a different function than BAT PDM, or that WAT CM have a different function than BAT CM. Indeed, BAT CM are specialized in oxidizing fatty acids for thermogenesis, a function inactive in CM from mature white adipocytes in WAT.

DISCUSSION

Here we describe an improved protocol to isolate PDM from BAT and WAT using ProtK treatment following high-speed centrifugation (**Figure 2-3A**). We find that addition of ProtK to the PDM isolation protocol significantly increases PDM yield, and most importantly solves the problem of extremely low yield of PDM isolation from WAT. PDM from WAT may have important implications in understanding the role of PDM in protection of lipotoxicity (Veliova *et al*, 2020).

Adding proteinase K to the PDM isolation protocol did not affect reproducing our previous observations that BAT PDM have higher respiratory capacity, ATP synthesis rate and a fuel preference for pyruvate and malate (**Figures 2-4A-C and 6E**) (Benador *et al*, 2018). Interestingly we find that in WAT, PDM have lower respiratory capacity than CM, but with similar ATP synthesis rates and fuel preference (**Figure 2-4D-F and 6F**). These data suggest that PDM in WAT might still serve triglyceride synthesis, but that ATP demand from CM might be larger. In this regard, one could hypothesize that other ATP-demanding processes in WAT, such as cytokine and peptide production, might rely on CM to explain their higher activity. Future studies will determine the function of PDM in WAT lipid esterification and LD homeostasis.

Interestingly we find that ProtK treatment provides mitochondria with higher ATP synthesizing capacity both in PDM and CM fractions (**Figure 2-4F**). These data suggest that including ProtK to the isolation protocol degrades/detaches some of the contaminants in the CM fraction (i.e. MAMs, ER membranes), thereby leading to a highly enriched mitochondrial isolation. However, future studies have to determine whether ProtK indeed increase mitochondrial purity.

Moreover, our data suggest that in both BAT and WAT smaller LDs have higher PDM content than larger ones (**Figures 2-4C and D**). These data are in partial agreement with a previous study showing that different sizes of LDs in BAT have different amounts of PDM associated to them (Zhang *et al*, 2016). In fact, Zhang et al. isolated 3 fractions of LDs from BAT using different centrifugation speeds. While Zhang et al. find that Fx2 contains more mitochondrial proteins than Fx1, the group shows lower expression of mitochondrial proteins in Fx3. However, in their protocol, Fx3 was created by centrifuging the lipid layer at 20,000 x g, a speed that likely stripped most mitochondria from the LDs.

Furthermore, we find that differently sized LDs in WAT and BAT are associated with PDM that have unique bioenergetics characteristics. Our data suggest that in BAT, PDM attached to larger LDs have higher respiratory capacity (**Figures 2-6A and C**). However, in WAT, PDM attached to smaller LDs have higher respiratory capacity both under pyruvate+malate and under palmitoyl-carnitine as substrates (**Figures 2-6C and D**). These data suggest that there are at least two different populations of PDM, which possibly have unique roles in mainlining LD homeostasis. Indeed functional differences between varying LD size have been also observed in hepatocytes (Schott *et al*, 2019), were large LDs were shown to be consumed by lipolysis, while larger LDs by lipophagy.

Future studies could investigate the role of PDM attached to small and large LDs in these two processes.

Furthermore our previous data suggest that under hormonal stimulation BAT PDM detach from the LDs, however some of the PDM remain attached, even after full BAT activation (Benador *et al*, 2018). It is conceivable that these PDM are more tightly associated and serve the role of re-building the LDs. Thus further characterization of PDM attached to differently sized LDs and also analysis of PDM that remain attached after cold exposure will aid our understanding on PDM function and their role in cellular energy metabolism.

MATERIALS AND METHODS

Mice

Mitochondria were isolated from 12-week-old male C57BL6/J mice and primary brown adipocytes were isolated from 3- to 4-week-old wild-type male C57BL6/J mice (Jackson lab, Bar Harbor, ME). Animals were fed standard chow (mouse diet 9F, PMI Nutrition International, Brentwood, MO) and maintained under controlled conditions (19–22°C and a 14:10 hr light-dark cycle) until euthanasia by isoflurane. All animal procedures were performed in accordance with the Guide for Care and Use of Laboratory Animals of the NIH, and were approved by the Animal Subjects Committee of the University of California, Los Angeles Institutional Guidelines for Animal Care.

Peridroplet mitochondria isolation

Peridroplet mitochondria were isolated as previously described in detail with (Benador *et al*, 2018; Ngo *et al*, 2021) with some modifications. BAT was homogenized using a glass-

teflon dounce homogenizer, and WAT has homogenized using a glass-glass dounce homogenizer in Sucrose-HEPES-EGTA buffer supplemented with BSA (SHE+BSA; 250 mM sucrose, 5 mM HEPES, 2 mM EGTA, 1% fatty acid-free BSA, pH 7.2). Homogenate was split into four equal parts to test protocol optimizations side-by side. Homogenates were centrifuged at 1000 x g for 10 min at 4°C. Supernatant was poured into a new tube and fat layer was scraped into a second tube and resuspended in SHE+BSA buffer. Fat layers and supernatant were left either untreated or, or treated with 2µg/ml Proteinase K (Thermo Fisher Scientific, Roskilde, Denmark). All fat-layers were incubated for 15 minutes at 4°C under constant rotation. For protocol including PMSF, 2 mM PMSF (Santa Cruz Biotechnology, Dallas, Tx) was added for an additional 20 minutes of incubation on ice while inverting the samples every 5 minutes. Then all the samples were were centrifuged again at 10,000 x g for 10 min at 4°C. The pellets were re-suspended in SHE+BSA and centrifuged with the same settings once more. The pellets were then re-suspended in SHE without BSA and again centrifuged with the same settings. Final pellets were resuspended in SHE without BSA and protein concentration was determined by BCA (Thermo Fisher Scientific, Roskilde, Denmark).

Isolation of Fx1 and Fx2 associated Peridroplet Mitochondria

Fat tissue was homogenized as for PDM isolation. Homogenates were sieved through a 630 µm mesh (Genesee Scientific, San Diego, CA), transferred into ice-cold tubes and kept on ice for 20 minutes. Homogenates were centrifuged at 500 x g for 3 min at 4ºC which created a fat layer (Fx1). Supernatant was carefully poured into a new tube and centrifuged at 2000 x g for 10 min at 4ºC which created a second fat layer (Fx2).

Supernatant containing CM was transferred into a new tube by carefully pipetting underneath the fat layer. Fx1 and Fx2 were resuspended in SHE+BSA. Fx1 was centrifuged again at 500 x g for 5 min at 4ºC and Fx2 ice-cold 1.5mL falcon mini tube at 2000 x g for 10 min at 4ºC. Fx1 and Fx2 were resuspended in 1 ml SHE+BSA and incubated with ProtK as described above. All fractions were centrifuged at 10,000 x g for 10 in at 4ºC to pellet mitochondria. Mitochondrial pellets were resuspended in SHE without BSA and protein concentrations were determined by BCA (Thermo Fisher Scientific, Roskilde, Denmark).

Isolated Mitochondria Respirometry

Respirometry in isolated mitochondria was performed as previously described in detail (Ngo et al, 2021). Briefly, isolated mitochondria were re-suspended in mitochondrial assay buffer (MAS; 100 mM KCl, 10 mM KH2PO4, 2 mM MgCl2, 5 mM HEPES, 1 mM EGTA, 0.1% BSA, 1 mM GDP, pH 7.2) and kept on ice. Two micrograms per well were loaded into Seahorse XF96 microplate in 20 µL volume containing substrates. The loaded plate was centrifuged at 2,000 x g for 5 min at 4°C and an additional 130 µL of MAS buffer+substrate was added to each well. Substrate concentrations in the well were as follow: i) 5 mM pyruvate + 5 mM malate + 4 mM ADP, or iii) 2mM malate + 4 mM ADP. For Pyruvate plus malate dependent respiration; oligomycin was injected at port A (3.5 µM), FCCP at port B (4 µM), N,N,N',N'-Tetramethyl-p-phenylenediamine (TMPD) + ascorbic acid (0.5mM + 1mM) at port C and azide (50 mM) at port D. For palmitoyl-carnitine dependent respiration; 5 mM malate + 4 mM ADP+ 40 µM palmitoyl-carnitine was injected at port A, oligomycin was injected at port B (3.5 µM), N,N,N',N'-Tetramethyl-

p-phenylenediamine (TMPD) + ascorbic acid (0.5mM + 1mM) at port C and azide (50 mM) at port D Mix and measure times were 0.5 min and 4 min, respectively. A 2 min wait time was included for oligomycin-resistant respiration measurements.

Peridroplet Mitochondria Quantification

Fat layer and stripped fat layer were incubated in MAS buffer containing mitotracker deep red (MTDR, 1 µM, final) and Bodipy493 (500 nM, final) for 10 minutes at 37^{o}C. Dye was removed by centrifuging the samples at 1000×g for 10 min and removing the infranatant. The stained fat layer or stripped fat layer was resuspended in 100 µl of MAS and fluorescence measured in clear-bottom black 96-well plate (Corning, NY). MTDR was excited at 625 nm and its emission recorded at 670 nm. Bodipy493 was excited 488nm laser and its emission recorded at 500-550nm. MTDR/BD493 was calculated for the fat cake and the stripped fat cake. For PDM quantification, we calculated the difference of the MTDR/BD493 in the fat cake and the one in the stripped fat cake.

ATP Synthesis Assay

10 µg of isolated mitochondria were re-suspended in 10 µl MAS buffer containing 5 mM pyruvate + 5 mM malate + 3.5 mM ADP and plated onto a clear-bottom black 96-well plate (Corning, NY). Luciferin-luciferase mix was added to the mitochondria and luminescence immediately. Luminescent counts were integrated over 0.5 s at 10 s intervals separated by 0.5 s orbital shaking on Spark M10 microplate reader (Tecan, Männedorf, Switzerland). The linear rate of luminescence increase was calculated to determine ATP synthesis rate.

Protein Gel Electrophoresis and Immunoblotting

5-15 mg of isolated mitochondrial protein or fat layer was re-suspended in NuPAGE LDS Sample Buffer (Thermo Fisher Scientific, Roskilde, Denmark) containing β-mercaptoethanol (Thermo Fisher Scientific, Roskilde, Denmark). Samples were then loaded into 4 %–12 % Bis-Tris precast gels (Thermo Fisher Scientific, Roskilde, Denmark) and electrophoresed, in constant voltage at 60V for 30 min (to clear stacking) and 140V for 60 min. Proteins were transferred to methanol-activated Immuno-Blot PVDF Membrane (Bio-Rad, Hercules, CA) in 30V constant voltage for 1 hr at 4°C. Blots were incubated over-night with primary antibody diluted in PBST (phosphate buffered saline with 1 mL/L Tween-20/PBS) + 5 % BSA (Thermo Fisher Scientific, Roskilde, Denmark) at 4°C. The next day, blots were washed in PBST and incubated with fluorescent secondary antibodies, diluted in PBST+ 5 % BSA for 1 hour at room temperature. Proteins were detected using the following antibodies: Anti-Perilipin-1 antibody (ab61682, Abcam, Cambridge, United Kingdom), Total Rodent OXPHOS Cocktail (ab110413, Abcam, Cambridge, United Kingdom), anti-VDAC (ab15895, Abcam, Cambridge, United Kingdom), Donkey anti-Goat IgG secondary antibody, Alexa Fluor® 568 conjugate (Thermo Fisher Scientific, Roskilde, Denmark), Goat anti-Mouse IgG secondary antibody, Alexa Fluor® 660 conjugate (Thermo Fisher Scientific, Roskilde, Denmark), Goat anti-Rabbit IgG secondary antibody DyLight 800 (Thermo Fisher Scientific, Roskilde, Denmark). Blots were imaged on the ChemiDoc MP imaging system (Bio-Rad Laboratories, Hercules, CA). Band densitometry was quantified using FIJI (ImageJ, NIH).

Fluorescence Microscopy

Imaging Apparatus

All imaging was performed on Zeiss LSM710 and LSM880. Super-resolution imaging was performed with 63x Apochromat oil-immersion lens and AiryScan super-resolution detector. Live cell imaging was performed with humidified 5% CO2 chamber on a temperature controlled stage.

Fluorophore Excitation/Emission

All fluorophores were excited on separate tracks to avoid artifacts due to bleed-through emission. BODIPY 493/503 and Alexa Fluor 488 were excited with 488 nm 25 mW Argon-ion laser and their emission captured through 500-550 nm band-pass filter. Alexa Fluor 568 was excited with 543 nm 1 mW Helium-Neon laser or 561 nm 20 mW diode-pumped solid-state laser and its emission captured through a 580-650 nm band-pass filter. MitoTracker deep red was excited using 633 nm 5 mW Helium-Neon laser and its emission captured through a 645 nm long-pass filter.

Fat Layer Imaging

Fat layers were stained with 1 mM BODIPY 493/503. 3-10 µl of each sample was pipetted onto a 1.0 mm glass slide (EMS 71867) and covered with #1.5 thickness coverglass (EMS 72222). Imaging was performed using 63x Apochromat oil-immersion lens.

Live Cells

Cells were seeded and differentiated in glass-bottom confocal plates (MatTek P35G-0.170-14-C). On the day of the experiment, cells were stained with BODIPY 493/503 was loaded at 200 nM and 200 nM MitoTracker Deep Red (MTDR) for 60 min. MTDR was washed out before imaging, while BODIPY 493/503 present during imaging.

Fixed cells

3T3L1 cells were cultured and differentiated on coverslips and fixed at 4% vol/vol PFA for 15 min at room temperature. After washing in PBS, cells were incubated in permeabilization buffer (2 mL/mL Triton X-100, 0.5 mg/mL Sodium Deoxycholate in PBS, pH 7.4) for 15 min at room temperature. Cells were then blocked with 3 g/100 mL BSA for 1 hr at room temperature. Next, cells were incubated with 1:200 primary antibody rabbit-anti-grp75 (mitochondria) and lipid goat-anti-Plin1 (LDs) at 4°C overnight. The next day, cells were washed in PBS and incubated secondary antibodies donkey-a-rabbit-Alexa488 and donkey-a-goat-Alexa568 for 1 hr at room temperature. After washing in PBS, coverslips were mounted in MOWIOL on glass slide, air-dried, and stored at 4°C.

Image Analysis

All image analysis was performed in FIJI (ImageJ, NIH).

Image Presentation

Image contrast and brightness were not altered in any quantitative image analysis protocols. Brightness and contrast were optimized to properly display representative images in figure panels.

FIGURES

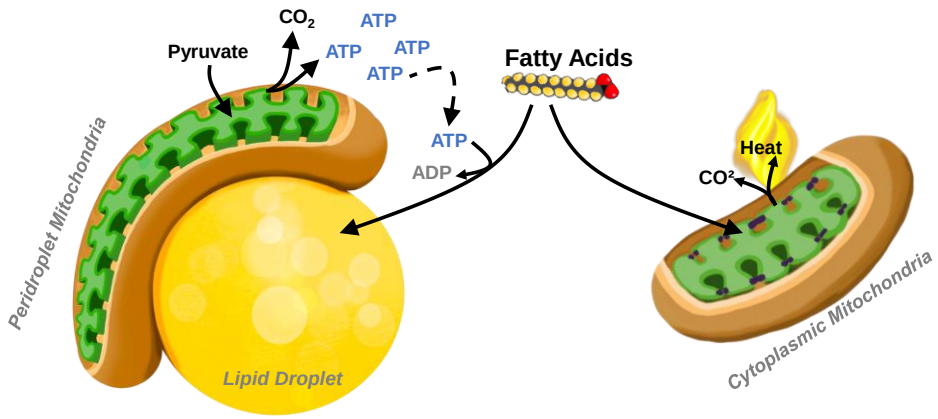

Figure 2-1: Peridroplet Mitochondria (PDM) and Cytoplasmic Mitochondria (CM).

PDM have a higher capacity to oxidize pyruvate and synthesize ATP. They provide ATP for TAG synthesis and thereby promote lipid droplet buildup. CM have a high capacity to oxidize fatty acids. The two mitochondrial populations do not fuse with each other.

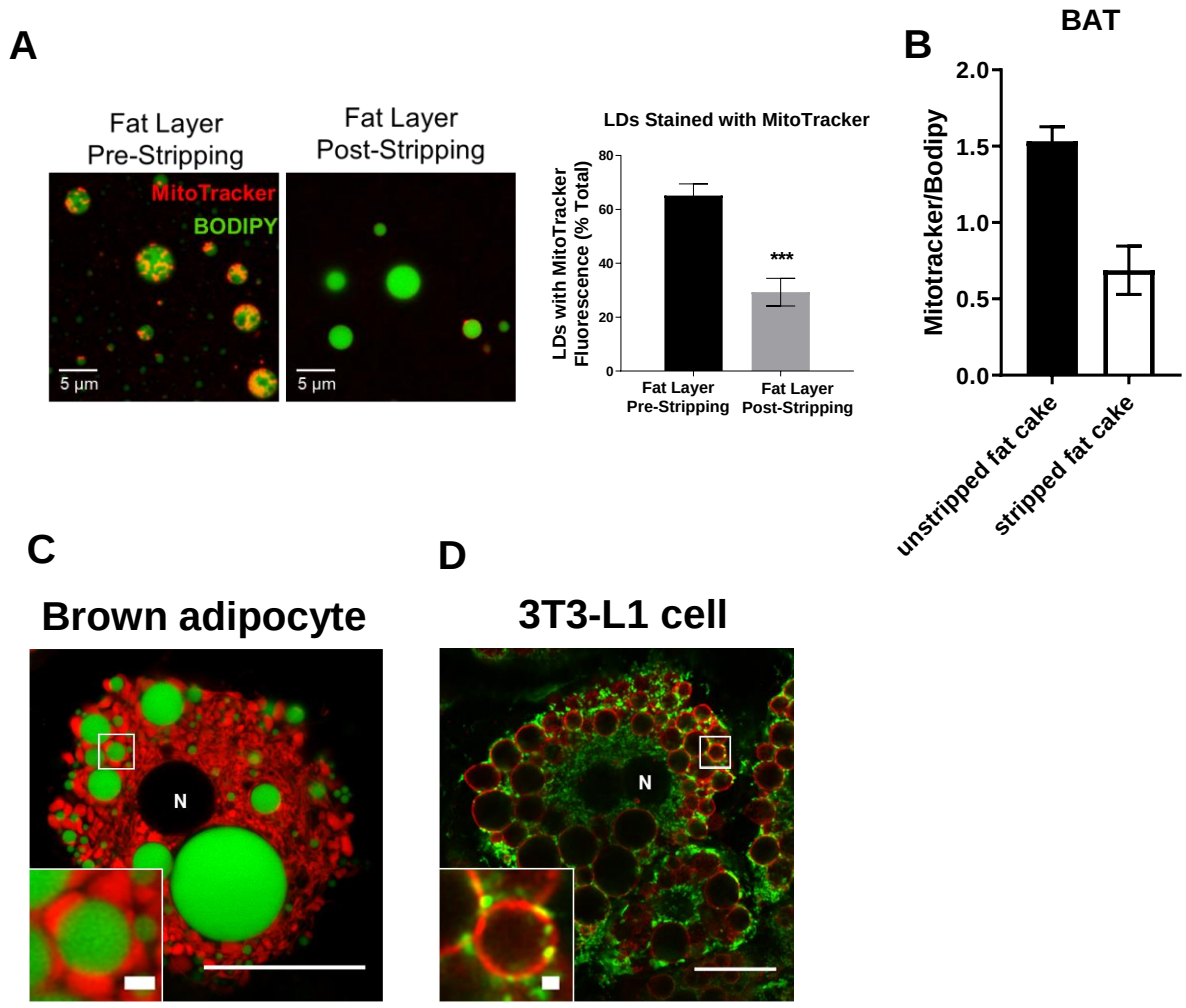

Figure 2-2: PDM isolation by high-speed centrifugation does not strip all mitochondria from lipid droplets.

(**A**) Super-resolution confocal microscopy of PDM attached to LDs before (pre-stripping) and after (post-stripping) high-speed centrifugation. Mitochondria were stained with Mitotracker deep red (MTDR) and lipid droplets with Bodipdy493. Bar graph shows quantification of LDs that contain MTDR signal. Note that even post-stripping there are still some mitochondria attached to LDs (adapted from Benador *et al*, 2018) . (**B**) PDM quantification using the fluorescence plate reader assay. Mitochondria were stained with Mitotracker deep red (MTDR) and lipid droplets with Bodipdy493. The ratio of

MTDR/Bodipy493 was quantified as a measure of PDM abundance from n=3 individual isolations. (**C**) Super-resolution confocal microscope image cultured primary mouse brown adipocyte differentiated for 7 days. Mitochondria were stained with MitoTracker Deep Red FM (red) and lipid droplets were stained with BODIPY 493/503 (green). Zoom-in box illustrates peridroplet mitochondria. N denotes nucleus. Note that smaller lipid droplets are surrounded by more mitochondria than larger lipid droplets. (**D**) Super-resolution confocal microscope image of cultured 3T3-L1 cells differentiated for 15 days. Cells were fixed in 4% PFA and mitochondria were stained with a primary antibody rabbit-anti-grp75 (green) and lipid droplets with goat-anti-Plin1 (red). Secondary antibodies used were donkey-a-rabbit-Alexa488 and donkey-a-goat-Alexa568. Zoom-in box illustrates peridroplet mitochondria. N denotes nucleus.

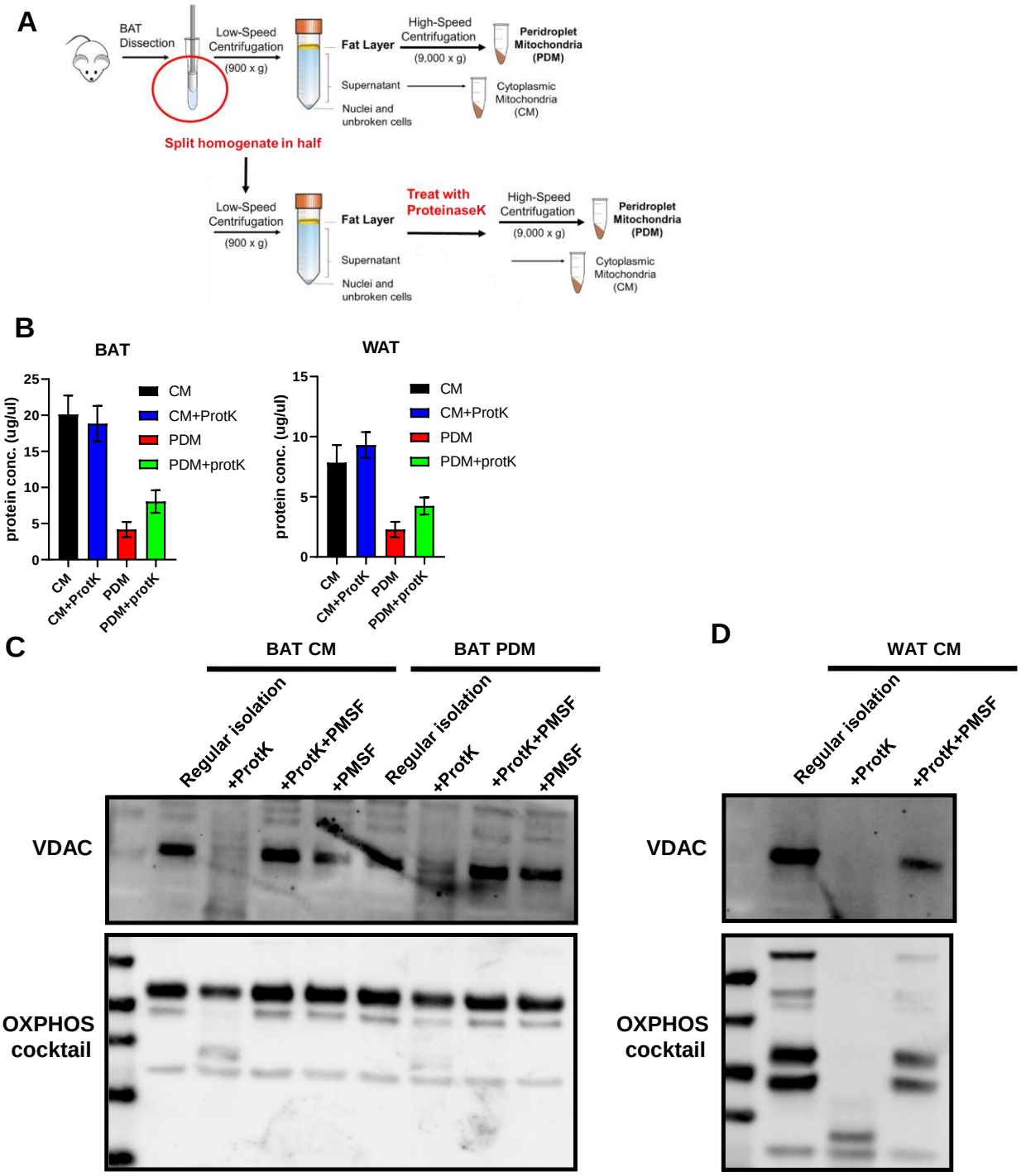

Figure 2-3: Proteolytic treatment of the fat layer increases the yield of PDM stripped from BAT and WAT lipid droplets.

(**A**) Schematic representation of optimized peridroplet (PDM) and cytoplasmic (CM) mitochondrial isolation from WAT and BAT. Fat homogenates were centrifuged at low speed to separate the fat layer containing PDM from supernatant containing CM. ProteinaseK (ProtK) was added to both fat layer and supernatant and incubated for 15 minutes. High-speed centrifugation stripped PDM from lipid droplets (LDs) and pelleted CM from the supernatant. (**B**) Protein concentration of PDM and CM after regular PDM isolation and PDM isolation with ProtK. Note that CM concertation is unchanged when isolating mitochondria using ProtK, while PDM concentration is increased when adding ProtK to the isolation protocol. (**C**) Western Blot analysis of PDM and CM isolated from BAT with regular PDM protocol or PDM isolation+ProtK. Note that ProtK treatment leads to degradation of mitochondrial proteins when samples are stored at -80C. The addition of PMSF after the 15min ProtK incubation period rescues the degradation of mitochondrial proteins. (**D**) Western Blot analysis of CM isolated from WAT with regular PDM protocol or PDM isolation+ProtK. Note that ProtK treatment leads to degradation of mitochondrial proteins when samples are stored at -80C until Western Blot analysis. The addition of PMSF after the 15min ProtK incubation period rescues the degradation of mitochondrial proteins.

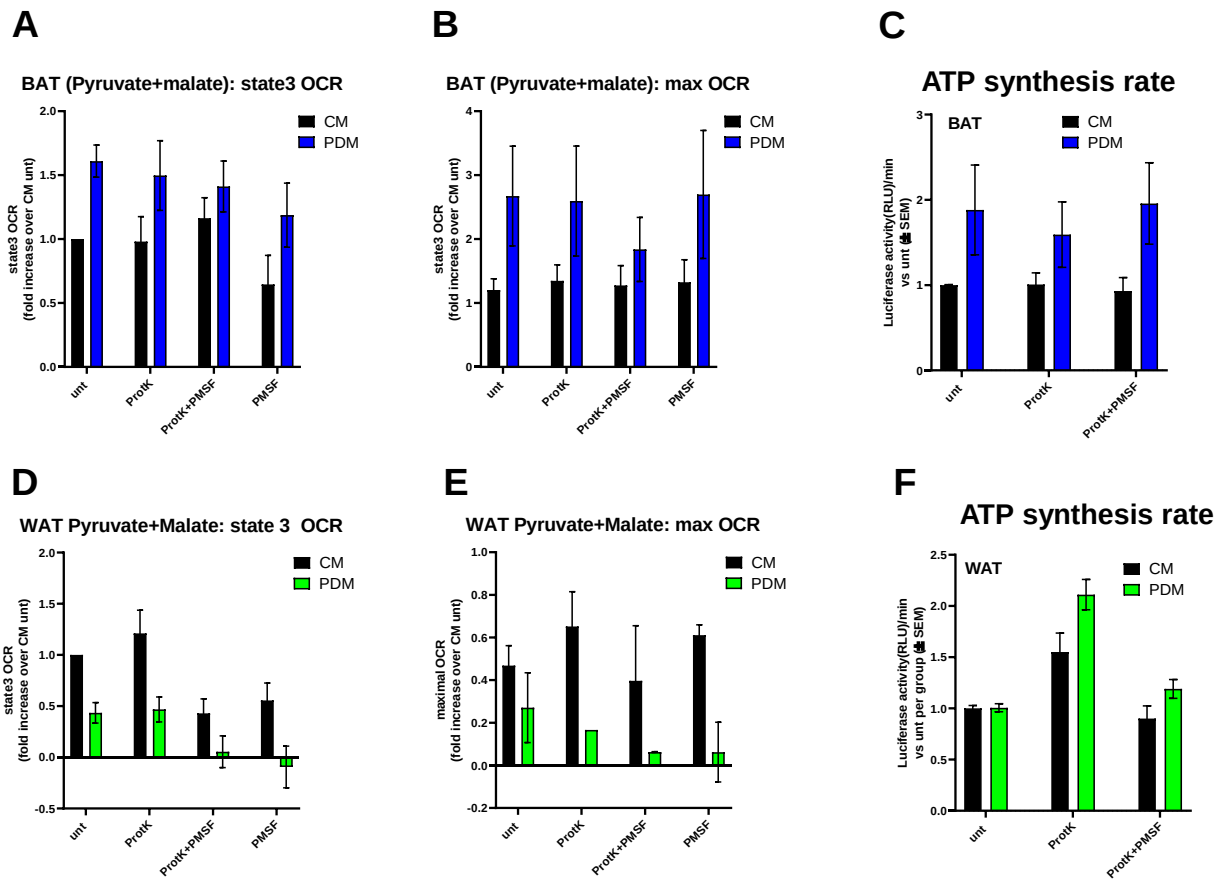

Figure 2-4: Isolation of PDM with ProtK does not inhibit mitochondrial function

(**A-C**) Assessing mitochondrial function in BAT after isolation with either regular isolation protocol, ProtK, ProtK+PMSF, or PMFS alone. (**A**) State 3 OCR of BAT mitochondria using pyruvate+malate as the substrate from n=6 independent isolations. Data were normalized to untreated CM for each individual experiment. (**B**) Maximal OCR after FCCP injection of BAT mitochondria using pyruvate+malate as the substrate from n=6 independent isolations. Data were normalized to untreated CM for each individual experiment. (**C**) Quantification of ATP synthase activity using pyruvate+malate as the substrate from n=5 independent isolations. ATP synthesis rates were determined by the rate of luminescence gain. Data were normalized to untreated CM for each individual

experiment. (**D-F**) Assessing mitochondrial function in WAT after isolation with either regular isolation protocol, ProtK, ProtK+PMSF, or PMFS alone. (**D**) State 3 OCR of WAT mitochondria using pyruvate+malate as the substrate from n=3-6 independent isolations. Data were normalized to untreated CM for each individual experiment. (**E**) Maximal OCR after FCCP injection of WAT mitochondria using pyruvate+malate as the substrate from n=3-6 independent isolations. Data were normalized to untreated CM for each individual experiment. (**F**) Quantification of ATP synthase activity using pyruvate+malate as the substrate from n=5 independent isolations. ATP synthesis rates were determined by the rate of luminescence gain. Data were normalized to untreated CM for each individual experiment.

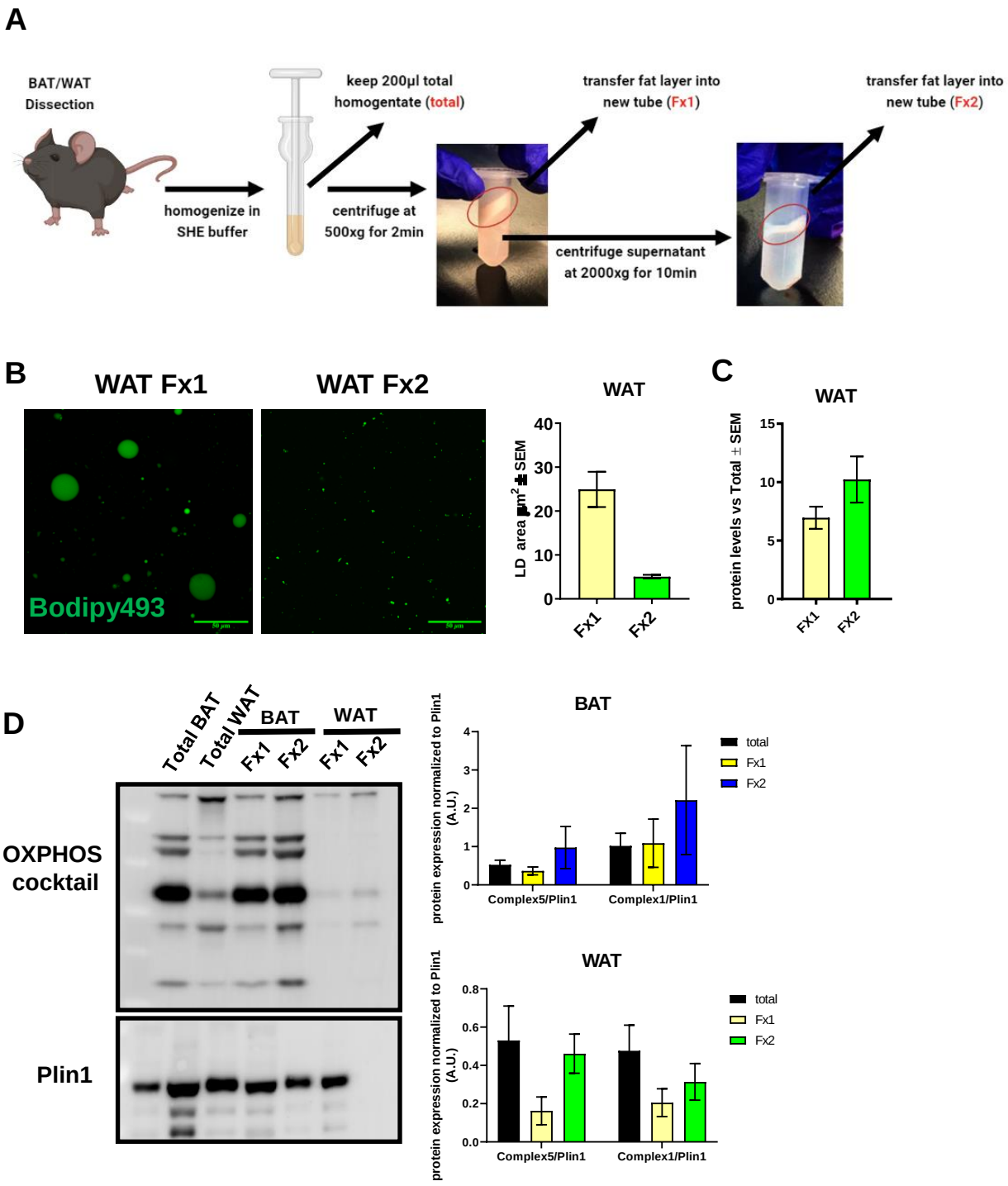

Figure 2-5: Proteinase K treatment enables the isolation of mitochondria attached to smaller LDs

(**A**) Schematic representation of the isolation protocol for small and large LDs. Tissue was homogenized and strained through a large filter. Homogenates were first centrifuged at 500g to create a fat layer containing large LDs (Fx1). After removing the first fat layer homogenates were centrifuged at 2000g to create a second fat layer containing small LDs (Fx2). (**B**) Super-resolution confocal microscopy of Fx1 and Fx2 fat layer isolated from WAT. The fat layer was stained with Bodipy494. Bar graph shows quantification of images. Note that Fx2 contains significantly smaller LDs than Fx1. (**C**) Assessing the amount of PDM associated with Fx1 versus Fx2 LD. The bar graph shows PDM quantification from WAT using the fluorescence plate reader assay. Mitochondria were stained with Mitotracker deep red and lipid droplets with Bodipdy493. The ratio of MTDR/Bodipy493 was quantified as a measure of PDM abundance. Note that Fx2 contains more PDM than Fx1. (**D**) Representative Western Blot of total fat homogenates (total), Fx1 and Fx2 from BAT and WAT. Bar graphs show quantification of n=3-4 independent isolations. Expression of mitochondrial complex 5 and 1 were normalized to Plin1 expression for each sample as a way to normalize for lipid droplet content in the sample.

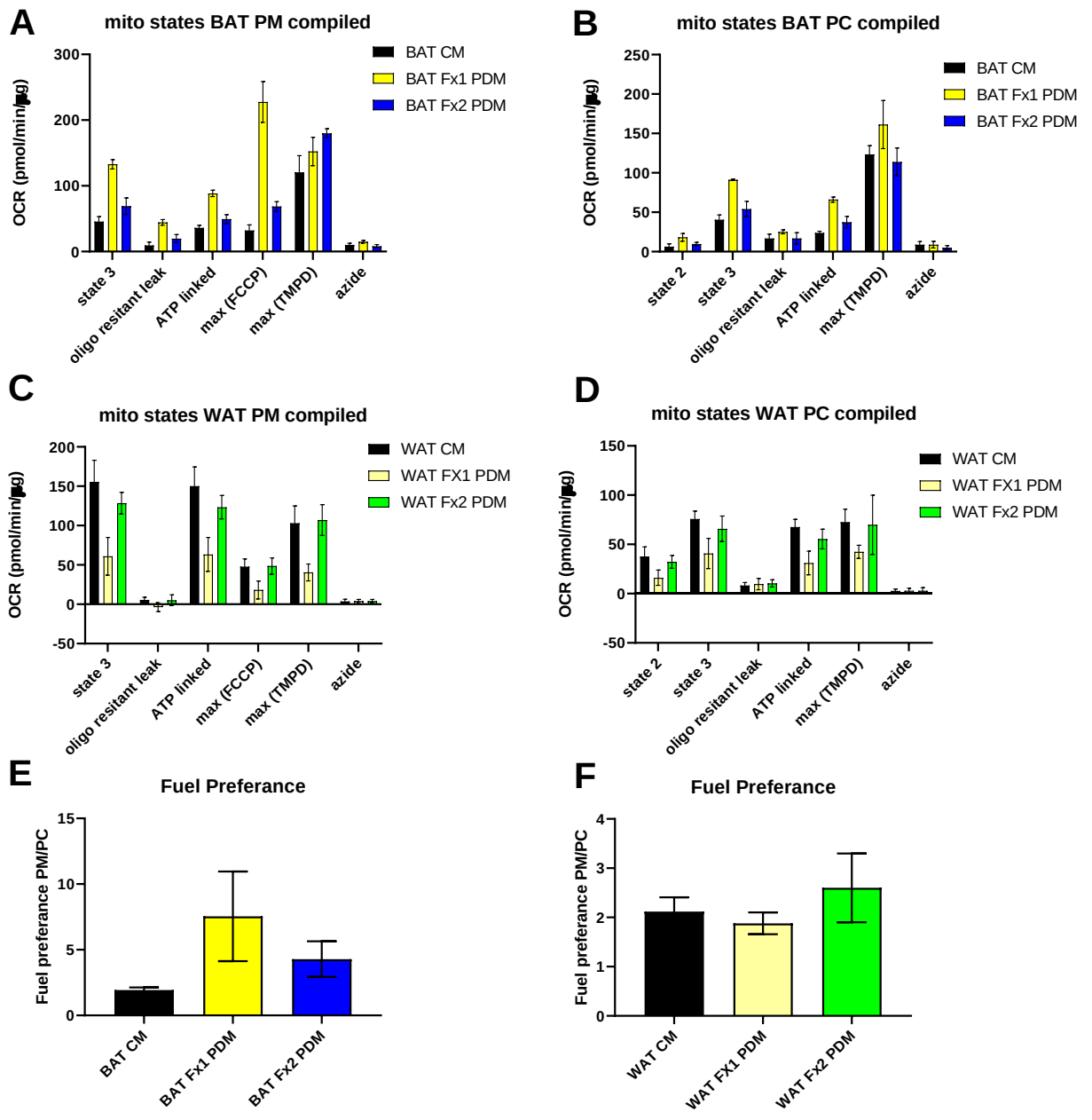

Figure 2-6: PDM from Fx2 have unique characteristics.

(**A-B**) Assessing mitochondrial function in PDM isolated from Fx1 and Fx2 compared to CM. All mitochondria were isolated from BAT using the ProtK protocol. (**A**) Quantification of state 3, mitochondrial proton leak, ATP-linked, maximal, and complex 4 OCR from n=4 individual isolations using pyruvate+malate as substrate. (**B**) Quantification of state 2,

state 3, mitochondrial proton leak, ATP-linked, and maximal OCR from n=4 individual isolations using palmitoyl-carnitine+malate as substrate. (**C-D**) Assessing mitochondrial function in PDM isolated from Fx1 and Fx2 compared to CM. All mitochondria were isolated from WAT using the ProtK protocol. (**C**) Quantification of state 3, mitochondrial proton leak, ATP-linked, maximal, and complex 4 OCR from n=4 individual isolations using pyruvate+malate as substrate. (**D**) Quantification of state 2, state 3, mitochondrial proton leak, ATP-linked, and maximal OCR from n=4 individual isolations using palmitoyl-carnitine+malate as substrate. (**E**) Quantification of mitochondrial fuel preference in BAT calculated as the ratio of maximal OCR from pyruvate+malate versus palmitoyl-carnitine+malate from n=2 individual isolations. (**F**) Quantification of mitochondrial fuel preference in WAT calculated as the ratio of maximal OCR from pyruvate+malate versus palmitoyl-carnitine+malate from n=2 individual isolations.

Table 2: Mechanisms of Mitochondria-Lipid Droplet Interaction

Proposed Tether	Mechanism of Tethering	Cell Type	Technique	Interaction with ER	Effects on *de novo* lipogenesis and fatty acid esterification	Reference
Perilipin5 (Plin5)	C-terminus of Plin5 regulates interaction with mitochondria	CHO, AML12, HL-1, primary brown adipocytes, INS1	site-directed mutagenesis, confocal fluorescence microscopy	N/A	*de novo*: N/A FA esterification: increased	Wang et al., 2011; Benador et al., 2018
DGAT2	N-terminus of DGAT2	COS-7	site-directed mutagenesis, confocal fluorescence microscopy, cell fractionation	Yes	*de novo*: increased FA esterification: N/A	Stone et al., 2009
Mfn2	Mfn2 interaction with Plin1	primary brown adipocytes	co-immunoprecipitation	Yes	*de novo*: N/A FA esterification: N/A	Boutant et al., 2017
MIGA2	C-terminus of MIGA2 targets mitochondria and N-terminus targets LDs	COS-7, 3T3-L1	site-directed mutagenesis, confocal fluorescence microscopy and electron microscopy	Yes	*de novo*: increased FA esterification: N/A	Freyre et al., 2019

CONCLUSIONS AND FUTURE DIRECTIONS

Potential for PDM as therapeutic target

*Evidence that PDM can be beneficial (**Table 3**)*

Previous publications suggest that one important role of PDM is to provide ATP for TAG synthesis and LD expansion (Benador *et al*, 2018). Although increasing PDM content may not be a good approach to increase fat consumption, it may represent an approach to prevent lipodystrophy and/or lipotoxicity by securing free fatty acids into TAG (**Figure 3-1**). Indeed, TAG accumulation was shown to protect from FFA-induced lipotoxicity by channeling palmitate into neutral lipid pools (Listenberger *et al*, 2003). Furthermore, ectopic accumulation of LDs in skeletal muscle is not only associated with increased body weight and type 2 diabetes, but, paradoxically, also observed in endurance athletes, further suggesting that TAG accumulation can have positive effects (Li *et al*, 2019; Amati *et al*, 2011).

While there are only few relevant studies assessing the role of PDM in adipose tissue to date, we can gain some ideas on the role of PDM in fat storing cells from other cell model and over-expression models. Most of our understanding of the possible role of PDM in protecting from lipotoxicity comes from studies using Plin5 overexpression (OE) models, or Plin5 knock-out (KO) models. Interpreting these studies in the context of PDM comes with various caveats, as Plin5 OE will not only induce PDM attachment, but also inhibit lipolysis through its function inhibiting ATGL (Sztalryd & Kimmel, 2014). Results from studies using Plin5 KO models might also be difficult to interpret, as these cells or mice usually have uncontrolled lipolysis, which could come from lack of Plin5 regulating ATGL,

or a lack of PDM, or a combination thereof. Keeping these caveats in mind there are still some interesting things to learn about PDM from Plin5 KO/gain-of-function models.

In agreement with the hypothesis that PDM are essential to protect from lipid induced damage, Plin5 KO in cardiac muscle caused increased sensitivity to ischemic injury (Drevinge *et al*, 2016; Zheng *et al*, 2017; Kuramoto *et al*, 2012), while Plin5 gain-of-function did not cause major cardiac damage, and was even cardio-protective despite LD accumulation (Pollak *et al*, 2013; Wang *et al*, 2013). In a recent study, Du and colleagues found endogenous Plin5 expression to be increased in cardiac epithelial cells in response to gluco-lipotoxicity, conferring a protective effect against FFA-ROS mediated microvascular injury. On the other hand, this type of injury was exacerbated by Plin5 KO in a model of type-2-diabetes with high circulating FFAs and in models of heart failure (Du *et al*, 2019; Wang *et al*, 2019). Furthermore, Plin5 deletion in hepatocytes led to reduced insulin sensitivity, which was associated with decreased fatty acid uptake and storage (Keenan *et al*, 2019). Remarkably, PDM may be linked to inflammatory processes in the liver, as Plin5 OE was shown to restore quiescence in hepatic stellate cells in a liver fatty acid-binding protein dependent manner (Chen *et al*, 2013; Lin *et al*, 2018; Lin & Chen, 2016). Endogenous Plin5 expression in pancreatic islets was stimulated upon fasting induced increases in serum FFAs, supported post-prandial insulin secretion, and Plin5-OE improved glucose tolerance (Trevino *et al*, 2015). Moreover, overexpression of Plin5 in INS1 pancreatic β-cells protected from palmitate induced lipotoxicity and ER stress (Zhu *et al*, 2019). Plin5 expression was found to be elevated in endurance conditioned human muscle, increasing metabolic flexibility, insulin sensitivity, and protection against lipotoxicity, which can also be recapitulated by Plin5 OE further implicating PDM

involvement in the metabolic health of the whole body and skeletal muscle (Bosma *et al*, 2013; Laurens *et al*, 2016). Furthermore, Gemmink et al. found that fasting induced endogenous Plin5 expression correlated with increased insulin sensitivity, and LDs generated de novo in the fasting phase were exclusively associated with Plin5, suggesting PDM as the essential protective mechanism against lipotoxicity in skeletal muscle (Gemmink *et al*, 2016).

Although it may seem counterintuitive to increase LD content as a therapy for diabetes, studies using the insulin sensitizers Thiazolidinediones (TZDs) suggest that increased adiposity is not in conflict with improved insulin sensitivity (Saltiel & Olefsky, 1996). TZDs are PPARgamma agonist that show very promising results in improving diabetic insulin sensitivity, despite their stimulatory effect on adipocyte differentiation and expansion. Indeed, Rosiglitazone has been shown to briten human WAT ex vivo in part through stimulation of PLIN5 expression, and the formation of small, satellite, PDM coated LDs (Lee *et al*, 2019). These studies are in favor of increasing PDM content to promote LD synthesis, as they suggest that an increase in overall fat mass may not be the problem, if the fat is partitioned to LD, and thereby stored in a safe place.

*Evidence that detaching PDM from the LD can be beneficial (**Table 3**)*

Previous studies show that upon adrenergic stimulation, BAT PDM detach from the LD, and that mitochondria undergo fragmentation (Benador *et al*, 2018; Wikstrom *et al*, 2014). While mitochondrial fragmentation is necessary for Norepinephrine-stimulated energy expenditure, it remains to be determined, whether PDM detachment is necessary as well,

in order to reach maximal thermogenic capacity. In addition, the observation that OCR upon adrenergic stimulation are not completely insensitive to the mitochondrial ATP synthase inhibitor oligomycin, may suggest that even under adrenergic stimulation there are PDM that remain attached, and possibly play a role in adrenergically stimulated lipid cycling. Detaching PDM from LDs may represent a promising approach to increase fat oxidation and energy expenditure, particularly in WAT or BAT. However, it is important to note that this strategy might result in accumulation of toxic free fatty acids, if it is not concurrent to UCP1 activation or increased mitochondrial fat oxidation. Although a direct assessment of the toxic effect of lack of PDM remains to be established, we can infer interesting information from studies using PLIN5 or DGAT2 KO models. In this context, DGAT2 KO mice die shortly after birth, due to severe lipopenia, which could not be rescued by OE of DGAT1 (Stone *et al*, 2004, 2). Even though the exact mechanism remains unclear, it is conceivable that part or the mechanism, by which DGAT2 KO is lethal, is through a lack of PDM. Possibly DGAT2 KO are void of PDM and are unable to esterify fatty acids, leading to exaggerated lipotoxicity.

Nonetheless, acute detachment in brown adipocytes, such as under Norepinephrine stimulation, could represent a valuable tool to promote fat oxidation. In this context, BAT-specific knock-out of Mfn2 resulted in resistance to diet induced obesity, and increased capacity of mitochondria to oxidize fatty acids in female mice, despite impaired cold tolerance (Mahdaviani *et al*, 2017). Given that Mfn2 KO in these mice also showed reduced interaction of mitochondria and LD, this may suggest that PDM detachment contributes to resistance to HFD and further suggests that PDM are necessary for regulation of inducible thermogenesis (Mahdaviani *et al*, 2017, 2; Boutant *et al*, 2017, 2).

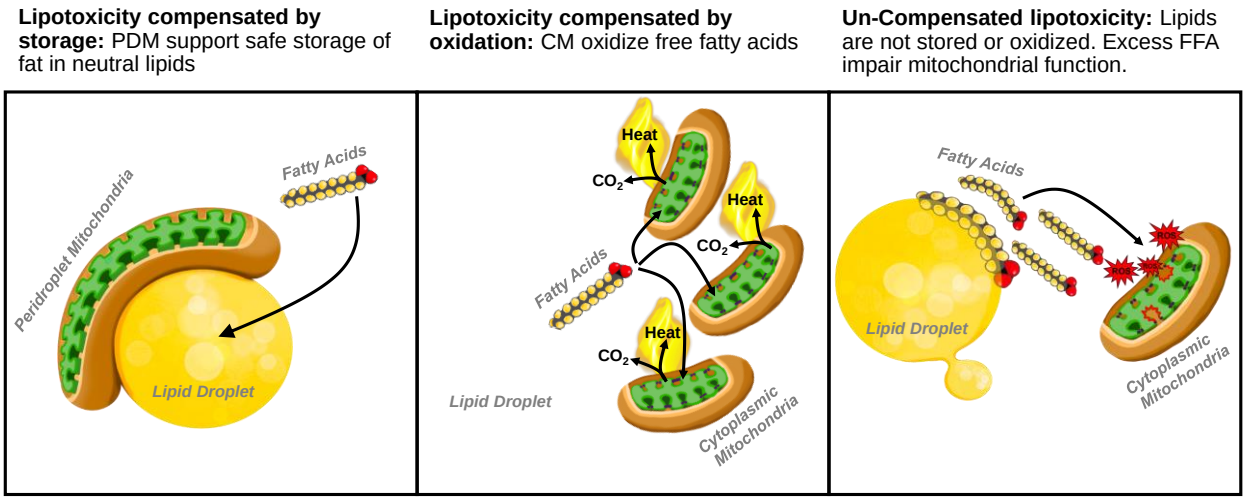

Figure 3-1: Possible role of PDM and CM in protection from lipotoxicity.

Both PDM and CM contribute to the removal of FFA and the prevention of lipotoxicity. While PDM support removal of FFA into storage, CM consume FFA as a fuel source. When lipids are not consumed or stored, lipotoxicity can impair mitochondrial function.

Table 3: Benefits and Pathologies related to PDM

Tissue/Cell type	Model	PDM increase or decrease	Observation	Reference
Whole body	DGAT2 KO	N/A	Lethal due to Lipopenia	Stone et al., 2004
Heart	Plin5 KO	Decreased (little to no lipid droplets)	Reduced lipid storage and increase in fatty acid oxidation; Increased sensitivity to ischemic injury by lipid induced oxidative stress; Aggravated myocardial hypertrophy in the model of heart failure	Kuramoto et al., 2012 Drevinge et. al., 2016; Zheng et al., 2017; Wang et al., 2019
Heart	Plin5 OE	increased	Increase in TAG content and reduced expression of FA oxidizing genes; cardiac steatosis with only mild impairment to cardiac function	Pollak et al., 2013; Wang et al., 2013
Hepatic stellate cells (HSC)	Plin5 OE	N/A	HSC lower Plin5 expression upon activation; exogenous expression of Plin5 lowers oxidative stress and inhibits HSC activation	Lin et al., 2016;
Hepatocytes	Plin5 KO	decreased	Reduced insulin sensitivity, reduced fatty acid uptake and storage	Keenan et al., 2019
Hepatocyte	Plin5 OE	increased	Resistance against H_2O_2 induced oxidative stress	Tan et al., 2019
Pancreatic β-cells	Plin5 OE	N/A	Improved glucose tolerance; Protection from lipotoxicity and ER stress	Trevino et al., 2015; Zhu et al., 2019
Brown adipose tissue	Mfn2 KO	decreased	Impaired cold tolerance, but increased resistance to HFD induced obesity in female mice; increased mitochondrial capacity to oxidize fatty acids	Boutant et al., 2017; Mahdaviani et al., 2017
Skeletal muscle	Plin5 OE	N/A	Increased LD size and improved mitochondrial function while maintaining insulin-sensitivity; Protection against lipotoxicity	Bosma et al., 2013; Laurens et al., 2016

REFERENCES

Alsabeeh N, Chausse B, Kakimoto PA, Kowaltowski AJ & Shirihai O (2018) Cell culture models of fatty acid overload: Problems and solutions. *Biochim Biophys Acta BBA - Mol Cell Biol Lipids* 1863: 143–151

Amati F, Dubé JJ, Alvarez-Carnero E, Edreira MM, Chomentowski P, Coen PM, Switzer GE, Bickel PE, Stefanovic-Racic M, Toledo FGS, *et al* (2011) Skeletal muscle triglycerides, diacylglycerols, and ceramides in insulin resistance: another paradox in endurance-trained athletes? *Diabetes* 60: 2588–2597

Angel A, Desai K & Halperin ML (1971) Free fatty acid and ATP levels in adipocytes during lipolysis. *Metabolism* 20: 87–99

Arruda AP, Pers BM, Parlakgül G, Güney E, Inouye K & Hotamisligil GS (2014) Chronic enrichment of hepatic endoplasmic reticulum–mitochondria contact leads to mitochondrial dysfunction in obesity. *Nat Med* 20: 1427–1435

Benador IY, Veliova M, Liesa M & Shirihai OS (2019) Mitochondria Bound to Lipid Droplets: Where Mitochondrial Dynamics Regulate Lipid Storage and Utilization. *Cell Metab* 29: 827–835

Benador IY, Veliova M, Mahdaviani K, Petcherski A, Wikstrom JD, Assali EA, Acín-Pérez R, Shum M, Oliveira MF, Cinti S, *et al* (2018) Mitochondria Bound to Lipid Droplets Have Unique Bioenergetics, Composition, and Dynamics that Support Lipid Droplet Expansion. *Cell Metab* 27: 869–885.e6

Bertholet AM, Kazak L, Chouchani ET, Bogaczyńska MG, Paranjpe I, Wainwright GL, Bétourné A, Kajimura S, Spiegelman BM & Kirichok Y (2017) Mitochondrial Patch Clamp of Beige Adipocytes Reveals UCP1-Positive and UCP1-Negative Cells Both Exhibiting Futile Creatine Cycling. *Cell Metab* 25: 811–822.e4

Bhatt-Wessel B, Jordan TW, Miller JH & Peng L (2018) Role of DGAT enzymes in triacylglycerol metabolism. *Arch Biochem Biophys* 655: 1–11

Bischof J, Salzmann M, Streubel MK, Hasek J, Geltinger F, Duschl J, Bresgen N, Briza P, Haskova D, Lejskova R, *et al* (2017) Clearing the outer mitochondrial membrane from harmful proteins via lipid droplets. *Cell Death Discov* 3

Blaszkiewicz M, Willows JW, Johnson CP & Townsend KL (2019) The Importance of Peripheral Nerves in Adipose Tissue for the Regulation of Energy Balance. *Biology* 8: 10

Bleck CKE, Kim Y, Willingham TB & Glancy B (2018) Subcellular connectomic analyses of energy networks in striated muscle. *Nat Commun* 9

Bosma M, Sparks LM, Hooiveld GJ, Jorgensen JA, Houten SM, Schrauwen P, Kersten S & Hesselink MKC (2013) Overexpression of PLIN5 in skeletal muscle promotes oxidative gene expression and intramyocellular lipid content without compromising insulin sensitivity. *Biochim Biophys Acta* 1831: 844–852

Boutant M, Kulkarni SS, Joffraud M, Ratajczak J, Valera-Alberni M, Combe R, Zorzano A & Cantó C (2017) Mfn2 is critical for brown adipose tissue thermogenic function. *EMBO J* 36: 1543–1558

Bricker DK, Taylor EB, Schell JC, Orsak T, Boutron A, Chen Y-C, Cox JE, Cardon CM, Van Vranken JG, Dephoure N, *et al* (2012) A Mitochondrial Pyruvate Carrier Required for Pyruvate Uptake in Yeast, *Drosophila* , and Humans. *Science* 337: 96–100

de Brito OM & Scorrano L (2008) Mitofusin 2 tethers endoplasmic reticulum to mitochondria. *Nature* 456: 605

Cannon B (2004) Brown Adipose Tissue: Function and Physiological Significance. *Physiol Rev* 84: 277–359

Cannon B & Nedergaard J (1979) The Physiological Role of Pyruvate Carboxylation in Hamster Brown Adipose Tissue. *Eur J Biochem* 94: 419–426

Cannon B & Nedergaard J (2004) Brown Adipose Tissue: Function and Physiological Significance. *Physiol Rev* 84: 277–359

Carobbio S, Pellegrinelli V & Vidal-Puig A (2017) Adipose Tissue Function and Expandability as Determinants of Lipotoxicity and the Metabolic Syndrome. In *Obesity and Lipotoxicity*, Engin AB & Engin A (eds) pp 161–196. Cham: Springer International Publishing

Chen A, Tang Y, Davis V, Hsu F-F, Kennedy SM, Song H, Turk J, Brunt EM, Newberry EP & Davidson NO (2013) Liver fatty acid binding protein (L-Fabp) modulates murine stellate cell activation and diet-induced nonalcoholic fatty liver disease. *Hepatol Baltim Md* 57: 2202–2212

Chitraju C, Mejhert N, Haas JT, Diaz-Ramirez LG, Grueter CA, Imbriglio JE, Pinto S, Koliwad SK, Walther TC & Farese RV (2017) Triglyceride Synthesis by DGAT1 Protects Adipocytes from Lipid-Induced ER Stress during Lipolysis. *Cell Metab* 26: 407–418.e3

Cordes T & Metallo CM (2019) Quantifying Intermediary Metabolism and Lipogenesis in Cultured Mammalian Cells Using Stable Isotope Tracing and Mass Spectrometry. In *High-Throughput Metabolomics*, D'Alessandro A (ed) pp 219–241. New York, NY: Springer New York

Cornell NW, Zuurendonk PF, Kerich MJ & Straight CB (1984) Selective inhibition of alanine aminotransferase and aspartate aminotransferase in rat hepatocytes. *Biochem J* 220: 707–716

Cui L, Mirza AH, Zhang S, Liang B & Liu P (2019) Lipid droplets and mitochondria are anchored during brown adipocyte differentiation. *Protein Cell* 10: 921–926

Cypess AM, Lehman S, Williams G, Tal I, Rodman D, Goldfine AB, Kuo FC, Palmer EL, Tseng Y-H, Doria A, *et al* (2009a) Identification and Importance of Brown Adipose Tissue in Adult Humans. *N Engl J Med* 360: 1509–1517

Cypess AM, Lehman S, Williams G, Tal I, Rodman D, Goldfine AB, Kuo FC, Palmer EL, Tseng Y-H, Doria A, *et al* (2009b) Identification and Importance of Brown Adipose Tissue in Adult Humans. *N Engl J Med* 360: 1509–1517

Deng Y, Wang ZV, Gordillo R, Zhu Y, Ali A, Zhang C, Wang X, Shao M, Zhang Z, Iyengar P, *et al* (2018) Adipocyte Xbp1s overexpression drives uridine production and reduces obesity. *Mol Metab* 11: 1–17

Divakaruni AS & Brand MD (2011) The Regulation and Physiology of Mitochondrial Proton Leak. *Physiology* 26: 192–205

Divakaruni AS, Hsieh WY, Minarrieta L, Duong TN, Kim KKO, Desousa BR, Andreyev AY, Bowman CE, Caradonna K, Dranka BP, *et al* (2018) Etomoxir Inhibits Macrophage Polarization by Disrupting CoA Homeostasis. *Cell Metab* 28: 490–503.e7

Divakaruni AS, Wallace M, Buren C, Martyniuk K, Andreyev AY, Li E, Fields JA, Cordes T, Reynolds IJ, Bloodgood BL, *et al* (2017) Inhibition of the mitochondrial pyruvate carrier protects from excitotoxic neuronal death. *J Cell Biol* 216: 1091–1105

Divakaruni AS, Wiley SE, Rogers GW, Andreyev AY, Petrosyan S, Loviscach M, Wall EA, Yadava N, Heuck AP, Ferrick DA, *et al* (2013) Thiazolidinediones are acute, specific inhibitors of the mitochondrial pyruvate carrier. *Proc Natl Acad Sci* 110: 5422–5427

Drevinge C, Dalen KT, Mannila MN, Täng MS, Ståhlman M, Klevstig M, Lundqvist A, Mardani I, Haugen F, Fogelstrand P, *et al* (2016) Perilipin 5 is protective in the ischemic heart. *Int J Cardiol* 219: 446–454

Du J, Hou J, Feng J, Zhou H, Zhao H, Yang D, Li D, Yang Y & Pei H (2019) Plin5/p-Plin5 Guards Diabetic CMECs by Regulating FFAs Metabolism Bidirectionally. *Oxid Med Cell Longev* 2019: 8690746

Duncan RE, Ahmadian M, Jaworski K, Sarkadi-Nagy E & Sul HS (2007) Regulation of Lipolysis in Adipocytes. *Annu Rev Nutr* 27: 79–101

Fain JN & Rosenthal JW (1971) Calorigenic Action of Triiodothyronine on White Fat Cells: Effects of Ouabain, Oligomycin, and Catecholamines. *Endocrinology* 89: 1205–1211

Fedorenko A, Lishko PV & Kirichok Y (2012) Mechanism of Fatty-Acid-Dependent UCP1 Uncoupling in Brown Fat Mitochondria. *Cell* 151: 400–413

Forner F, Kumar C, Luber CA, Fromme T, Klingenspor M & Mann M (2009) Proteome Differences between Brown and White Fat Mitochondria Reveal Specialized Metabolic Functions. *Cell Metab* 10: 324–335

Freyre CAC, Rauher PC, Ejsing CS & Klemm RW (2019) MIGA2 Links Mitochondria, the ER, and Lipid Droplets and Promotes De Novo Lipogenesis in Adipocytes. *Mol Cell*

Gallardo-Montejano VI, Saxena G, Kusminski CM, Yang C, McAfee JL, Hahner L, Hoch K, Dubinsky W, Narkar VA & Bickel PE (2016) Nuclear Perilipin 5 integrates lipid droplet lipolysis with PGC-1α/SIRT1-dependent transcriptional regulation of mitochondrial function. *Nat Commun* 7

Geiger T, Velic A, Macek B, Lundberg E, Kampf C, Nagaraj N, Uhlen M, Cox J & Mann M (2013) Initial Quantitative Proteomic Map of 28 Mouse Tissues Using the SILAC Mouse. *Mol Cell Proteomics* 12: 1709–1722

Gemmink A, Bosma M, Kuijpers HJH, Hoeks J, Schaart G, van Zandvoort MAMJ, Schrauwen P & Hesselink MKC (2016) Decoration of intramyocellular lipid droplets with PLIN5 modulates fasting-induced insulin resistance and lipotoxicity in humans. *Diabetologia* 59: 1040–1048

Goldman SJ, Zhang Y & Jin S (2011) Autophagic Degradation of Mitochondria in White Adipose Tissue Differentiation. *Antioxid Redox Signal* 14: 1971–1978

Gorin E, Tal-Or Z & Shafrir E (1969) Glyceroneogenesis in Adipose Tissue of Fasted, Diabetic and Triamcinolone Treated Rats. *Eur J Biochem* 8: 370–375

Gray LR, Sultana MR, Rauckhorst AJ, Oonthonpan L, Tompkins SC, Sharma A, Fu X, Miao R, Pewa AD, Brown KS, *et al* (2015) Hepatic Mitochondrial Pyruvate Carrier 1 Is Required for Efficient Regulation of Gluconeogenesis and Whole-Body Glucose Homeostasis. *Cell Metab* 22: 669–681

Halestrap AP (1975) The mitochondrial pyruvate carrier. Kinetics and specificity for substrates and inhibitors. *Biochem J* 148: 85–96

Hammond VA & Johnston DG (1987) Substrate cycling between triglyceride and fatty acid in human adipocytes. *Metabolism* 36: 308–313

Hankir MK, Kranz M, Keipert S, Weiner J, Andreasen SG, Kern M, Patt M, Klöting N, Heiker JT, Brust P, *et al* (2017) Dissociation Between Brown Adipose Tissue ^{18}F-FDG Uptake and Thermogenesis in Uncoupling Protein 1–Deficient Mice. *J Nucl Med* 58: 1100–1103

Harms M & Seale P (2013) Brown and beige fat: development, function and therapeutic potential. *Nat Med* 19: 1252–1263

Harper RD & Saggerson ED (1975) Some aspects of fatty acid oxidation in isolated fat-cell mitochondria from rat. *Biochem J* 152: 485–494

Heaton GM, Wagenvoord RJ, Kemp A & Nicholls DG (1978) Brown-Adipose-Tissue Mitochondria: Photoaffinity Labelling of the Regulatory Site of Energy Dissipation. *Eur J Biochem* 82: 515–521

Herms A, Bosch M, Reddy BJN, Schieber NL, Fajardo A, Rupérez C, Fernández-Vidal A, Ferguson C, Rentero C, Tebar F, *et al* (2015) AMPK activation promotes lipid droplet dispersion on detyrosinated microtubules to increase mitochondrial fatty acid oxidation. *Nat Commun* 6

Hernández-Alvarez MI, Sebastián D, Vives S, Ivanova S, Bartoccioni P, Kakimoto P, Plana N, Veiga SR, Hernández V, Vasconcelos N, *et al* (2019) Deficient Endoplasmic Reticulum-Mitochondrial Phosphatidylserine Transfer Causes Liver Disease. *Cell* 177: 881–895.e17

Herzig S, Raemy E, Montessuit S, Veuthey J-L, Zamboni N, Westermann B, Kunji ERS & Martinou J-C (2012) Identification and Functional Expression of the Mitochondrial Pyruvate Carrier. *Science* 337: 93–96

Ikeda K, Kang Q, Yoneshiro T, Camporez JP, Maki H, Homma M, Shinoda K, Chen Y, Lu X, Maretich P, *et al* (2017) UCP1-independent signaling involving SERCA2b-mediated calcium cycling regulates beige fat thermogenesis and systemic glucose homeostasis. *Nat Med* 23: 1454–1465

Indiveri C, Palmieri F, Bisaccia F & Krämer R (1987) Kinetics of the reconstituted 2-oxoglutarate carrier from bovine heart mitochondria. *Biochim Biophys Acta BBA - Bioenerg* 890: 310–318

Irshad Z, Dimitri F, Christian M & Zammit VA (2017) Diacylglycerol acyltransferase 2 links glucose utilization to fatty acid oxidation in the brown adipocytes. *J Lipid Res* 58: 15–30

Kauppinen RA, Sihra TS & Nicholls DG (1987) Aminooxyacetic acid inhibits the malate-aspartate shuttle in isolated nerve terminals and prevents the mitochondria from utilizing glycolytic substrates. *Biochim Biophys Acta BBA - Mol Cell Res* 930: 173–178

Kazak L, Chouchani ET, Jedrychowski MP, Erickson BK, Shinoda K, Cohen P, Vetrivelan R, Lu GZ, Laznik-Bogoslavski D, Hasenfuss SC, *et al* (2015) A Creatine-Driven Substrate Cycle Enhances Energy Expenditure and Thermogenesis in Beige Fat. *Cell* 163: 643–655

Keenan SN, Meex RC, Lo JCY, Ryan A, Nie S, Montgomery MK & Watt MJ (2019) Perilipin 5 Deletion in Hepatocytes Remodels Lipid Metabolism and Causes Hepatic Insulin Resistance in Mice. *Diabetes* 68: 543–555

Kershaw EE & Flier JS (2004) Adipose Tissue as an Endocrine Organ. *J Clin Endocrinol Metab* 89: 2548–2556

Kiorpes TC, Hoerr D, Ho W, Weaner LE, Inman MG & Tutwiler GF (1984) Identification of 2-tetradecylglycidyl coenzyme A as the active form of methyl 2-tetradecylglycidate (methyl palmoxirate) and its characterization as an irreversible, active site-directed inhibitor of carnitine palmitoyltransferase A in isolated rat liver mitochondria. *J Biol Chem* 259: 9750–9755

Koh EH, Park J-Y, Park H-S, Jeon MJ, Ryu JW, Kim M, Kim SY, Kim M-S, Kim S-W, Park IS, *et al* (2007) Essential Role of Mitochondrial Function in Adiponectin Synthesis in Adipocytes. *Diabetes* 56: 2973–2981

Kolleritsch S, Kien B, Schoiswohl G, Diwoky C, Schreiber R, Heier C, Maresch LK, Schweiger M, Eichmann TO, Stryeck S, *et al* (2019) Low cardiac lipolysis reduces mitochondrial fission and prevents lipotoxic heart dysfunction in Perilipin 5 mutant mice. *Cardiovasc Res*

Kotzbeck P, Giordano A, Mondini E, Murano I, Severi I, Venema W, Cecchini MP, Kershaw EE, Barbatelli G, Haemmerle G, *et al* (2018) Brown adipose tissue whitening leads to brown adipocyte death and adipose tissue inflammation. *J Lipid Res* 59: 784–794

Krawczyk SA, Haller JF, Ferrante T, Zoeller RA & Corkey BE (2012) Reactive Oxygen Species Facilitate Translocation of Hormone Sensitive Lipase to the Lipid Droplet During Lipolysis in Human Differentiated Adipocytes. *PLoS ONE* 7: e34904

Kuramoto K, Okamura T, Yamaguchi T, Nakamura TY, Wakabayashi S, Morinaga H, Nomura M, Yanase T, Otsu K, Usuda N, *et al* (2012) Perilipin 5, a lipid droplet-binding protein, protects heart from oxidative burden by sequestering fatty acid from excessive oxidation. *J Biol Chem* 287: 23852–23863

Kusminski CM, Holland WL, Sun K, Park J, Spurgin SB, Lin Y, Askew GR, Simcox JA, McClain DA, Li C, *et al* (2012) MitoNEET-driven alterations in adipocyte mitochondrial activity reveal a crucial adaptive process that preserves insulin sensitivity in obesity. *Nat Med* 18: 1539–1549

Kusminski CM & Scherer PE (2012) Mitochondrial dysfunction in white adipose tissue. *Trends Endocrinol Metab* 23: 435–443

Kwok KHM, Lam KSL & Xu A (2016) Heterogeneity of white adipose tissue: molecular basis and clinical implications. *Exp Mol Med* 48: e215–e215

Laurens C, Bourlier V, Mairal A, Louche K, Badin P-M, Mouisel E, Montagner A, Marette A, Tremblay A, Weisnagel JS, *et al* (2016) Perilipin 5 fine-tunes lipid oxidation to metabolic demand and protects against lipotoxicity in skeletal muscle. *Sci Rep* 6: 38310

Lee M-J, Jash S, Jones JEC, Puri V & Fried SK (2019) Rosiglitazone remodels the lipid droplet and britens human visceral and subcutaneous adipocytes ex vivo. *J Lipid Res* 60: 856–868

Li X, Li Z, Zhao M, Nie Y, Liu P, Zhu Y & Zhang X (2019) Skeletal Muscle Lipid Droplets and the Athlete's Paradox. *Cells* 8: 249

Liesa M, Palacín M & Zorzano A (2009) Mitochondrial Dynamics in Mammalian Health and Disease. *Physiol Rev* 89: 799–845

Lin J & Chen A (2016) Perilipin 5 restores the formation of lipid droplets in activated hepatic stellate cells and inhibits their activation. *Lab Investig J Tech Methods Pathol* 96: 791–806

Lin J, Zheng S, Attie AD, Keller MP, Bernlohr DA, Blaner WS, Newberry EP, Davidson NO & Chen A (2018) Perilipin 5 and liver fatty acid binding protein function to restore quiescence in mouse hepatic stellate cells. *J Lipid Res* 59: 416–428

Listenberger LL, Han X, Lewis SE, Cases S, Farese RV, Ory DS & Schaffer JE (2003) Triglyceride accumulation protects against fatty acid-induced lipotoxicity. *Proc Natl Acad Sci* 100: 3077–3082

Luong Q, Huang J & Lee KY (2019) Deciphering White Adipose Tissue Heterogeneity. *Biology* 8: 23

Mahdaviani K, Benador I & Shirihai O (2015) Assessment of Brown Adipocyte Thermogenic Function by High-throughput Respirometry. *BIO-Protoc* 5

Mahdaviani K, Benador IY, Su S, Gharakhanian RA, Stiles L, Trudeau KM, Cardamone M, Enríquez-Zarralanga V, Ritou E, Aprahamian T, *et al* (2017) Mfn2 deletion in brown adipose tissue protects from insulin resistance and impairs thermogenesis. *EMBO Rep* 18: 1123–1138

van Marken Lichtenbelt WD, Vanhommerig JW, Smulders NM, Drossaerts JMAFL, Kemerink GJ, Bouvy ND, Schrauwen P & Teule GJJ (2009a) Cold-Activated Brown Adipose Tissue in Healthy Men. *N Engl J Med* 360: 1500–1508

van Marken Lichtenbelt WD, Vanhommerig JW, Smulders NM, Drossaerts JMAFL, Kemerink GJ, Bouvy ND, Schrauwen P & Teule GJJ (2009b) Cold-Activated Brown Adipose Tissue in Healthy Men. *N Engl J Med* 360: 1500–1508

Mottillo EP, Balasubramanian P, Lee Y-H, Weng C, Kershaw EE & Granneman JG (2014) Coupling of lipolysis and de novo lipogenesis in brown, beige, and white adipose tissues during chronic β3-adrenergic receptor activation. *J Lipid Res* 55: 2276–2286

Murphy DJ & Vance J (1999) Mechanisms of lipid-body formation. *Trends Biochem Sci* 24: 109–115

Napolitano L & Fawcett D (1958) The Fine Structure of Brown Adipose Tissue in the Newborn Mouse and Rat. *J Biophys Biochem Cytol* 4: 685–692

Newsholme EA, Arch JRS, Brooks B & Surholt B (1983) The role of substrate cycles in metabolic regulation. *Biochem Soc Trans* 11: 52–56

Ngo J, Benador IY, Brownstein AJ, Vergnes L, Veliova M, Shum M, Acín-Pérez R, Reue K, Shirihai OS & Liesa M (2021) Isolation and functional analysis of peridroplet mitochondria from murine brown adipose tissue. *STAR Protoc* 2: 100243

Nguyen TB, Louie SM, Daniele JR, Tran Q, Dillin A, Zoncu R, Nomura DK & Olzmann JA (2017) DGAT1-Dependent Lipid Droplet Biogenesis Protects Mitochondrial Function during Starvation-Induced Autophagy. *Dev Cell* 42: 9–21.e5

Nicholls DG & Ferguson SJ (2013) Bioenergetics Fourth edition. Amsterdam: Academic Press, Elsevier

Nielsen J, Mogensen M, Vind BF, Sahlin K, Højlund K, Schrøder HD & Ørtenblad N (2010) Increased subsarcolemmal lipids in type 2 diabetes: effect of training on localization of lipids, mitochondria, and glycogen in sedentary human skeletal muscle. *Am J Physiol-Endocrinol Metab* 298: E706–E713

O'Mara AE, Johnson JW, Linderman JD, Brychta RJ, McGehee S, Fletcher LA, Fink YA, Kapuria D, Cassimatis TM, Kelsey N, *et al* (2020) Chronic mirabegron treatment increases human brown fat, HDL cholesterol, and insulin sensitivity. *J Clin Invest*

Palade, G.E. (1959) Subcellular particles. *Funct Chang Struct Cell Compon*: 64–83

Palmieri L, Pardo B, Lasorsa FM, del Arco A, Kobayashi K, Iijima M, Runswick MJ, Walker JE, Saheki T, Satrústegui J, *et al* (2001) Citrin and aralar1 are Ca2+-stimulated aspartate/glutamate transporters in mitochondria. *EMBO J* 20: 5060–5069

Panic V, Pearson S, Banks J, Tippetts TS, Lee S, Simcox J, Geoghegan G, Bensard C, van Ry T, Holland WL, *et al* (2019) Mitochondrial pyruvate carrier is required for optimal brown fat thermogenesis. *bioRxiv*

Papa S, Francavilla A, Paradies G & Meduri B (1971) The transport of pyruvate in rat liver mitochondria. *FEBS Lett* 12: 285–288

Peirce V, Carobbio S & Vidal-Puig A (2014) The different shades of fat. *Nature* 510: 76

Pfannenberg C, Werner MK, Ripkens S, Stef I, Deckert A, Schmadl M, Reimold M, Haring H-U, Claussen CD & Stefan N (2010) Impact of Age on the Relationships of Brown Adipose Tissue With Sex and Adiposity in Humans. *Diabetes* 59: 1789–1793

Poekes L, Lanthier N & Leclercq IA (2015) Brown adipose tissue: a potential target in the fight against obesity and the metabolic syndrome. *Clin Sci* 129: 933–949

Pollak NM, Schweiger M, Jaeger D, Kolb D, Kumari M, Schreiber R, Kolleritsch S, Markolin P, Grabner GF, Heier C, *et al* (2013) Cardiac-specific overexpression of perilipin 5 provokes severe cardiac steatosis via the formation of a lipolytic barrier. *J Lipid Res* 54: 1092–1102

Prentki M & Madiraju SRM (2008) Glycerolipid Metabolism and Signaling in Health and Disease. *Endocr Rev* 29: 647–676

Pribasnig M, Kien B, Pusch L, Haemmerle G, Zimmermann R & Wolinski H (2018) Extended-resolution imaging of the interaction of lipid droplets and mitochondria. *Biochim Biophys Acta BBA - Mol Cell Biol Lipids* 1863: 1285–1296

Qi J, Lang W, Giardino E, Caldwell GW, Smith C, Minor LK, Darrow AL, Willemsens G, DeWaepenaert K, Roevens P, *et al* (2010) High-content assays for evaluating cellular and hepatic diacylglycerol acyltransferase activity. *J Lipid Res* 51: 3559–3567

Rambold AS, Cohen S & Lippincott-Schwartz J (2015) Fatty Acid Trafficking in Starved Cells: Regulation by Lipid Droplet Lipolysis, Autophagy, and Mitochondrial Fusion Dynamics. *Dev Cell* 32: 678–692

Reshef L, Olswang Y, Cassuto H, Blum B, Croniger CM, Kalhan SC, Tilghman SM & Hanson RW (2003) Glyceroneogenesis and the Triglyceride/Fatty Acid Cycle. *J Biol Chem* 278: 30413–30416

Saltiel AR & Olefsky JM (1996) Thiazolidinediones in the Treatment of Insulin Resistance and Type II Diabetes. *Diabetes* 45: 1661–1669

Schell JC, Wisidagama DR, Bensard C, Zhao H, Wei P, Tanner J, Flores A, Mohlman J, Sorensen LK, Earl CS, *et al* (2017) Control of intestinal stem cell function and proliferation by mitochondrial pyruvate metabolism. *Nat Cell Biol* 19: 1027–1036

Schott MB, Weller SG, Schulze RJ, Krueger EW, Drizyte-Miller K, Casey CA & McNiven MA (2019) Lipid droplet size directs lipolysis and lipophagy catabolism in hepatocytes. *J Cell Biol* 218: 3320–3335

Schrepfer E & Scorrano L (2016) Mitofusins, from Mitochondria to Metabolism. *Mol Cell* 61: 683–694

Seale P, Conroe HM, Estall J, Kajimura S, Frontini A, Ishibashi J, Cohen P, Cinti S & Spiegelman BM (2011) Prdm16 determines the thermogenic program of subcutaneous white adipose tissue in mice. *J Clin Invest* 121: 96–105

Sharma A, Oonthonpan L, Sheldon RD, Rauckhorst AJ, Zhu Z, Tompkins SC, Cho K, Grzesik WJ, Gray LR, Scerbo DA, *et al* (2019) Impaired skeletal muscle mitochondrial pyruvate uptake rewires glucose metabolism to drive whole-body leanness. *eLife* 8

Stone SJ, Levin MC, Zhou P, Han J, Walther TC & Farese RV (2009) The Endoplasmic Reticulum Enzyme DGAT2 Is Found in Mitochondria-associated Membranes and Has a Mitochondrial Targeting Signal That Promotes Its Association with Mitochondria. *J Biol Chem* 284: 5352–5361

Stone SJ, Myers HM, Watkins SM, Brown BE, Feingold KR, Elias PM & Farese RV (2004) Lipopenia and Skin Barrier Abnormalities in DGAT2-deficient Mice. *J Biol Chem* 279: 11767–11776

Sztalryd C & Kimmel AR (2014) Perilipins: Lipid droplet coat proteins adapted for tissue-specific energy storage and utilization, and lipid cytoprotection. *Biochimie* 96: 96–101

Tajima K, Ikeda K, Chang H-Y, Chang C-H, Yoneshiro T, Oguri Y, Jun H, Wu J, Ishihama Y & Kajimura S (2019) Mitochondrial lipoylation integrates age-associated decline in brown fat thermogenesis. *Nat Metab* 1: 886–898

Tan GD, Debard C, Tiraby C, Humphreys SM, Frayn KN, Langin D, Vidal H & Karpe F (2003) A “futile cycle” induced by thiazolidinediones in human adipose tissue? *Nat Med* 9: 811–812

Tan, Jin, Wang, Huang, Wu & Ren (2019) Perilipin 5 Protects against Cellular Oxidative Stress by Enhancing Mitochondrial Function in HepG2 Cells. *Cells* 8: 1241

Tarnopolsky MA, Rennie CD, Robertshaw HA, Fedak-Tarnopolsky SN, Devries MC & Hamadeh MJ (2007) Influence of endurance exercise training and sex on intramyocellular lipid and mitochondrial ultrastructure, substrate use, and mitochondrial enzyme activity. *Am J Physiol-Regul Integr Comp Physiol* 292: R1271–R1278

Tompkins SC, Sheldon RD, Rauckhorst AJ, Noterman MF, Solst SR, Buchanan JL, Mapuskar KA, Pewa AD, Gray LR, Oonthonpan L, *et al* (2019) Disrupting Mitochondrial Pyruvate Uptake Directs Glutamine into the TCA Cycle away from Glutathione Synthesis and Impairs Hepatocellular Tumorigenesis. *Cell Rep* 28: 2608–2619.e6

Trevino MB, Machida Y, Hallinger DR, Garcia E, Christensen A, Dutta S, Peake DA, Ikeda Y & Imai Y (2015) Perilipin 5 regulates islet lipid metabolism and insulin

secretion in a cAMP-dependent manner: implication of its role in the postprandial insulin secretion. *Diabetes* 64: 1299–1310

Vacanti NM, Divakaruni AS, Green CR, Parker SJ, Henry RR, Ciaraldi TP, Murphy AN & Metallo CM (2014) Regulation of substrate utilization by the mitochondrial pyruvate carrier. *Mol Cell* 56: 425–435

Vadvalkar SS, Matsuzaki S, Eyster CA, Giorgione JR, Bockus LB, Kinter CS, Kinter M & Humphries KM (2017) Decreased Mitochondrial Pyruvate Transport Activity in the Diabetic Heart: ROLE OF MITOCHONDRIAL PYRUVATE CARRIER 2 (MPC2) ACETYLATION. *J Biol Chem* 292: 4423–4433

Valm AM, Cohen S, Legant WR, Melunis J, Hershberg U, Wait E, Cohen AR, Davidson MW, Betzig E & Lippincott-Schwartz J (2017) Applying systems-level spectral imaging and analysis to reveal the organelle interactome. *Nature* 546: 162–167

Vanderperre B, Bender T, Kunji ER & Martinou J-C (2015) Mitochondrial pyruvate import and its effects on homeostasis. *Curr Opin Cell Biol* 33: 35–41

Vanderperre B, Herzig S, Krznar P, Hörl M, Ammar Z, Montessuit S, Pierredon S, Zamboni N & Martinou J-C (2016) Embryonic Lethality of Mitochondrial Pyruvate Carrier 1 Deficient Mouse Can Be Rescued by a Ketogenic Diet. *PLoS Genet* 12: e1006056

Varghese M, Kimler VA, Ghazi FR, Rathore GK, Perkins GA, Ellisman MH & Granneman JG (2019) Adipocyte lipolysis affects Perilipin 5 and cristae organization at the cardiac lipid droplet-mitochondrial interface. *Sci Rep* 9

Veliova M, Petcherski A, Liesa M & Shirihai OS (2020) The biology of lipid droplet-bound mitochondria. *Semin Cell Dev Biol* 108: 55–64

Vernochet C, Damilano F, Mourier A, Bezy O, Mori MA, Smyth G, Rosenzweig A, Larsson N-G & Kahn CR (2014) Adipose tissue mitochondrial dysfunction triggers a lipodystrophic syndrome with insulin resistance, hepatosteatosis, and cardiovascular complications. *FASEB J* 28: 4408–4419

Vigueira PA, McCommis KS, Schweitzer GG, Remedi MS, Chambers KT, Fu X, McDonald WG, Cole SL, Colca JR, Kletzien RF, *et al* (2014) Mitochondrial Pyruvate Carrier 2 Hypomorphism in Mice Leads to Defects in Glucose-Stimulated Insulin Secretion. *Cell Rep* 7: 2042–2053

Virtanen KA, Lidell ME, Orava J, Heglind M, Westergren R, Niemi T, Taittonen M, Laine J, Savisto N-J, Enerbäck S, *et al* (2009) Functional Brown Adipose Tissue in Healthy Adults. *N Engl J Med* 360: 1518–1525

Walther TC & Farese RV (2009) The life of lipid droplets. *Biochim Biophys Acta BBA - Mol Cell Biol Lipids* 1791: 459–466

Wang C, Yuan Y, Wu J, Zhao Y, Gao X, Chen Y, Sun C, Xiao L, Zheng P, Hu P, *et al* (2019) Plin5 deficiency exacerbates pressure overload-induced cardiac hypertrophy and heart failure by enhancing myocardial fatty acid oxidation and oxidative stress. *Free Radic Biol Med* 141: 372–382

Wang H, Sreenivasan U, Gong D-W, O'Connell KA, Dabkowski ER, Hecker PA, Ionica N, Konig M, Mahurkar A, Sun Y, *et al* (2013) Cardiomyocyte-specific perilipin 5

overexpression leads to myocardial steatosis and modest cardiac dysfunction. *J Lipid Res* 54: 953–965

Wang H, Sreenivasan U, Hu H, Saladino A, Polster BM, Lund LM, Gong D, Stanley WC & Sztalryd C (2011) Perilipin 5, a lipid droplet-associated protein, provides physical and metabolic linkage to mitochondria. *J Lipid Res* 52: 2159–2168

Wang H & Sztalryd C (2011) Oxidative tissue: perilipin 5 links storage with the furnace. *Trends Endocrinol Metab* 22: 197–203

Wang T, Si Y, Shirihai OS, Si H, Schultz V, Corkey RF, Hu L, Deeney JT, Guo W & Corkey BE (2010) Respiration in Adipocytes is Inhibited by Reactive Oxygen Species. *Obesity* 18: 1493–1502

Wang T, Yao W, Li J, He Q, Shao Y & Huang F (2018) Acetyl-CoA from inflammation-induced fatty acids oxidation promotes hepatic malate-aspartate shuttle activity and glycolysis. *Am J Physiol-Endocrinol Metab* 315: E496–E510

Wikstrom JD, Mahdaviani K, Liesa M, Sereda SB, Si Y, Las G, Twig G, Petrovic N, Zingaretti C, Graham A, *et al* (2014) Hormone-induced mitochondrial fission is utilized by brown adipocytes as an amplification pathway for energy expenditure. *EMBO J*: n/a-n/a

Wilson-Fritch L, Burkart A, Bell G, Mendelson K, Leszyk J, Nicoloro S, Czech M & Corvera S (2003) Mitochondrial Biogenesis and Remodeling during Adipogenesis and in Response to the Insulin Sensitizer Rosiglitazone. *Mol Cell Biol* 23: 1085–1094

Wilson-Fritch L, Nicoloro S, Chouinard M, Lazar MA, Chui PC, Leszyk J, Straubhaar J, Czech MP & Corvera S (2004) Mitochondrial remodeling in adipose tissue associated with obesity and treatment with rosiglitazone. *J Clin Invest* 114: 1281–1289

Wolins NE, Quaynor BK, Skinner JR, Tzekov A, Croce MA, Gropler MC, Varma V, Yao-Borengasser A, Rasouli N, Kern PA, *et al* (2006) OXPAT/PAT-1 Is a PPAR-Induced Lipid Droplet Protein That Promotes Fatty Acid Utilization. *Diabetes* 55: 3418–3428

Wu J, Boström P, Sparks LM, Ye L, Choi JH, Giang A-H, Khandekar M, Virtanen KA, Nuutila P, Schaart G, *et al* (2012) Beige Adipocytes Are a Distinct Type of Thermogenic Fat Cell in Mouse and Human. *Cell* 150: 366–376

Yang C, Ko B, Hensley CT, Jiang L, Wasti AT, Kim J, Sudderth J, Calvaruso MA, Lumata L, Mitsche M, *et al* (2014a) Glutamine Oxidation Maintains the TCA Cycle and Cell Survival during Impaired Mitochondrial Pyruvate Transport. *Mol Cell* 56: 414–424

Yang C, Ko B, Hensley CT, Jiang L, Wasti AT, Kim J, Sudderth J, Calvaruso MA, Lumata L, Mitsche M, *et al* (2014b) Glutamine Oxidation Maintains the TCA Cycle and Cell Survival during Impaired Mitochondrial Pyruvate Transport. *Mol Cell* 56: 414–424

Yang L, Kombu RS, Kasumov T, Zhu S-H, Cendrowski AV, David F, Anderson VE, Kelleher JK & Brunengraber H (2008) Metabolomic and Mass Isotopomer

Analysis of Liver Gluconeogenesis and Citric Acid Cycle: I. INTERRELATION BETWEEN GLUCONEOGENESIS AND CATAPLEROSIS; FORMATION OF METHOXAMATES FROM AMINOOXYACETATE AND KETOACIDS. *J Biol Chem* 283: 21978–21987

Yen C-LE, Stone SJ, Koliwad S, Harris C & Farese RV (2008) *Thematic Review Series: Glycerolipids.* DGAT enzymes and triacylglycerol biosynthesis. *J Lipid Res* 49: 2283–2301

Yin X, Lanza IR, Swain JM, Sarr MG, Nair KS & Jensen MD (2014) Adipocyte Mitochondrial Function Is Reduced in Human Obesity Independent of Fat Cell Size. *J Clin Endocrinol Metab* 99: E209–E216

Yoneshiro T, Aita S, Matsushita M, Okamatsu-Ogura Y, Kameya T, Kawai Y, Miyagawa M, Tsujisaki M & Saito M (2011) Age-Related Decrease in Cold-Activated Brown Adipose Tissue and Accumulation of Body Fat in Healthy Humans. *Obesity* 19: 1755–1760

Yoo H, Antoniewicz MR, Stephanopoulos G & Kelleher JK (2008) Quantifying Reductive Carboxylation Flux of Glutamine to Lipid in a Brown Adipocyte Cell Line. *J Biol Chem* 283: 20621–20627

Yu J, Zhang S, Cui L, Wang W, Na H, Zhu X, Li L, Xu G, Yang F, Christian M, *et al* (2015) Lipid droplet remodeling and interaction with mitochondria in mouse brown adipose tissue during cold treatment. *Biochim Biophys Acta BBA - Mol Cell Res* 1853: 918–928

Zechner R, Zimmermann R, Eichmann TO, Kohlwein SD, Haemmerle G, Lass A & Madeo F (2012) FAT SIGNALS - Lipases and Lipolysis in Lipid Metabolism and Signaling. *Cell Metab* 15: 279–291

Zhang H, Wang Y, Li J, Yu J, Pu J, Li L, Zhang H, Zhang S, Peng G, Yang F, *et al* (2011) Proteome of Skeletal Muscle Lipid Droplet Reveals Association with Mitochondria and Apolipoprotein A-I. *J Proteome Res* 10: 4757–4768

Zhang J, Ahn WS, Gameiro PA, Keibler MA, Zhang Z & Stephanopoulos G (2014) 13C Isotope-Assisted Methods for Quantifying Glutamine Metabolism in Cancer Cells. In *Methods in Enzymology* pp 369–389. Elsevier

Zhang S, Wang Y, Cui L, Deng Y, Xu S, Yu J, Cichello S, Serrero G, Ying Y & Liu P (2016) Morphologically and Functionally Distinct Lipid Droplet Subpopulations. *Sci Rep* 6

Zhang Y, Goldman S, Baerga R, Zhao Y, Komatsu M & Jin S (2009) Adipose-specific deletion of autophagy-related gene 7 (atg7) in mice reveals a role in adipogenesis. *Proc Natl Acad Sci* 106: 19860–19865

Zheng P, Xie Z, Yuan Y, Sui W, Wang C, Gao X, Zhao Y, Zhang F, Gu Y, Hu P, *et al* (2017) Plin5 alleviates myocardial ischaemia/reperfusion injury by reducing oxidative stress through inhibiting the lipolysis of lipid droplets. *Sci Rep* 7

Zhu Y, Zhang X, Zhang L, Zhang M, Li L, Luo D & Zhong Y (2019) Perilipin5 protects against lipotoxicity and alleviates endoplasmic reticulum stress in pancreatic β-cells. *Nutr Metab* 16

Zou S, Lang T, Zhang B, Huang K, Gong L, Luo H, Xu W & He X (2018a) Fatty acid oxidation alleviates the energy deficiency caused by the loss of MPC1 in MPC1+/− mice. *Biochem Biophys Res Commun* 495: 1008–1013

Zou S, Zhu L, Huang K, Luo H, Xu W & He X (2018b) Adipose tissues of MPC1 ± mice display altered lipid metabolism-related enzyme expression levels. *PeerJ* 6: e5799